AN EVALUATION OF ACCELERATED DRYING OF RECLAMATION SOIL COVERS BY CONVECTIVE AIRFLOW

A Thesis Submitted to the College of

Graduate and Postdoctoral Studies

In Partial Fulfillment of the Requirements

for the Degree of Master of Science

In the Department of Civil, Geological and Environmental Engineering

University of Saskatchewan

Saskatoon, SK

By

Bryan Koehler

PERMISSION TO USE

In presenting this thesis in partial fulfilment of the requirements for a Postgraduate degree from the University of Saskatchewan, I agree that the Libraries of this University may make it freely available for inspection. I further agree that permission for copying of this thesis in any manner, in whole or in part, for scholarly purposes may be granted by the professor or professors who supervised my thesis work or, in their absence, by the Head of the Department or the Dean of the College in which my thesis work was done. It is understood that any copying or publication or use of this thesis or parts thereof for financial gain shall not be allowed without my written permission. It is also understood that due recognition shall be given to me and to the University of Saskatchewan in any scholarly use which may be made of any material in my thesis.
Requests for permission to copy or to make other use of material in this thesis in whole or part should be addressed to:

Department of Civil, Geological and Environmental Engineering
University of Saskatchewan
3B48 Engineering building
57 Campus Drive
Saskatoon, Saskatchewan S7N 5A9

Alternatively, requests for permission to copy or to make other use of material in this thesis in whole or part may also be addressed to:

College of Graduate and Postdoctoral Studies
Room 116 Thorvaldson Building, 110 Science Place
Saskatoon, Saskatchewan S7N 5C9

ABSTRACT

The coke beach instrumented watershed is a reclamation cover test site constructed in 2005 on top of petroleum coke at the Mildred Lake mine operated by Syncrude Canada Ltd in Fort McMurray, Alberta. Petroleum coke is a by-product of the oil sands extraction process. The cover system monitoring has shown an annual water loss which cannot be readily accounted for based on a standard water balance analyses. The water loss is most pronounced in late spring/early summer. It is hypothesized that the cause of the enhanced water loss is a result of convective drying of the cover as a result of airflow from the atmosphere into the underlying coke. This airflow could be the result of density gradients across the cover system as a result of temperature contrasts between the atmosphere and the coke or could be the result of oxygen consumption processes associated with the oxidation of methane released from the underlying fine tailings. The primary purpose of this study was to design and implement a field monitoring system to determine whether convective airflow was occurring across a series of trial closure cover systems overlying petroleum coke, and to utilize the resulting data in a water-loss calculation and determine the effect on the overall water balance for the site.

The coke beach instrumented watershed contains two cover system trials: a shallow cover system and a deep cover system, with nominal cover depths of 0.40 m and 1.0 m respectively. Each cover system was instrumented with soil monitoring instrumentation which has been continuously monitored since cover construction. The shallow cover system included a meteorological monitoring system to complete the water balance monitoring. Additional studies have been carried out on each cover system including regular vegetation monitoring, and hydraulic conductivity testing. The major field research associated with this thesis was the installation and monitoring of differential pressure between the subsurface soil air and the ambient conditions. Three clusters at variable depths (0.4 m, 1.1 m, and 2.0 m) were installed on each cover system. In addition, air permeability testing of the cover system and underlying coke was performed to collect more data points for which to assess airflow rates.

The results of the field monitoring program showed that differential pressure gradients existed across the cover systems relative to ambient conditions, and each cover system showed enhanced drying during the field monitoring years. The pressure gradients measured at each cover system were sufficient to induce substantial airflows, with measured differential pressures exceeding 40

Pa during peak periods. However, the estimated airflow rates did not appear to be sufficient to account for all of the enhanced drying observed in the water balance. This lack of airflow is likely a result of low permeability of the cover system material where the differential pressure systems were installed. However, it should be noted that across both cover systems, substantial cracking has occurred as a result of the dry conditions of the soil material. These cracks create macro-pores through which increased flow rates are possible due to larger void space. Given the differential pressure gradients measured across the cover systems, airflow through these cracks is possible and may have an effect on the soil moisture in material in the area surrounding the cracks. Further refinement in the research may be able to determine the effect the cracks have on airflow and cover drying.

In addition to allowing for potential increased airflow rates, the macro-pores and cracks may also give rise to increased net percolation/bypass flow during snow melt infiltration and/or heavy rainfall events. The cover systems have approximately a 1% slope with substantial surface roughness and consequently runoff from the covers is unlikely. However, very little to no ponded water was observed on top of the cover systems even following large rainfall events. This indicates that there is a high potential for bypass flow or increased net percolation which may not have been represented by point measurements of permeability. No monitoring of net-percolation or infiltration was included as a component of the water balance; lysimeters were installed as part of the initial meteorological system installed in 2005, however, they were not regularly maintained or monitored since installation and as such were not usable.

Hypothetical analyses were carried out in order to determine the water removal via airflow under higher permeability conditions. This analysis found that an increase in permeability of three orders of magnitude would result in sufficient airflow to cause enhanced drying of each cover system such that the additional moisture loss not currently accounted for by the water balance was completely accounted for by airflow alone. It is possible that the water balance of the covers is affected by both enhanced drying as a result of airflow as well as some form of preferential or bypass flow during infiltration events. Further research is required to more fully characterize the latter mechanism.

ACKNOWLEDGEMENTS

The completion of this thesis would not have been possible without the input and support from many people and parties. Firstly, I would like to give my thanks and gratitude to Syncrude Canada Ltd. and the Environmental Department staff for funding the research, providing me access to the project location, providing me the resources necessary to complete the work, and answering any and all questions regarding site operations, site safety requirements, and anything else that arose while carrying out the work. I would also like to thank Dyan Pratt and Thomas Baer of the University of Saskatchewan for helping with field work, including but not limited to data downloads, sensor installation, field measurements, and all other work that was required to complete the project. Lastly, I would like to thank my supervisors Dr. Lee Barbour and Dr. Grant Ferguson with the University of Saskatchewan; it has been a long road from inception of the project to thesis completion, and their undying patience and support got me through to the end.

TABLE OF CONTENTS

LIST OF TABLES

LIST OF FIGURES

LIST OF ABBREVIATIONS

AET	Actual Evapotranspiration
PET	Potential Evapotranspiration
FC	Field Capacity
WP	Wilting Point
AWHC	Available water holding capacity
AWR	Additional water removal
CS229	Campbell Scientific thermal conductivity sensors
CS616	Campbell Scientific TDR sensors
TDR	Time domain reflectometry
DP	Differential pressure
CBIW	Coke beach instrumented watershed
SCL	Syncrude Canada, ltd.
OKC	O'Kane Consultants, Inc.
g	Acceleration due to gravity
K	Intrinsic permeability (m^2)
K_{sat}	Saturated hydraulic conductivity
K_{air}	Air conductivity
m	metres
g	Gravitational constant

m^2	square metres
m^3	Cubic metres
Pa	Pascals
kPa	Kilopascals
PPT	Precipitation
SWE	Snow-water equivalence
SWCC	Soil water characteristic curve
S	Degree of saturation
RI	Runoff and interflow
VWC	Volumetric water content
VAC	Volumetric air content
LNAPL	Light non-aqueous phase liquid
P_{sat}	Saturated vapour pressure
P_{vap}	Actual vapour pressure
RH	Relative humidity
Q	Flow rate

Chapter 1
Introduction

Syncrude Canada Ltd. (SCL) constructed two instrumented watersheds overtop of unsaturated petroleum coke (coarse textured carbon sand like deposit from the upgrading process) which had been hydraulically deposited over fluid fine tailings (FFT) in 2004. The covers were part of a study of reclamation cover performance for landforms constructed out of coke. The two instrumented watersheds were constructed near the top of a sand dyke at the Mildred Lake Settling Basin (MLSB), the main tailings disposal basin for the SCL Base Mine operation. The cover systems are referred to as the Coke Beach Instrumented Watershed (CBIW).

Oil sands mining activities have greatly altered the landscapes of the Fort McMurray region. Following mining activities, the land will be returned to the government, but prior to this occurring the oil sands mining companies are required to reclaim the landscape and demonstrate that the reclaimed land will provide "an equivalent land capability" (Cumulative Environment Management Association (CEMA), 2006). This equivalent land capability applies to water storage (soil moisture storage) and nutrient supply to sustain fauna/flora in the area. The CBIW will be part of that reclaimed landscape, and SCL is required to reclaim the landscape in order to meet regulatory requirements.

An initial water balance for the CBIW covers for 2005-2006 by Fenske (2012) found that in spite of a high-water storage capacity, the covers did not provide sufficient water to the vegetation during dryer periods of the year. Subsequent interpretations of the water balance for the covers (Huang et al., 2010) suggested there was additional drying of the covers beyond that which could reasonably be ascribed to evapotranspiration. As a consequence, it has been hypothesized that the enhanced drying is due to convective airflow in which dry atmospheric air is drawn across the cover system resulting in removal of water from the cover.

There have been a number of mechanisms for convective airflow through unsaturated soils documented in the literature. The primary one, most often associated with coarse unsaturated mine waste such as waste rock, is the generation of airflow driven by gradients in air density created by temperature differences in the waste rock. This form of convective airflow is also known as free

convection (Lu, 2001). The other less common cause of convective airflow is that associated with the rapid consumption of oxygen within the soil profile such as might occur as a result of upward methane migration. This reaction induced convection is due to a loss of partial pressures (or molar volume) of gas as oxygen and methane react (Thorstenson 1989, Amos et al., 2005, Jones et al., 2014).

1.1 Study Objectives and Scope

The primary purpose of this study was to design and implement a field monitoring system to establish if downward airflow was occurring through the cover and if so, whether this airflow was sufficient to account for the observed enhanced drying of the covers. The specific objectives of this thesis are as follows:

- Design and install field instrumentation and testing to characterize the presence and magnitude of airflow through the cover profiles at the CBIW.
- Quantify the water loss from the covers that is in excess of what can be explained by normal evapotranspiration processes based on a daily water balance for each year of monitoring and identify time periods which actual evapotranspiration trends diverge from expected trends.

Soil monitoring stations used for the determination of the site water balances were installed in 2004 by O'Kane Consultants Inc. (OKC) (OKC, 2004)

1.2 Thesis Layout

Chapter 2 provides a brief summary of background literature. Chapter 3 describes the field program, including all equipment and sensors installed at the site location. Chapter 4 presents the key data collected during the monitoring program. Chapter 5 presents a discussion and interpretation of the data presented in Chapter 4. Finally, Chapter 6 summarizes the key findings and conclusions drawn from interpretations of the field data and provides recommendations for future work.

Chapter 2
Literature Review

The purpose of this chapter is to provide an introduction into mine waste cover systems, instrumented watersheds, and the basic processes of gas flow through a porous medium.

2.1 Airflow in Unsaturated Soil

The flow of air through a dry soil is analogous to the flow of water through a saturated soil in that a basic Darcian relationship can be used to describe the flow rate in response to a hydraulic gradient comprised of both a pressure and gravitational (*i.e.* density) gradient. The driving mechanism of free convection in a system is the variation in air density that occurs as a result of the difference in temperature from one location to the next.

Temperature and concomitant density variations can have an effect on the airflow in a system which is open to the atmosphere. Air is a compressible fluid whose density changes significantly with variations in temperature or pressure, and density dependent convective airflow in a porous media is a well-documented process, and has been observed in coarse waste rock piles (Lu, 2001), gravel embankments (Goering & Kumar, 1996), and has been used to encourage permafrost aggradation (Arenson et. al, 2007).

Variations in air density within a deposit relative to ambient atmospheric conditions are primarily caused by temperatures within the deposit that are different from those in the atmosphere. The presence of a temperature induced density gradient results in variable pressures at differing depths throughout the soil. The flow equation for airflow can be written as follows (Geostudio, 2013):

$$m_a = \rho_a q_a dxdz = \frac{-k_a}{g}\left(\frac{\partial u_a}{\partial y} + \rho_a g \frac{\partial y}{\partial y}\right) dxd \qquad 2.1$$

where k_a is the (dry) air hydraulic conductivity (L T^{-1}), ρ_a is the density of air (M L^{-3}), qa is the airflow velocity (L T^{-1}), u_a is the air pressure, and m_a is the mass flow rate.

If isothermal conditions and a constant water content (*i.e.* single phase air transfer) are assumed the equation can be reduced to the following equation (Geostudio, 2013):

$$\rho_a \frac{\theta_a}{\bar{u}_a} = \frac{\partial}{\partial y}\left[\frac{k_a}{g}\left(\frac{\partial u_a}{\partial y} + \rho_a g \frac{\partial y}{\partial y}\right)\right] \quad 2.2$$

which is the governing equation for airflow through a soil and is similar to Darcy's Law for liquid water flow.

Theoretically, the correct method to determine airflow in an unsaturated soil is to use the compressible flow equation presented in Equation 2.2, however, due to the complexity of compressible flow calculations it is sometimes more simple and appropriate to use an assumption of incompressible flow. In these situations, a basic Darcian analysis can be utilized to determine airflow rates due to a density gradient, as presented in Equation 2.3 (Geostudio, 2012).

$$f_g = \left(\frac{K_{air}}{\rho_{air} g}\right)\left(\frac{dP_a}{dx}\right) \quad 2.3$$

where f_g is the airflow rate (L T-1), Pa is the measured differential air pressure (M L^{-1} T^{-2}) ρ_a is the density of air (M L^{-3}), and g is the gravitational constant (L T^{-2}). In order to use the preceding equation, several assumptions are required (Massman, 1989):

- Laminar, incompressible flow;
- Slip flow is negligible (valid when pore radii > 10^{-3} m);
- Isothermal flow;
- Uniform water content and permeability along axis of flow;
- Gravitational effects are minimal; and
- Air behaves as an ideal gas.

Previous studies have shown that by assuming air behaves as an incompressible fluid to determine airflow rates is a valid assumption if the differential pressure between two measurement points is less than 50 kPa (Massman,1989).

2.1.1 Case Histories – Temperature Driven Mechanisms

Convective airflow within an unsaturated waste rock dump at the Sullivan Mine in British Columbia, Canada, resulted in four fatalities in an otherwise innocuous monitoring shed on the

mine property (Hockley et al. 2009, Philips et al., 2009). Differences in temperature in the waste rock relative to atmospheric conditions resulted in airflow out of the pile and into the monitoring shed through a drainage pipe. It was found that during certain periods of the year and under specific climatic conditions, variable pressure gradients existed within the pile which resulted in the flow of pore-gas either in or out of the pile through the cover material. A downward pressure gradient existed while the soil temperatures within the waste rock pile were less than ambient temperature; *i.e* gas pressure at the base of the pile was higher than ambient pressure. This created a downward airflow which pulled air through the cover and into the waste rock pile resulting in an outward airflow from the base of the waste rock pile into a open pipe which led to an enclosed monitoring shed. The open pipe was used to monitor water flow from the pile. It was found that that the driving force behind these mass air movements was primarily related to changes in dump temperature, as opposed to fluctuations in barometric pressure, and the phenomenon only occurred once a specific ambient temperature had been exceeded. This study showed that differential pressures of only 10 Pa were sufficient to generate airflow rates in excess of 1 m/s.

Arenson & Sego (2007) found that in Arctic regions, the long winters and short summers could be used to design tailings ponds to encourage permafrost aggradation, and thus, isolation of contaminants within the stored tailings. By increasing the air permeability of the cover system on top of the tailings, the authors were able to prove that permafrost depth increased over the winter as the colder, denser air was readily able to infiltrate the high permeability material and displace the relatively warm air in the subsurface. This effect caused maximum freezing of the tailings. During the summer, the cooler air in the higher permeability cover system layer "insulated" the tailings from the warm, less dense ambient air, thus minimizing the degradation of the frozen tailings and successfully containing the waste. This cover system design maintained a mean annual temperature of the interface between the tailings and the cover system below $0^{o}C$.

Temperature driven convective systems have been utilized to limit the degradation of permafrost in highway embankments in Canada's Arctic (Goering, 1997). Frost heave effects can be mitigated on roads in the Arctic by maintaining a continually frozen foundation. By minimizing annual temperature fluctuations causing freezing/thaw cycles in the road base, surface heave is minimized, thus maintaining the integrity of the road surface. These roadway foundation designs incorporated a higher air permeability base, which allowed cold, denser air to infiltrate readily in

the winter. This infiltrating air created convective cells beneath the entire extent of the roadway, displacing all warmer, lower density air. In the summer the cold foundation created convective cells beneath the roadway that equalized temperatures below that of ambient temperatures, and thus prevented the lower density warm air from infiltrating resulting in a thermal insulation effect. This effect maintained integrity of the permafrost in the subsurface and provided a more stable foundation for the road.

2.1.2 Reaction Driven Mechanisms

The density of a fluid may change due to changes in the concentrations of various constituents through chemical reactions such as oxidation or consumption in biological processes (Amos et al., 2005). Reaction driven advective processes have been observed in cases of light non-aqueous phase liquid (LNAPL) releases on top of groundwater. Natural biological processes will utilize (oxidize) the released LNAPL as a source of energy through both aerobic and anaerobic processes, releasing carbon dioxide (CO_2) as a by-product. As hydrocarbons are oxidized, a density gradient is formed, thus creating a pressure difference which can drive advective flow processes.

Reactive driven convective flow having magnitudes between 5×10^{-4} m/s and 6×10^{-4} m/s were observed by Amos et al. (2005) by using non-reactive tracer elements (Nitrogen and Argon) when observing biodegradation of LNAPLs and methane above an aquifer. Using the principle that the concentration of a non-reactive gas will be enriched in the direction of net mass flux (and subsequently depleted in the opposing direction), the authors were able to show areas of both enrichment and depletion. The field observations indicated that an upward mass flux from the zone of LNAPL impact to the surface existed, as indicated by a depletion in nitrogen/argon levels which varied from atmospheric levels. The results indicated that at the surface of the water table there was generally a depletion of tracer elements, indicating the direction of flow was depleting these tracer elements from the area. The tracers were then noted to have elevated concentrations above the LNAPL plume in the vadose zone, but below ground surface. These zones and inferred directions of flow are outlined in Figure 2.1, and show the zones of depletion, enrichment, and inferred pressure gradients indicating the presence of convective cells above the reaction system.

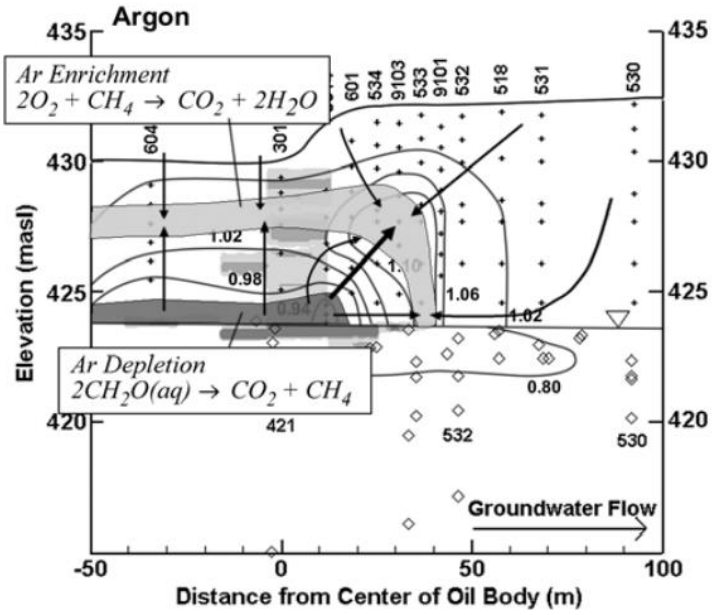

Figure 2.1 Aquifer cross section showing LNAPL impact zone and enrichment/depletion zones of conservative tracer Argon illustrating convective cells due to biodegradation (Amos et al., 2005).

Other instances of reaction driven convective airflow have been observed by Birkham et al., (2010) and Birkham et al. (2011) in which non-reactive tracers (nitrogen) were used in sulfur storage facilities at SCL Fort McMurray to observe oxygen consuming processes (formation of sulfuric acid). These tracers indicated that advective airflow was occurring during the consumption process and generating density driven convective cycles.

Advective/convective cycles at the CBIW may be driven by the presence of methane released from the stored tailings, as observed by Fenske (2012). The biodegradation of the released methane may have been the cause of the low oxygen/high carbon dioxide levels observed by Fenske (2012), and as a result, contributions to a convective cycle are possible.

2.1.3 Air Permeability of a Soil and Effect of Soil Saturation

Air permeability of a soil is heavily influenced by the volumetric water content (VWC) of a soil (Ball & Schjønning, 2002), as well as the soil structure (Olson et al., 2001). The air permeability is one of the determining factors as to how air moves through the soil, and is typically inversely proportional to the soil water characteristic curve (SWCC) (D.G. Fredlund et al., 2012).

Air conductivity (k_a) functions were estimated by assuming a maximum air conductivity (K_{dry_air}) based on the material properties assumed and grain sizes (Bear, 1972). Knowing the K_{dry_air} in conjunction with the SWCC of a soil allows for use of the following equation to estimate the air conductivity as a function of saturation (Brooks and Corey, 1966):

$$K_{air} = K_{dry\_air}(1 - S)^{0.5}(1 - S^{\frac{1}{q}})^{2q} \quad 2.4$$

where q is and empirical value equal to 2.9 and S is the water saturation of the material.

The relationship between the degree of saturation of a soil and the total suction of the material at respective levels of saturation is known as the soil water characteristic curve (SWCC) (Barbour, 1998). The maximum value of air permeability for a soil is found when the soil is completely dry (*i.e.* VWC = 0), and lowest or negligible when the soil is saturated (*i.e.* VWC = porosity) (Ball & Schjønning, 2002). As the matric suction of the soil increases, the SWCC decreases, while the air permeability of the soil increases; this relationship can be seen in Figure 2.2 (a) and (b), respectively.

A bulk (*i.e.* whole cover layer) air permeability in the vertical direction can be determined using multiple measurements of permeability as shown in Equation 2.5(Freeze and Cherry, 1979);

$$K_z = \frac{d}{\sum_{i=1}^{n}\left(\frac{d_i}{K_i}\right)} \quad 2.5$$

where K_z is an equivalent vertical permeability for the system having discontinuous permeabilities (L^2), d is the depth of the entire system (L), d_1, d_2,…d_n are the depths of the soil layers in the system (m), and K_1, K_2,…K_n are permeability values of each soil layer in the system. The estimated air permeability required which represents the threshold for onset of forced convection in soils is approximately 10^{-9} m^2 (Ritchie, 2003).

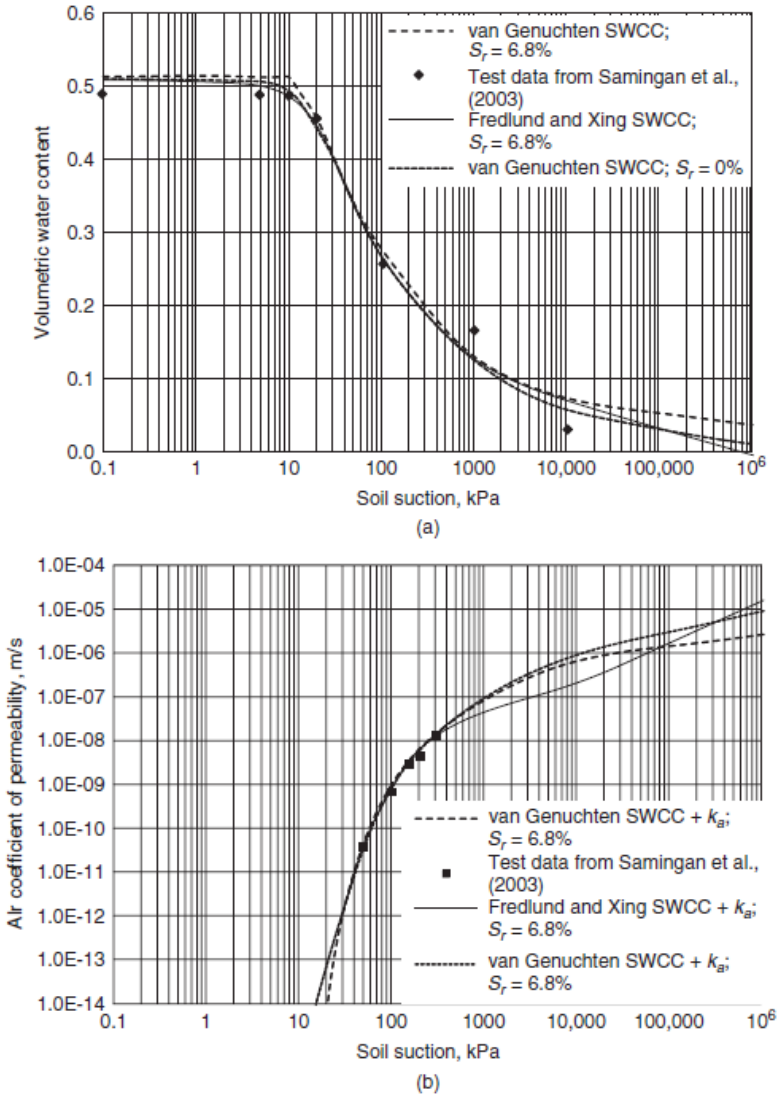

Figure 2.2 Relationship between soil water characteristic curve (a) and air permeability of a soil (b). As the soil suction increases in the soil, a decline in the VWC is noted, while an increase in the air coefficient of permeability is noted (D.G. Fredlund et al., 2012).

The upper and lower bound for air permeability is associated with the fully dry and saturated states of the soil, respectively (D.G. Fredlund et al., 2012). As such, the air permeability can be described in one of two ways: with respect to the saturation value of the soil (*i.e.*, with respect to VWC), or with respect to the suction of the soil (*i.e.* with respect to volumetric air content (VAC)).

2.2 Water Balance Method

The water balance method can be used to assess the processes controlling changes in the water stored within a specified depth (volume) of soil. (Savenjie, 1997). The water balance method relies on the *in situ* measurement of soil water contents along with climate data including precipitation and atmospheric conditions from which potential evapotranspiration (PET) can be estimated. The following components should be measured in order to actual evapotranspiration (AET) in a system:

- Total precipitation, including snowmelt (PPT);
- Actual evapotranspiration (AET);
- Runoff and Interflow (RI); and
- Net Percolation (NP).

By measuring or estimating the above parameters, 2.6 can be solved to determine an overall change in storage (ΔS) within the system (modified from (Savenjie, 1997)):

$$\Delta S = PPT - AE - RI - NP \qquad 2.6$$

However, many of these parameters are difficult to measure accurately. In situations where there is only one unknown in the system, the remainder of the equation can be solved by setting it equivalent to 0 by assuming continuity and changing the unknown parameter until a null condition is met.

2.2.1 Potential and Actual Evapotranspiration

ET is the amount of water that would be evaporated under an optimal set of conditions (*e.g.*, unlimited supply of water) and can be computed from climatic inputs using Penman's method (Penman, 1948). Evapotranspiration is the combined effect of evaporation (the process by which liquid water is transformed into the vapour phase via an energy input) and transpiration (the water uptake by vegetation) (Chin, 2006). Evapotranspiration is defined as the quantity of water leaving a soil per unit area, per unit time. A difficulty arises in differentiating between evaporation from the ground and transpiration by plants when a vegetated surface is taken into consideration.

In practice, there are two primary terms used to describe the water loss from a system due to evapotranspiration: PET and AET. These terms are typically used synonymously with potential evaporation (PE) and actual evaporation (AE), respectively. Due to the difficulties in assessing water movement through a soil, there have been hundreds of contrasting methods developed to predict the AET and PET from a system over the years. The most generally accepted method of prediction of PET is the Penman (1948) method, later adapted to the Penman-Monteith (1965) method. This method utilizes a number data points measured using meteorological instrumentation and is presented in Equation 2.7.

$$ET_o = \frac{\Delta\left((Rn - G) + \rho_a c_p(\delta_e) g_a\right)}{\Delta + \gamma\left(1 + \frac{g_a}{g_s}\right) L_v} \qquad 2.7$$

where ET_o is the water volume evaporated per unit time (mm $^{s-1}$), Δ is the rate of change of saturation specific humidity with air temperature (Pa K^{-1}), R_n is the net irradiance (w m^{-2}), G is the ground heat flux (w m^{-2}), ρ_a is the dry air density (kg m^{-3}), c_p is the specific heat capacity of air (J kg^{-1} K^{-1}), δ_e is the specific humidity (Pa), g_a is the atmospheric conductance (m s^{-1}), γ is the psychrometric constant (~66 Pa K^{-1}), g_s is the surface conductance (m s^{-1}), and L_v is the volumetric latent heat of vaporization (MJ m^{-3}).

The measurement of PET by the Penman-Monteith (1965) method assumes that the soil surface remains saturated throughout the evaporation process. Unfortunately, this is typically never the case in true real-world scenarios, and as such, the measured PET is typically an overestimate of the actual evaporation (AET) occurring.

AET is the rate of water removal that the deposit actually experiences due to evaporation. The AET/PET ratio is 1.0 when available water at the deposit surface is adequate. In typical soil and mine waste deposits, the ratio falls below 1.0 and experiences temporal fluctuations due to a number of factors, including rainfall, salinity changes, and surface desiccation. If the ratio is very low (*i.e.*, practically nil), then minimal water can be removed from the deposit by evaporation. The following sub-sections describe the methods utilized to estimate the AET at the site.

Determining the actual evapotranspiration in field scenario is a difficult task due to the large number of variables and influencing factors (density of vegetation, variable solar radiation,

variable wind velocities, etc.). Using the Penman-Monteith (1965) method to estimate the PET allows for an estimate of the maximum evaporation rates from a specific vegetated area, however, several methods can further refine this estimate to calculate an AET rate.

If the field capacity and wilting point of a soil are known, a linear relationship relating the AWHC can be used to determine the AET from a soil as follows (Brooks et al., 2013).

$$AET = PET * \frac{VWC - WP}{FC - WP} \quad 2.8$$

Using the above equation, when the soil moisture is at or near to the field capacity, the AET is equivalent to the PET, whereas when the soil moisture is at or below the WP, the AET is equivalent to 0. The remainder of the range between the FC and the WP will show a linear relationship between the AET/PET ratios as determined from the equation. The measurement of field capacity and wilting point are drawn directly from measurements of *in situ* Volumetric Water Content (VWC), using methods described in Section 3.2.5.

2.2.2 Precipitation

Precipitation is formed as a rising mass of humid air cools to the dew point temperature. As the rising mass of air cools, the evaporated moisture will condense around particulates in the air, creating droplets of water (Fetter, 1994). When these water droplets reach a certain size, they will begin descending to the earth, resulting in precipitation. In Fort McMurray, Alberta, this may occur in the form of rainfall, hail, or snowfall.

Measurement of rainfall can be performed using an open topped container, and it has been shown that the size of the opening has little effect on the total volume of rainfall measured (Fetter, 1994). Rain gauges used at the CBIW are tipping bucket style rain gauge (TE525) with a CS705 snowfall adapter containing ethylene glycol which melts snowfall and subsequently measures the snow water equivalence (SWE) at the site.

In addition to measurement of SWE via the ethylene glycol measurement, prior to snowmelt manual snow surveys are performed by SCL environmental field staff. In general, it can be said that approximately 10% of the total snow depth is the equivalence of water in the snow pack.

However, as time progresses, and more snow falls, this number tends to become less accurate as the snowpack is compressed under the weight of the overlying snow, resulting in a denser snow pack. As such, manual snow surveys are required to obtain a more accurate density measurement of the snow pack to correlate to an equivalent depth of water. The most accurate measurement of snowpack occurs as close to spring melt as possible, as this is when the greatest amount of snow is present at its most dense state.

A snow survey utilizes a thin walled tube driven into the snow pack. A field measurement of mass of the tube and snow are taken, and the subsequent density of the snow can be calculated from the known mass of the dry tube and dimensions of the tube. The snow water equivalence can be calculated as follows in 2.9 (Pomeroy and Gray, 1995):

$$SWE = \frac{d_s \rho_s}{\rho_w} \qquad 2.9$$

where d_s is the average depth of the snow pack at the point of measurement, and ρ_s and ρ_w are the average densities of the snow and water respectively.

2.2.3 Infiltration / Net Percolation

The process by which water enters the soil as a result of precipitation is known as infiltration (Chin, 2006). Infiltration is not to be confused with net percolation. Net percolation is a term which is used to describe the movement of water through the soil within a specified soil body *(i.e.*, a cover system) and is the water which remains following all removal processes (evapotranspiration, interflow, *etc.*), while infiltration is specific to the movement of water into the soil at the surface. The capacity for infiltration for a specific soil is primarily determined by the amount of surface cover material and the specific soil moisture properties. For a vegetated surface such as at the CBIW, the infiltration capacity is typically higher than that of a bare soil as a result of flow pathways through the soil surface resulting from vegetation stalks.

The net percolation will vary from the infiltration rate depending on the level of vegetation at the surface, flow pathways within the subsurface, and various other influencing factors. Alternative flow pathways may exist in the form of macro-pores and cracking at the surface which can greatly increase net percolation rates through preferential bypass flow through which water can flow

significantly faster than flow through micropores, as governed by Darcian flow (Saravanathiiban D.S. et al., 2014). Water flowing through continuous macropores essentially results in water short-circuiting around the cover system and rooting zone of the plants. Water entering the cracks may infiltrate into the vertical walls of the cracks but may also bypass the soil entirely through the base of the crack; as a result, the majority of water balances do not accommodate the potential for bypass flow.

2.2.4 Runoff & Interflow

In general, two forms of runoff are typically used to describe the potential overland runoff from a given storm event: infiltration excess and saturation excess (Chin, 2006). Infiltration excess occurs when the rainfall exceeds the infiltration capacity of the soil in question at the surface, whereas saturation excess occurs when the soil is saturated at the surface, resulting in a decreased infiltration rate. At first glance these may seem to indicate the same process, however, the differentiation arises between what is used to describe and calculate the actual infiltration capacity of the soils in each method. Infiltration excess limits its analysis to contributing roles of soil type and land use, however, saturation excess runoff includes landscape position, local topography, and soil depth.

The other component of runoff is interflow, which is the lateral flow of water in the subsurface. Baseflow is the flow of water in the subsurface into the system and is typically independent of rainfall events. Interflow is the subsurface flow of water which lands on the system and continues to flow out of the system boundaries.

Chapter 3
Field and Laboratory Program

Instrumentation designed to measure the cover water balance had been previously installed by OKC (2006) and was expanded upon by Fenske (2012). This chapter describes the field programs undertaken at the SCL CBIW through the duration of this study (2012-2014), as well as the instrumentation which was installed and monitored at the site and which was used as part of the analyses undertaken in the present study.

The magnitude of convective airflow across the cover is controlled primarily by the air permeability of the cover and underlying unsaturated coke and the air pressure deficiency present within the waste below the cover. In order to assess the potential for convective airflow across the cover system profile, a system of differential pressure sensors (pressure relative to atmospheric pressure) was installed for this study at various depths across the covers and into the underlying coke at multiple locations. This differential pressure monitoring system included a high accuracy barometric pressure sensor to determine absolute pressure in the system. A component of this *in situ* monitoring program included point measurements of air permeability in the cover profile for all of the various material types.

3.1 Airflow Conceptual Model

The hypothesized cause of the convective airflow system being investigated at the CBIW is the geometry of both the deposit and the berm adjacent to the deposit coupled with the porous nature of the sand tailings and coke tailings and temperature gradients between subsurface and ambient air. Both the sand tailings and coke are covered by a peat-clay mixture which provides a low-permeability isolation boundary layer to the system. This cover system typically would inhibit air and moisture movement into the stored materials, however, due to the unsaturated condition of the coke, proximity of the coke to the edge of the berms downslope, and the temperature variances across the cover system, a density dependant convective cell may develop.

This conceptual model is what is hypothesized to drive the convective airflow in the system, however, due to the scale is difficult to measure and quantify. As such, in order to isolate the conceptual model to the cover system, all analyses have been carried out across the cover system

with the assumption that any downward flowing air is driven towards the berm due to natural topography of the deposit and airflow forcing caused by the temperature gradients down the slope. This process may be investigated further with enhanced numerical modelling but is outside the scope of this thesis.

When considering the design of the berm sloping at a downward angle and maintaining vadose conditions throughout the slope, this temperature trend is likely maintained down the entire slope of the berm, as the cover depth profile is approximately the same. In this situation, the more dense air in the subsurface will tend to exit the tail of the slope. This action would then result in a negative pressure in the subsurface which would then draw in air through the cover system at the point of highest pressure gradient. It is this action which is likely driving any convective airflow across the cover system.

3.2 Description of Test Covers and Existing Instrumentation

Fluid coke was hydraulically deposited and graded in 2004 to create two prototype watersheds, each approximately 4.5 ha in area. Two-layer soil covers were then constructed overtop of the deposited coke in the fall/winter of 2004. The cover was constructed with a negligible slope of less than 1%. The lower layer consisted of a layer of salvaged glacial till overlain by a mixture of peat-mineral soil (glacial till) salvaged by over-stripping surficial peat deposits prior to mining.

The purpose of these cover system trials was to assess the viability of various cover system designs for reclamation of coke beaches. The two different cover systems were constructed as follows:

- Shallow cover system: a nominal depth of 40 cm, comprised of a 15 cm layer of peat-mineral mix and an underlying layer of till with a depth of 25 cm
- Deep cover system: a nominal depth of 100 cm comprised of a 15 cm layer of peat-mineral mix at the surface, and an underlying layer of till having a depth of 85 cm.

Installation of the field monitoring at the CBIW was undertaken by OKC (2006) with additional site characterization and field testing undertaken by Fenske (2012). The field monitoring included a climate station, soil profile monitoring as well as the construction of a collection lysimeter under each cover. Details of each of these systems are outlined in the following subsections.

A complete summary of all existing OKC installed instrumentation is presented in Table 3.1. The layout of the site is shown Figure 3.1 and Figure 3.2.

Table 3.1
Summary of existing instrumentation installed in each cover system and along adjacent berm

Location	Instrumentation by OKC (2004)
Deep Cover System	• Soil VWC sensors (8) • Soil matric suction and temperature sensors (8) • Data acquisition system
Shallow Cover System	• Soil VWC sensors (8) • Soil matric suction and temperature sensors (8) • Meteorological station • Data acquisition system

Figure 3.1 Aerial view of MLSB and specific location of project study area, including two cover systems configuration

Figure 3.2 Aerial view of project study area showing two cover systems configuration

3.2.1 Meteorological Station

The meteorological station was installed in 2004 by OKC (O'Kane Consultants Inc., 2004) near the centre of the shallow cover system. The monitoring consisted of a tipping bucket rain gauge (Model TE525) as well as the following instrumentation mounted on a single tripod (Figure 3.3):

- Temperature and RH monitoring performed using a Betatherm 0.3K1A1A thermistor and a Vaisala HUMICAP® 180 capacitive RH sensor, respectively; both of which are built into the single instrument that is the Campbell Scientific Model HMP45CF probe.
- Wind speed and 360^{o} direction measurement done using an R.M. Young Model 05103 anemometer.
- Net radiation measured using an NR-Lite Net Radiometer mounted 2.5 m above the surface of the cover system.

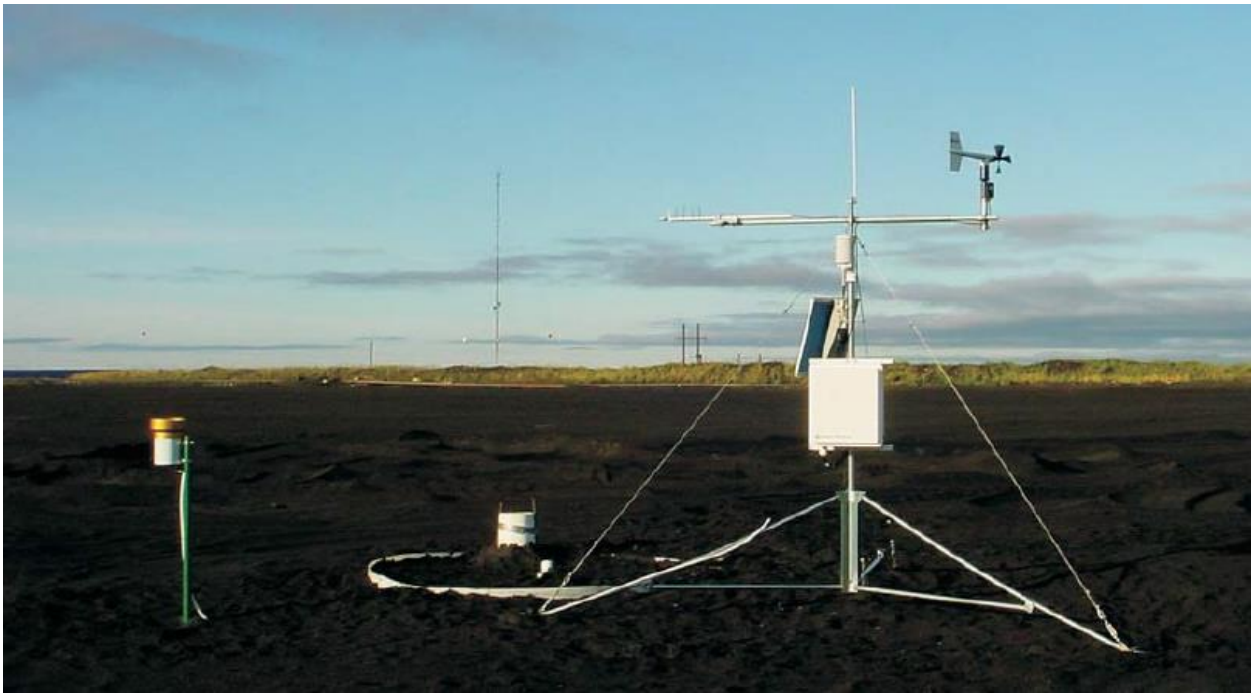

Figure 3.3 Meteorological station installed on shallow cover at MLSB CBIW (September 24, 2003)

3.2.2 Automated Soil Monitoring Stations

OKC installed automated soil monitoring stations and associated data acquisition systems on each cover system in 2004. The soil monitoring stations included sensors to monitor soil temperature and matric suction (Campbell Scientific 229 sensors), and volumetric water content (Campbell Scientific 616 TDR sensors). The installation depths and sensors installed at each depth on the deep cover system are outlined in Table 3.2, and for the shallow cover system in

Installation Depth (cm from surface)
5
10
20
25
30
40
90
180

Table 3.3. Each sensor type (CS229 and CS616) was installed alongside each other at equivalent depths.

Table 3.2
Soil monitoring instrumentation depths installed by OKC at Shallow Cover System in 2004

Installation Depth (cm from surface)
5
10
20
25
30
40
90
180

Table 3.3
Soil monitoring instrumentation depths installed by OKC at Deep Cover System in 2004

Installation Depth (cm from surface)
5
20
30
45
70
90
100
180

The soil monitoring sensors were wired into a CR1000 datalogger, manufactured by Campbell Scientific. Each cover system uses its own datalogger for data collection and storage purposes. The soil monitoring systems and datalogging equipment were located at S02 and D02 in Figure 3.4.

3.2.3 Infiltration, Net Percolation, and Runoff/Interflow

At the CBIW, the net percolation through the cover system was measured *in situ* using a lysimeter until the close of 2006. Following 2006, no net percolation measurements were recorded. The lysimeters were designed and installed by OKC in 2004, and have a diameter of 2.44 m and a height of 2.5 m (O'Kane Consultants Inc., 2004). The tanks were hollow, and as such, required that the inside be filled with native material to the same level of compaction of the material outside the tank to ensure a representative measurement of percolation. Each tank was installed to a depth of 2.5 m below the surface of the coke, measured from the bottom of the lysimeter tank, resulting in the top of the lysimeter resting at the base of each respective cover system. This allowed for direct measurement of total net percolation through the cover systems. Measurements of water

volume in the lysimeter were facilitated using a piezometer installed in the centre of each lysimeter, with regular measurements of water height recorded. The piezometer tube also allowed for the removal of water as required.

At the close of the 2006 monitoring year, no percolation was recorded through the shallow cover system during the 2 year monitoring period, while only 21.6 mm of percolation were recorded through the deep cover system for the same period (Fenske, 2012).

In the system being studied at the CBIW, changes in surface grade are negligible, and as such, no runoff or interflow has been measured or recorded since the commencement of the project. For the purposes of analysis, the runoff and interflow in the system is assumed to be negligible.

3.2.4 Soil Temperature and Matric Suction

The measurement of the soil temperature and the soil matric suction is carried out using a Campbell Scientific 229 (CS229) matric potential sensor. The CS229 sensor uses a heating element and a thermocouple which is encapsulated in epoxy within a hypodermic needle. This setup is then encased in a porous ceramic matrix which allows for equilibration with the surrounding soil moisture. The air entry value (*i.e.* minimum suction measurement threshold of the sensor) is 10 kPa, and the maximum measurement potential of the sensor is 2500 kPa of suction.

The soil suction in the soil surrounding the CS229 sensor is measured by using a current exciting module to induce an electrical current through the thermocouple. This electrical current causes an increase in the temperature of the thermocouple, and the magnitude of the temperature rise is dependent on the amount of water content of the ceramic matrix surrounding the thermocouple setup. The ceramic is assumed to be in equilibrium with the suction within the surrounding soil. The rate of temperature rise is then related to the matric suction of the soil using a second order polynomial derived from a laboratory calibration of each sensor. This calibration was carried out by OKC prior to installation. The temperature of the soil surrounding the CS229 sensor must be taken and recorded prior to each reading of the sensor using the built in thermocouple in order to provide a reference temperature for the total temperature rise. As a consequence, this sensor functions as both a matric suction sensor and a soil temperature sensor.

The volume of water in the air within unsaturated soils can be assumed to be saturated when above wilting point. The saturation vapour pressure of the air within soil voids can be calculated using Equation 3.1 (National Oceanic Atmospheric Institute, 2015).

$$P_{sat} = 6.11\ x\ 10^{\left(\frac{7.5\ x\ T}{237.3+T}\right)} \quad 3.1$$

The vapour pressure of the soil air can be determined using Equation 3.2 (National Oceanic Atmospheric Institute, 2015).

$$RH = \frac{P_{vap}}{P_{sat}} \quad 3.2$$

The calculated maximum potential moisture removal rates are based on the calculated airflow and the moisture removal potential (discussed in Sections 5.5.1 and 5.3.1, respectively). These values are calculated based on the measured temperature conditions within the cover system and the air. The estimated moisture removal rate is calculated as follows:

$$T_v = f_g * M_a \quad 3.3$$

where T_v is the total volume of moisture removed (grams), f_g is the total airflow rate per day (m^3/day), and M_a is the total moisture availability for removal from the soil profile (grams/m^3). The total moisture availability for removal is assumed to be the difference between the actual vapour pressure of the ambient air, and the saturated vapour pressure of the soil void air.

3.2.5 Volumetric Water Content

The soil volumetric water content (VWC) is measured using Campbell Scientific 616 (CS616) time-domain reflectometry (TDR) sensors. These sensors are based on water content reflectometry technology and are capable of measuring a wide range of water content in various soil materials.

The CS616 probe consists of two 300 mm long stainless steel probes connected to a circuit board for the measurement system. The circuit board is encapsulated in epoxy to protect the wiring from soil moisture. A measurement of dielectric permittivity is taken by allowing an electromagnetic pulse to propagate along a waveguide surrounded by soil, using the stainless-steel rods as a guideline for the wave (Hu et al., 2006). The travel time of the electromagnetic wave through the

soil, and the reflection of the pulse back to the sensor is measured, and is correlated back to the soil VWC using the Topp et al., (1980) equation. This equation (1980) is generally considered to be universal and can be applied directly to measured dielectric permittivity to determine soil VWC. There are exceptions to the "universal" nature of the Topp et al. (1980) equation, which includes unsaturated clay soils, however, these exceptions do not affect this study and as such the Topp et al. (1980) equation can be used directly.

3.3 Instrumentation Installed as a Component of this Thesis

In order to adapt the current monitoring system to be able to measure differential airflow, the author designed and installed a differential pressure monitoring system across the cover system. The installation locations are shown in Figure 3.4. The details of these systems are outlined in Table 3.4.

Figure 3.4 Detailed instrumentation installation locations at the coke beach instrumented watershed

Table 3.4
Differential Pressure Monitoring Systems installed by the Author in 2012

Location	Instrumentation as part of this study (Spring 2013)
Deep Cover System	• Differential gas pressure sensors, 3 locations (D01, D02, D03), 3 sensors each location • Data acquisition systems
Shallow Cover System	• Differential gas pressure sensors, 3 locations (S01, S02, S03), 3 sensors each location • Data acquisition systems

Figure 3.5 Installing gas probes at monitoring location using AMS International system.

Gas inlet ports were installed using the AMS International® gas sampler (Figure 3.5). The advantage of this system is that it uses dedicated vapour sampling tips which can be installed in the subsurface without pre-boring. This system utilizes steel gas vapour tips attached to fluoropolymer tubing which is then fed through a hollow steel pipe. Using a manual impact hammer, this steel pipe is gradually hammered into the ground to the desired depth. As the steel

pipe forces the gas vapour tip further into the ground, extensions to the steel pipe are added to accommodate the additional depth to which the gas vapour tip is being placed.

The differential pressure measurements were obtained using differential pressure monitoring sensors. Table 3.5 shows the installation depths and identifications assigned to each sensor installation on top of the CBIW, as well as the GPS coordinate of each instrumentation cluster.

Table 3.5
Installation depths and identification numbers for differential pressure sensors at each cover system

	Site ID	Full Installation ID	Depth Below Surface (m)	Easting	Northing
Deep Cover	D01	D01-30	0.33	459975.36	6323805.46
		D01-110	1.1		
		D01-200	2		
	D02	D02-30	0.5	460063.8	6323804.83
		D02-110	1.1		
		D02-200	2		
	D03	D03-30	0.5	460113.59	6323810.02
		D03-110	1.1		
		D03-200	2		
Shallow Cover	S01	S01-30	0.25	459985.51	6323706.39
		S01-70	1.1		
		S01-200	2		
	S02	S02-30	0.25	460047.83	6323702.23
		S02-80	1.1		
		S02-190	1.9		
	S03	S03-50	0.25	460099.64	6323709.41
		S03-110	1.1		
		S03-200	1.5		

The measurement of differential pressure was performed using PA-699 differential air pressure sensor and is manufactured by Sontay Instruments and distributed by Omni Instruments. The PA-699 differential pressure sensor can measure low-range differential gas pressure (0-100 Pa). The sensors are powered by an external 1.2 Ah sealed lead-acid (SLA) battery. The differential pressure sensors were connected to Logbox-AA datalogging systems, manufactured by Novus®. These

systems are capable of recording data from two analog sensors per unit. As such, for locations with more than two differential pressure sensors, two datalogging units were required. The completed monitoring system can be seen in Figure 3.6.

Figure 3.6 Completed differential pressure monitoring system and data acquisition system

Each differential pressure sensor utilizes a low pressure and a high-pressure port, with the difference in pressure across the two ports resulting in a voltage drop which can be converted to a relative differential pressure. The differential pressure measurements are made at the same elevation and consequently no pressure corrections for hydrostatic air pressures or density were applied to the measurements.

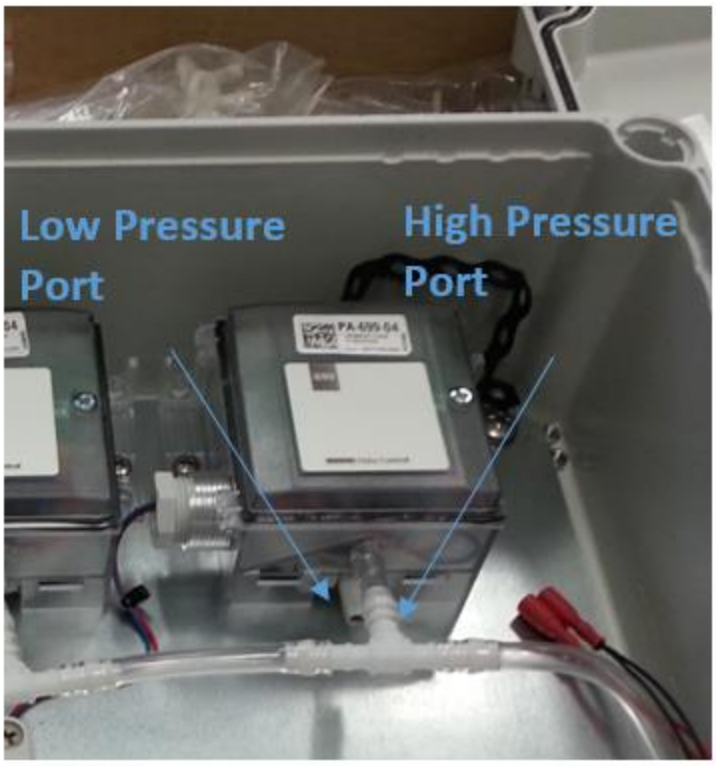

Figure 3.7 Differential pressure sensor configuration.

Early iterations of the project design included the measurement of differential pressures along the western berm of MLSB, adjacent to the CBIW. Differential pressure monitoring systems were installed as indicated in Table 3.6.

Table 3.6
Installation depths and identification numbers for differential pressure sensors on side berm of MLSB

	Site ID	Full Installation ID	Depth Below Surface (m)	Easting	Northing
MLSB Berm	B01	B01-40	0.4	459715.15	6323764.01
		B01-100	1		
		B01-200	2		
	B02	B02-40	0.4	459661.8	6323766.98
		B02-100	1		
		B02-200	2		
	B03	B03-40	0.4	459767.13	6323763.06
		B03-100	1		
		B03-200	2		
	B04	B04-40	0.4	459822.87	6323756.06
		B04-100	1		
		B04-200	2		
	B05	B05-40	0.4	459874.2	6323751.55
		B04-100	1		
		B04-200	2		

The sensors listen in Table 3.6 were monitored early in the investigative process, however, monitoring was eventually ceased due to lack of results/correlation and were omitted from this thesis.

3.3.1 Barometric Pressure

The measurement of the ambient barometric pressure was done using a Vaisala BAROCAP® Digital Barometer PTB210. This sensor was selected due to its high accuracy (+/- 15 Pa using a digital output), and its suitability for harsh environments, such as the exposed condition on top of MLSB. Due to the lack of appropriate dataloggers at the actual site of the study (MLSB CBIW), the PTB210 barometer was installed approximately 300 m away at the same elevation at an alternate OKC datalogging system. The sensor was shielded using a shield designed and distributed by the manufacturer of the sensor. The purpose of the shielding was to prevent influences from solar radiation and wind effects. This datalogger was a CR1000 manufactured by

Campbell Scientific. This data was downloaded by OKC on quarterly basis and forwarded to the author.

3.4 Field Testing Program

The field testing program consisted of air permeability testing carried out by the author, assisted by University of Saskatchewan Research Engineer, Dyan Pratt.

3.4.1 Air Permeability Testing

Air permeability testing was carried out using a method developed by Rodgers (2008), and further utilized in Huang et al. (2014) and Huang et al. (2016) at the University of Saskatchewan. This air permeameter, shown in Figure 3.8, was tested at the CBIW by Rodgers (2008) as a component of her master's research. These measurements were used to supplement the results obtained in this study.

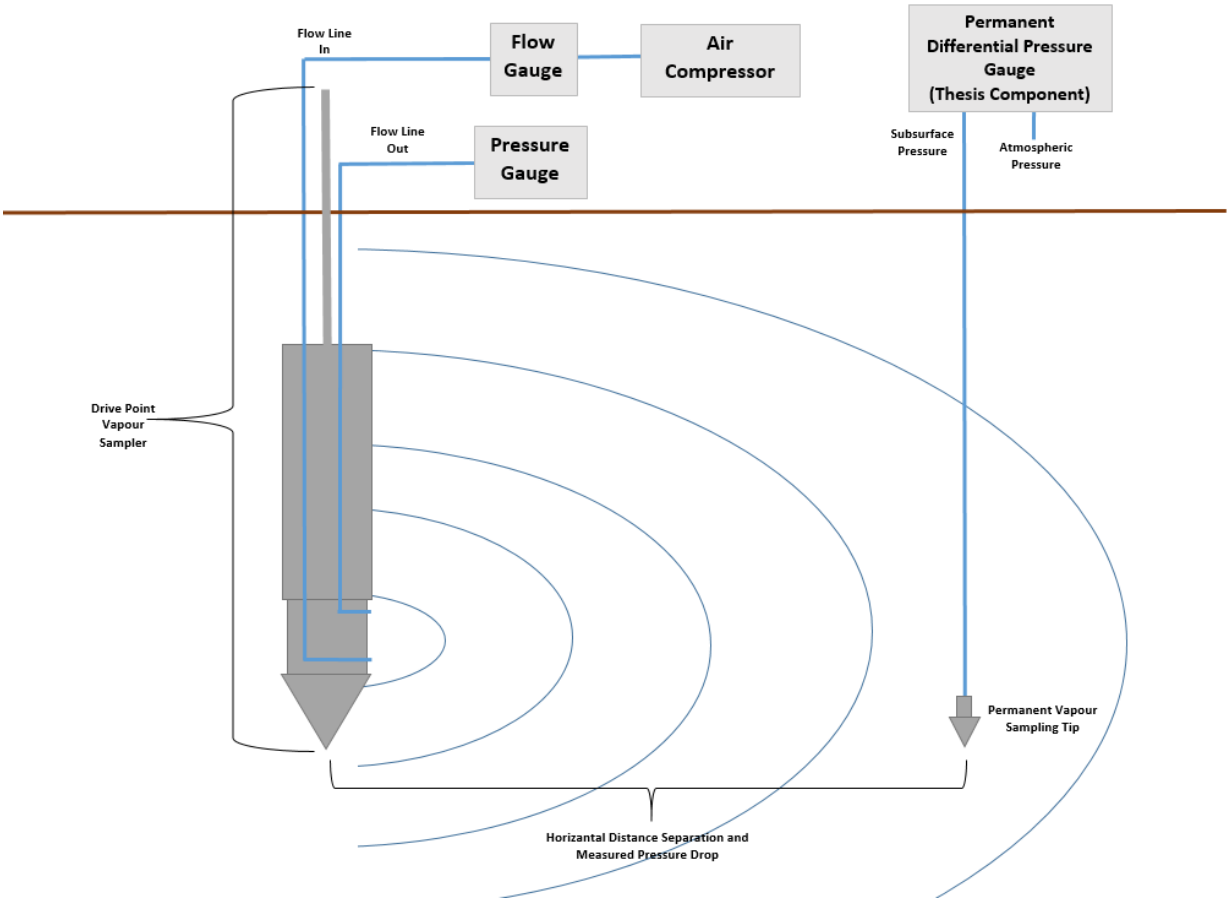

Figure 3.8 Conceptual design or air permeameter used in determination of air permeability (not to scale).

The system outlined in Figure 3.8 was adapted such that it could be driven to a specified depth into the soil cover profile using the AMS International soil gas probe kit used to install the DP sensors. The soil vapour probe is approximately 3 cm in diameter, and approximately 15 cm long. Two hoses were connected to the retractable gas vapour sampler. The airflow entered the vapour sampler through one hose, where it was allowed to diffuse into the surrounding soil until a constant pressure condition was achieved, as measured from the second hose attached to a pressure sensor at the surface. The functionality of the system was determined using the permanent vapour sampling tips installed to measure differential pressures; these were located between 2-3 m from the permeameter location. The airflow rate and air pressures through the system were recorded using an automated flow meter. The airflow rates and pressures measured across the screened length were interpreted using a numerical flow model (SEEP/W, Geo-Slope International 2012) to estimate permeability (K). The flow rates (Q) and pressure responses (dH) were used to set up a

2-D numerical model using axisymmetric coordinate system to simulate a pumping well using Geostudio SEEP/W software. The numerical model utilized a unit geometry (1 m^2 cross sectional area); the boundary conditions of the unit geometry were assumed to be a no-flow boundary, while the surface of the soil geometry was assumed to have a pressure of 0 kPa (no differential pressure gradient between subsurface air and ambient). The point of the drive-point permeameter was assumed to be a constant head as the test was run until a constant pressure head was measured by the permeater test gauges. The numerical model was run in steady state using an arbitrary geometry but with a nominal differential head and conductivity of unity to define a shape factor (F) for the test (*i.e.* F = Q/(Kdh). This shape factor was then used to obtain a value of K from the field tests for the test specific flowrates and measured pressure responses.

Air permeability was measured for the till cover layer and the underlying coke in September, 2013. The testing locations were isolated to S01 and D01 due to limitations associated with moving equipment across the rugged terrain of the cover system. Each cover system and underlying coke were tested at each trial cover system location, as per Table 3.7

Table 3.7
Air Permeability Test Depths and Flow Rates

	Shallow Cover System		Deep Cover System		
	80 cm	20 cm	110 cm	80 cm	20 cm
Air Permeameter Flow Rate	5	5	5	5	5
	10	10	10	10	10
	15	15	15	15	15
	20	20	20	20	20

It should be noted that these air permeability testing represent conditions at a single point in time, and as such, for a single soil VWC. The procedure to simulate air permeability (K-air) was to simply simulate the test geometry (*e.g.* screen depth and length) using differential air heads (dh) of unity and a unit media fluid conductivity (*i.e.* K-air = 1). The simulation then defines the relationship between differential head between the screen and the atmosphere and flow rate (Q). This defines the shape factor (F) which is set equal to Q/(Kdh). The value of K can then be calculated from the actual measured values of Q and dh from the field test.

Chapter 4
Presentation of Data

This chapter presents and discusses particular observations pertinent to the hypothesis of enhanced drying of the covers due to convective airflow. Soil volumetric water content (VWC) and suction data collected from CS616 and CS29 sensors, respectively, are presented in Appendix A. The full set of data from all sensors used while investigating this thesis is included as an electronic supplement (Appendix B); this data is used in Chapter 5 (Analyses) to evaluate the water balance for the covers. The specific elements of this data set that are important to the potential for convective airflow include the following:

- The magnitude, direction, and timing of differential pressures between the atmosphere and underlying coke which may be creating conditions for airflow.
- Soil cover, coke, and air temperatures to identify the timing and magnitude of the temperature contrasts which may create differences in air density which may in turn lead airflow and subsequent differential pressures.

Taken together, these observations provide evidence as to the timing and extent of potential mechanisms for convective airflow or evidence of enhanced drying. The extent of this drying will be further quantified in Section 5 (Analyses) by estimating the contribution of the enhanced drying in the cover water balance.

This section of the thesis will also present the data obtained from the monitoring of pressure differentials and the measurement of *in situ* air permeability.

4.1 Temperature Gradient across Cover Systems

The potential for free convection to develop across the cover can also be illustrated by looking at the temperature gradient between the atmosphere and the underlying unsaturated coke. The detailed temperature data presented in Appendix A show the deep soil temperatures to fluctuate seasonally between 5^{o}C and 15^{o}C. The deep soil air temperature can be used to represent the temperature of the bulk air mass in the subsurface and is subsequently used to assess temperature gradients relative to the ambient atmosphere.

The temperature difference between the ambient and the deep soil air temperatures at the shallow cover system is shown in Figure 4.1 for the 2013 monitoring year, while Figure 4.2 shows the same for the deep cover system; these figures were isolated to months in which the soil was unfrozen in order to highlight temperature gradients which would allow for unimpeded airflow through unfrozen soil. Months not shown were during periods in which the cover system was frozen, preventing effective airflow. It can be seen that starting in early May and continuing throughout the duration of the summer the temperature in the subsurface is much lower than the ambient atmospheric temperature. As a consequence, the subsurface air is more dense than ambient air and consequently in the presence of a sloping geometry could result in downward airflow through the cover and underlying coke out towards the dyke slope and the outlet drains installed within the sand dyke.

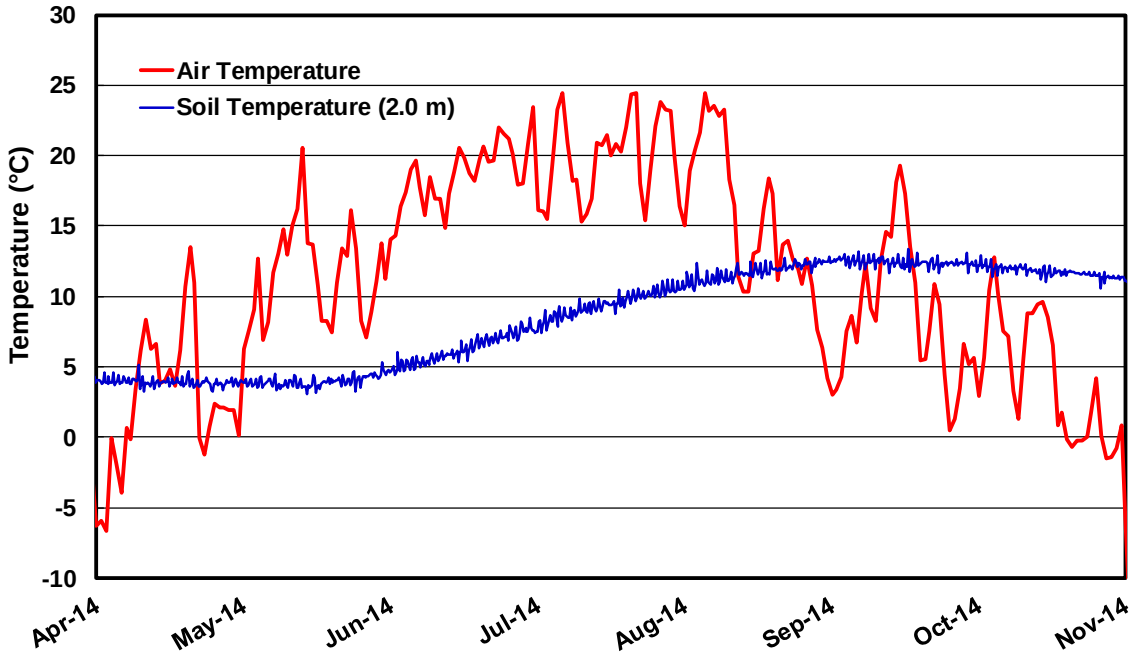

Figure 4.1 2013 differential air temperature, shallow cover system

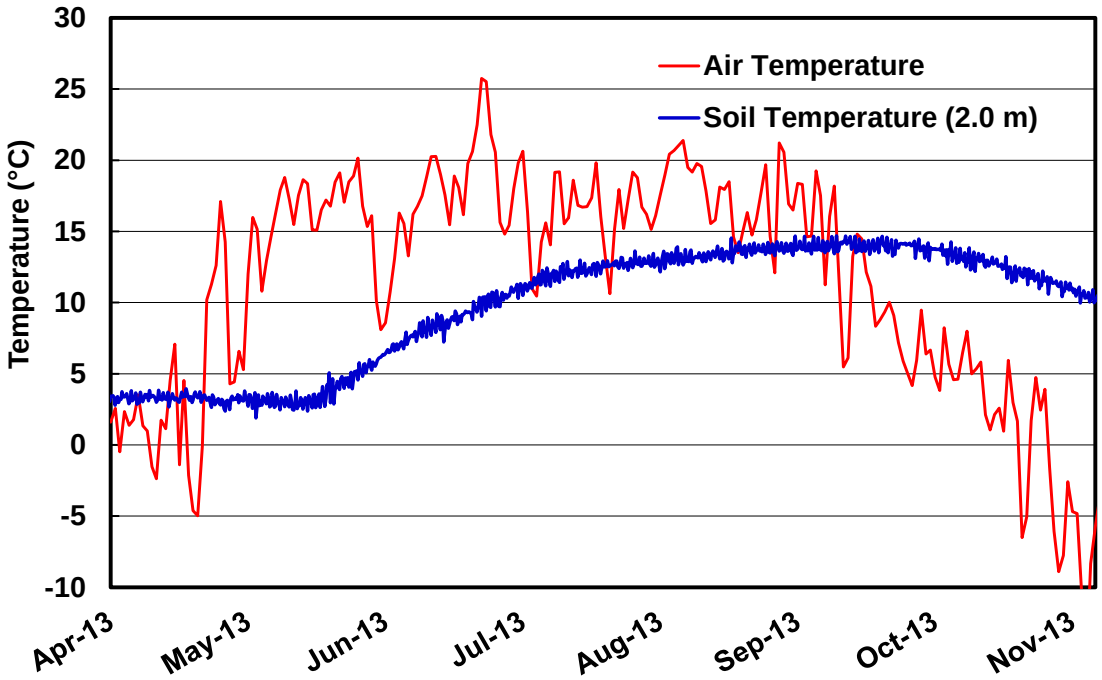

Figure 4.2 2013 differential air temperature, deep cover system

Temperature trends in 2014 showed similar results, indicating more dense air in the subsurface, which could result in downward flow for the duration of the summer months (Figure 4.3, Figure 4.4); again, these figures were isolated to months in which the soil was unfrozen in order to highlight temperature gradients which would allow for unimpeded airflow through unfrozen soil. Months not shown were during periods in which the cover system was frozen, preventing effective airflow.

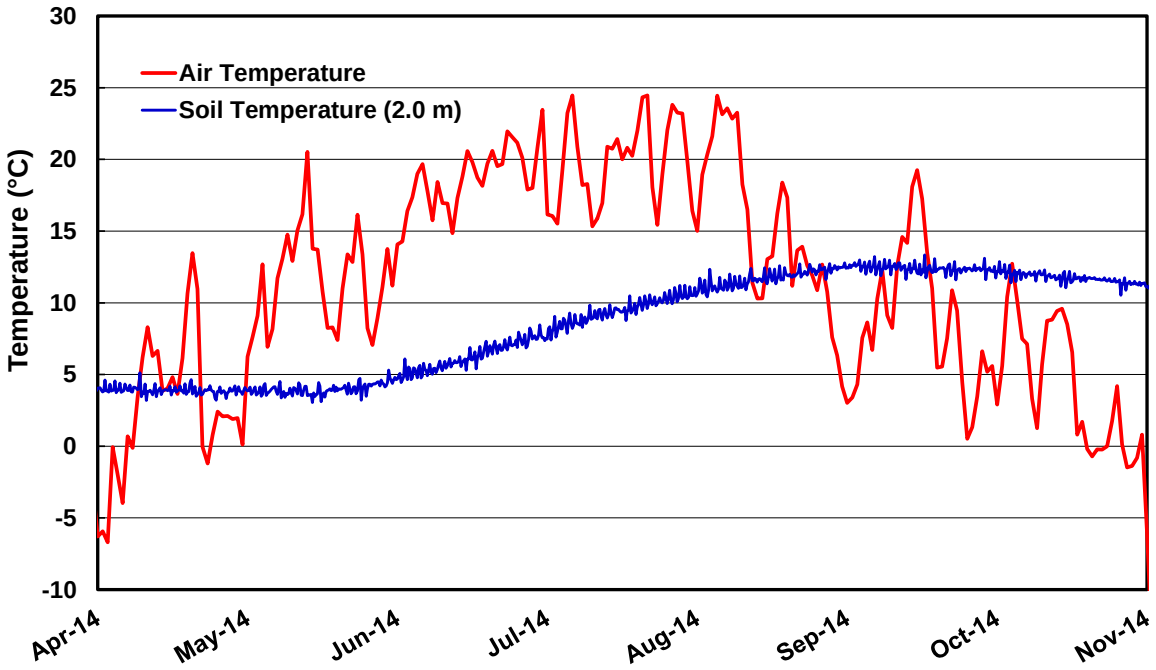

Figure 4.3 2014 differential air temperature, shallow cover system

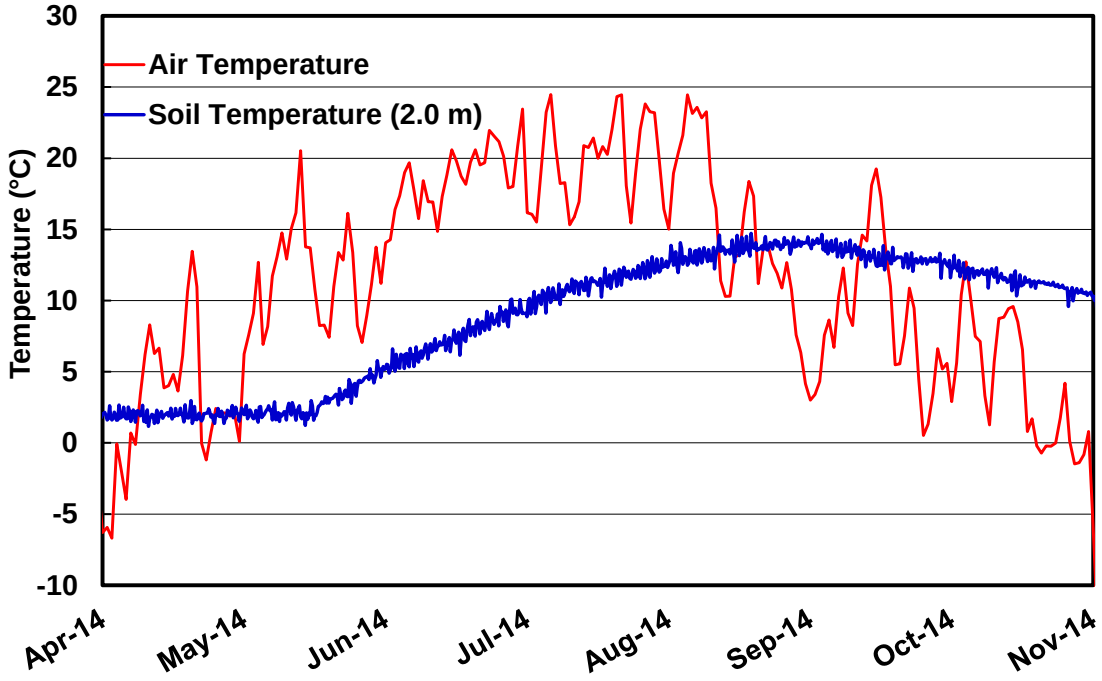

Figure 4.4 2014 differential air temperature, deep cover system

The large temperature gradient present predominantly during spring/summer at both locations proves conceptually that the necessary conditions for convective airflow exist. The determination of true convective airflow requires further analysis and will be presented later in the thesis.

4.2 *In situ* Differential Pressure Monitoring

The sensors available for monitoring the differential pressure in the cover system were only capable of monitoring differential pressure between an inlet (low pressure) and outlet (high pressure) port. The effect of an elevation gradient (*i.e.* gravity gradient) on flow is also essentially taken into account by the fact that the difference in the two pressures (soil and atmosphere) are measured at a common elevation. As a result, the focus of this discussion will be on the measured difference between the high pressure outlet and the low pressure outlet and is referred to as the measured differential pressure (dP). The dP sensor is only capable of measuring a positive value for dP. A negative dP (*i.e.* the inlet pressure becomes higher than the outlet pressure) cannot be measured.

In 2013 the sensor configuration was connected such that the inlet port was connected to the subsurface measurement points and the outlet port was vented to the atmosphere. Detection of a differential pressure was then associated with lower pressures within the soil profile than in the air. This configuration was reversed in 2014 to evaluate if dP creating upward airflow in the system. As such, the sensor configuration was set up differently for each monitoring year. In 2013, the only measurable differential air pressure measurements occurred when atmospheric pressure was greater than soil air pressure, while in 2014 the only measurable differential pressures where for the period when soil air pressures were greater than atmospheric pressures. The subsequent sections detail the differential pressure data measured at each location during each monitoring setup.

The fluctuations in dP over the course of 2013 at all 3 shallow cover system monitoring locations (S01, S02, S03) are presented in the following 3 figures (Figure 4.5, Figure 4.6, Figure 4.7). The fluctuations in dP over the course of 2013 at all 3 deep cover system monitoring locations (D01, D02, D03) are presented in the following 3 figures (Figure 4.8, Figure 4.9, Figure 4.10).

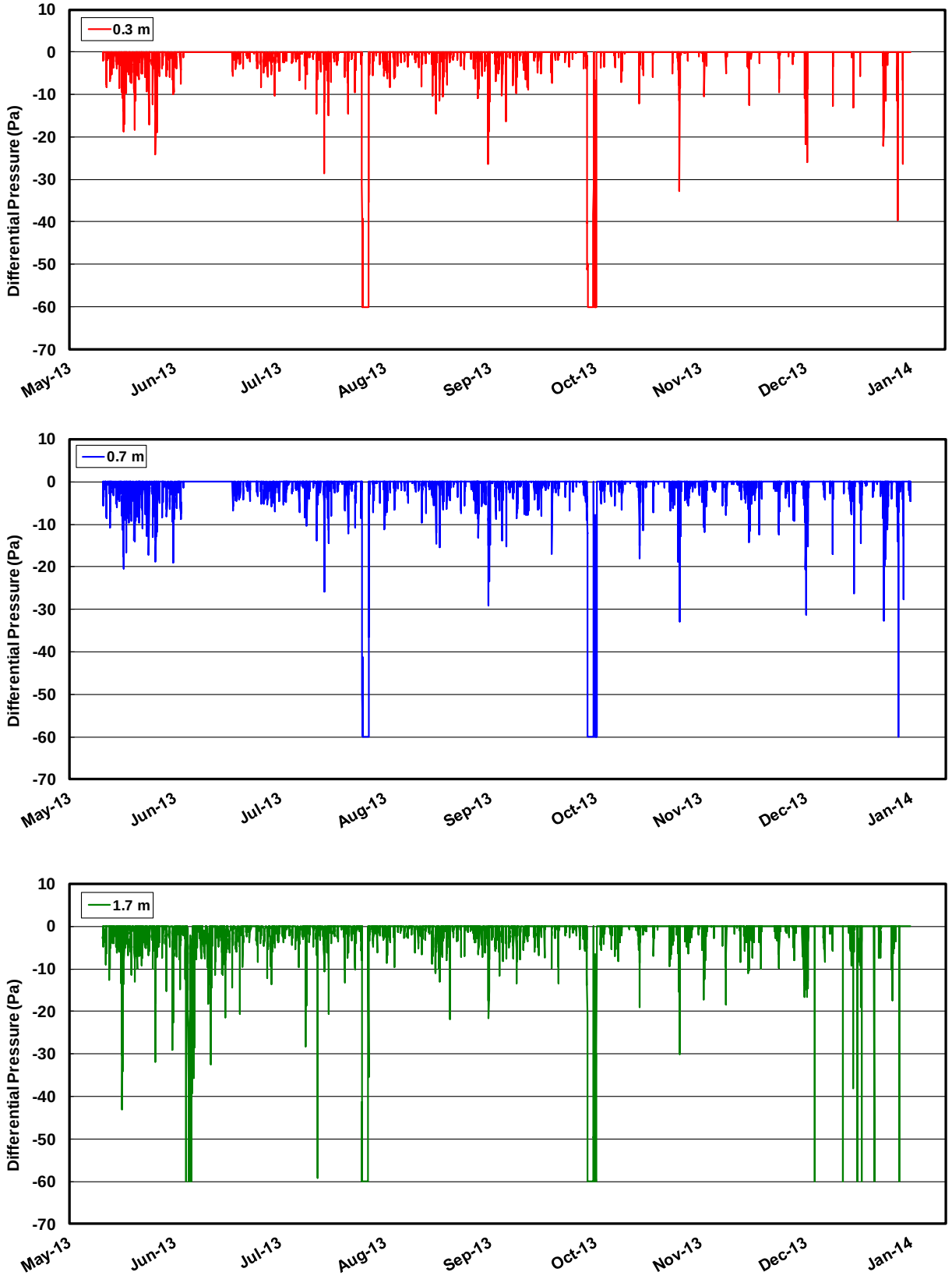

Figure 4.5 Differential pressure measured at S01 (2013).

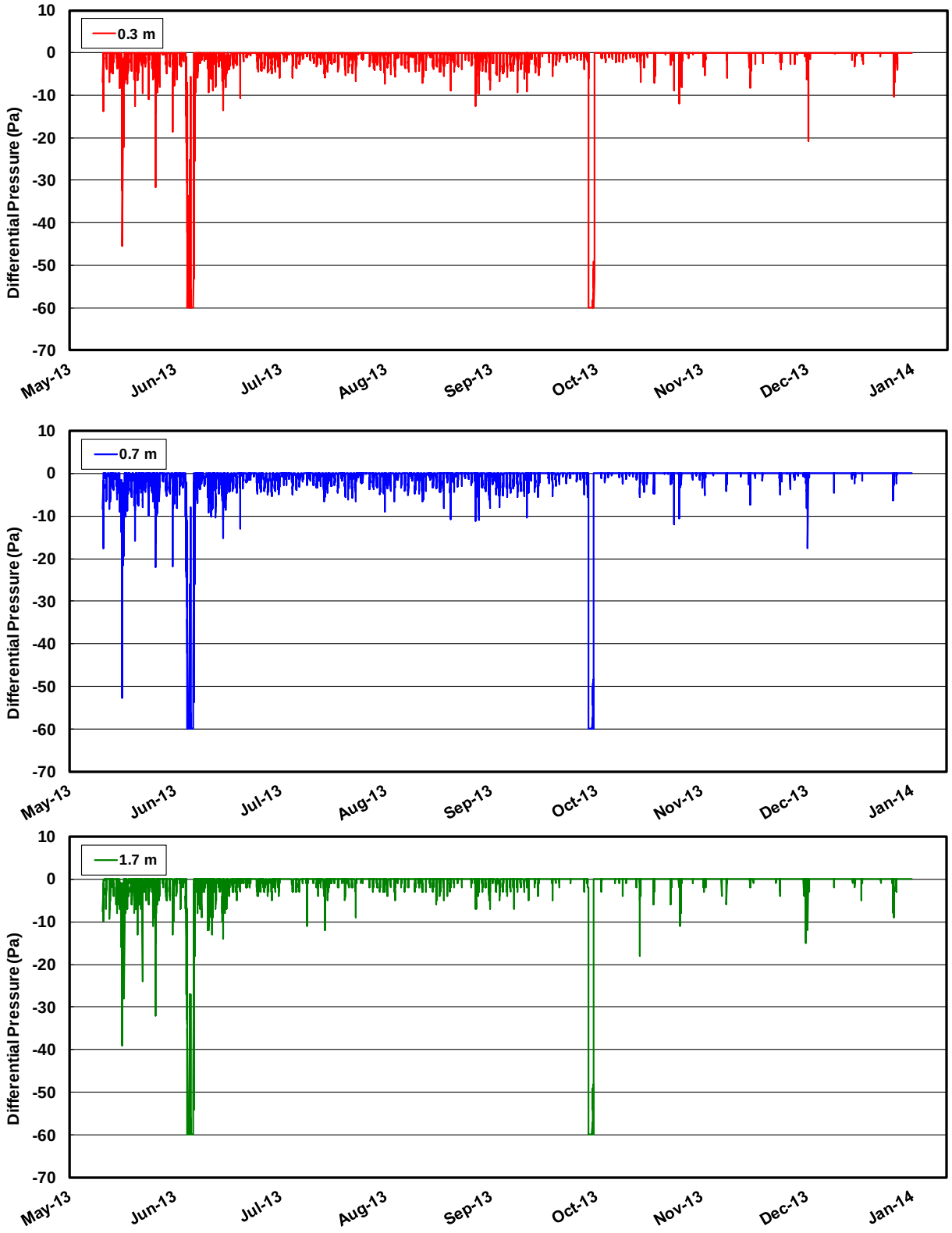

Figure 4.6 Differential pressure measured at S02 (2013).

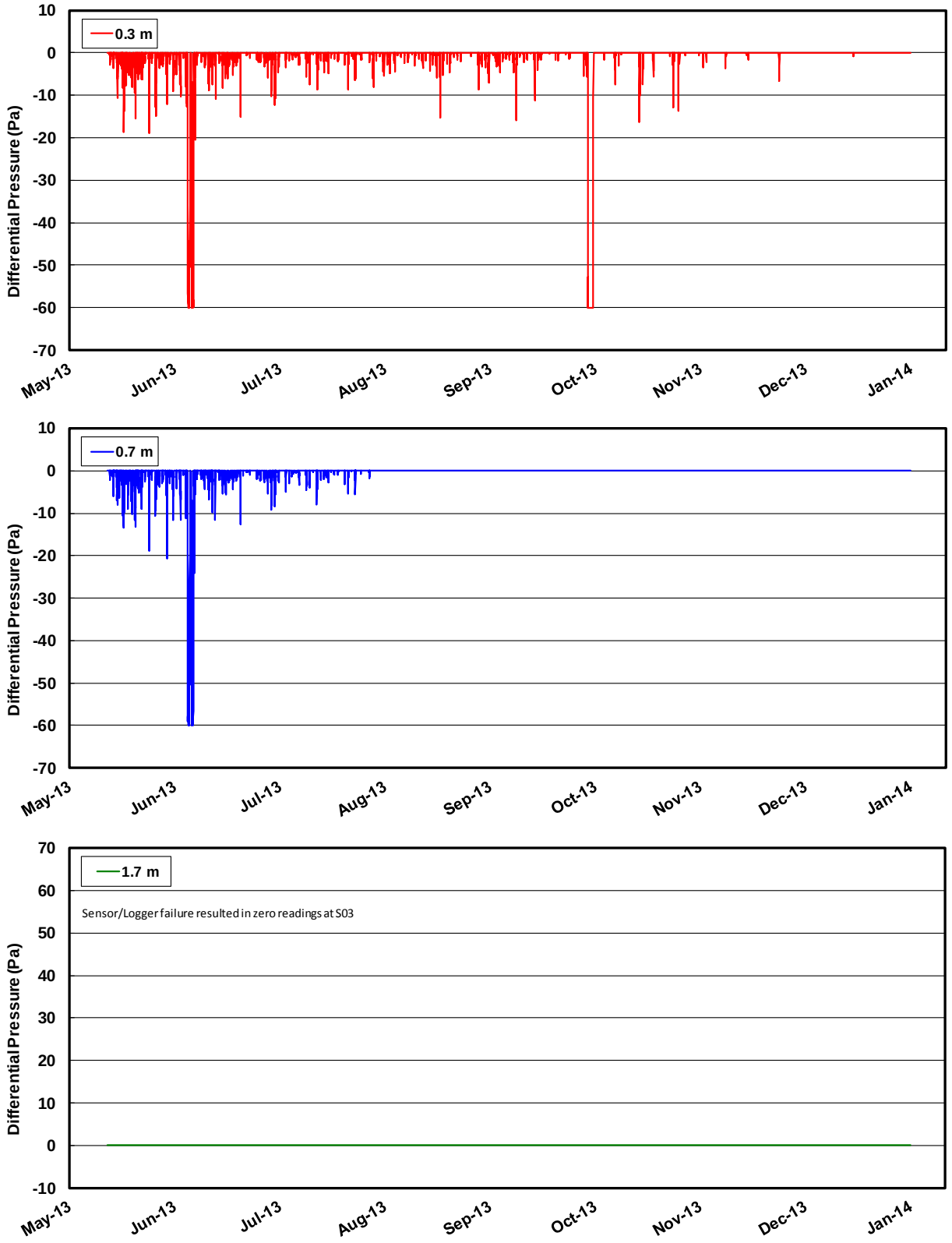

Figure 4.7 Differential pressure measured at S03 (2013).

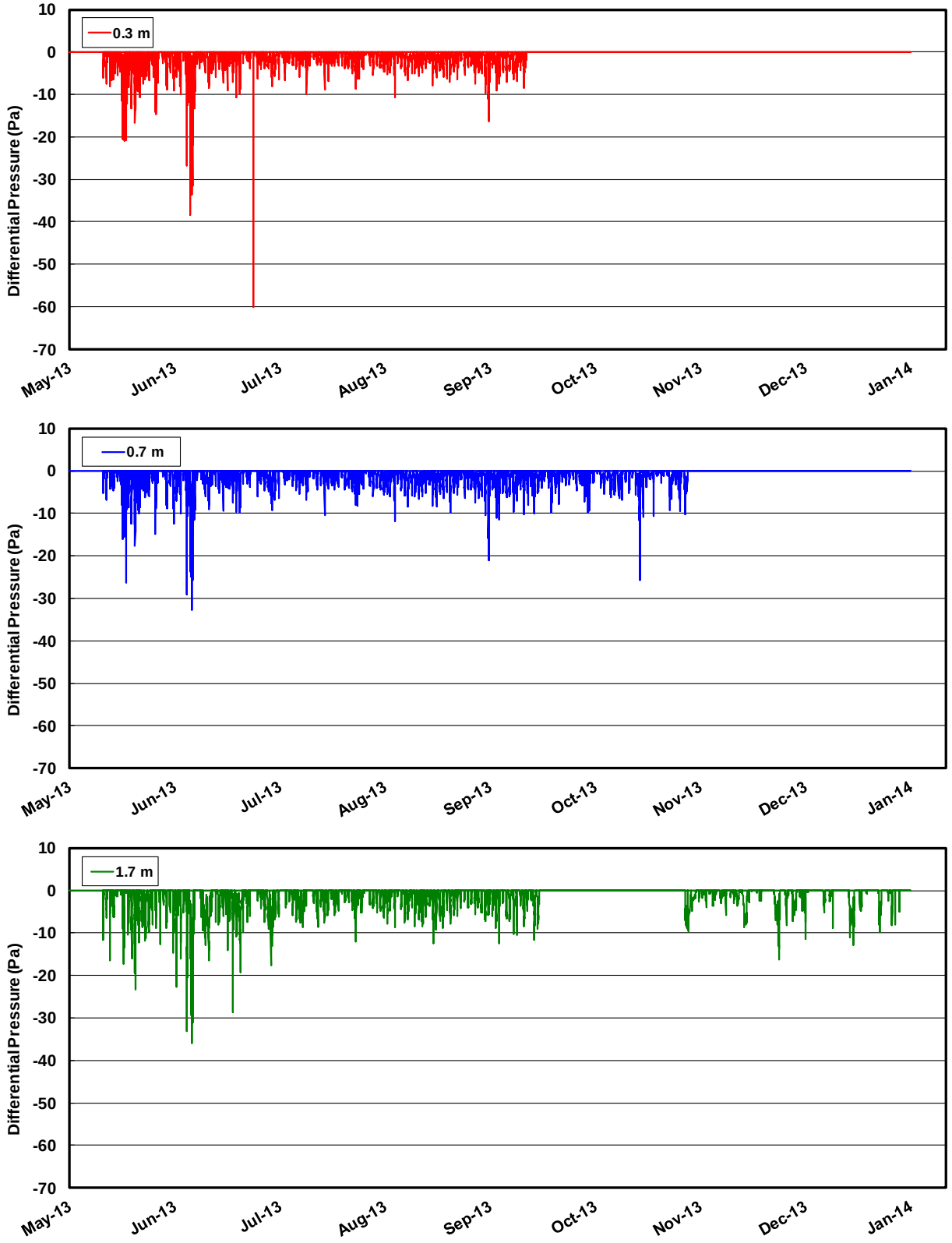

Figure 4.8 Differential pressure measured at D01 (2013).

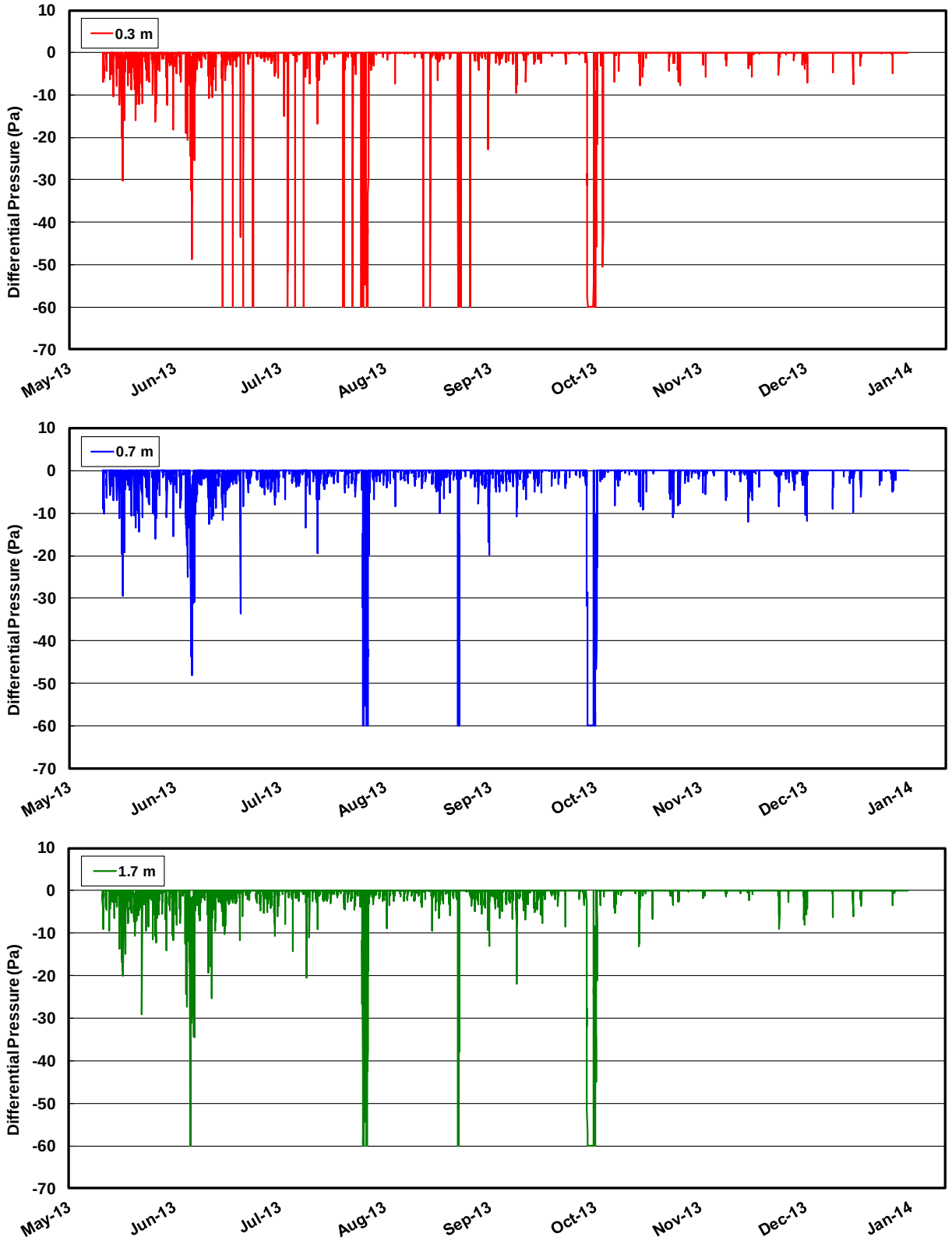

Figure 4.9 Differential pressure measured at D02 (2013).

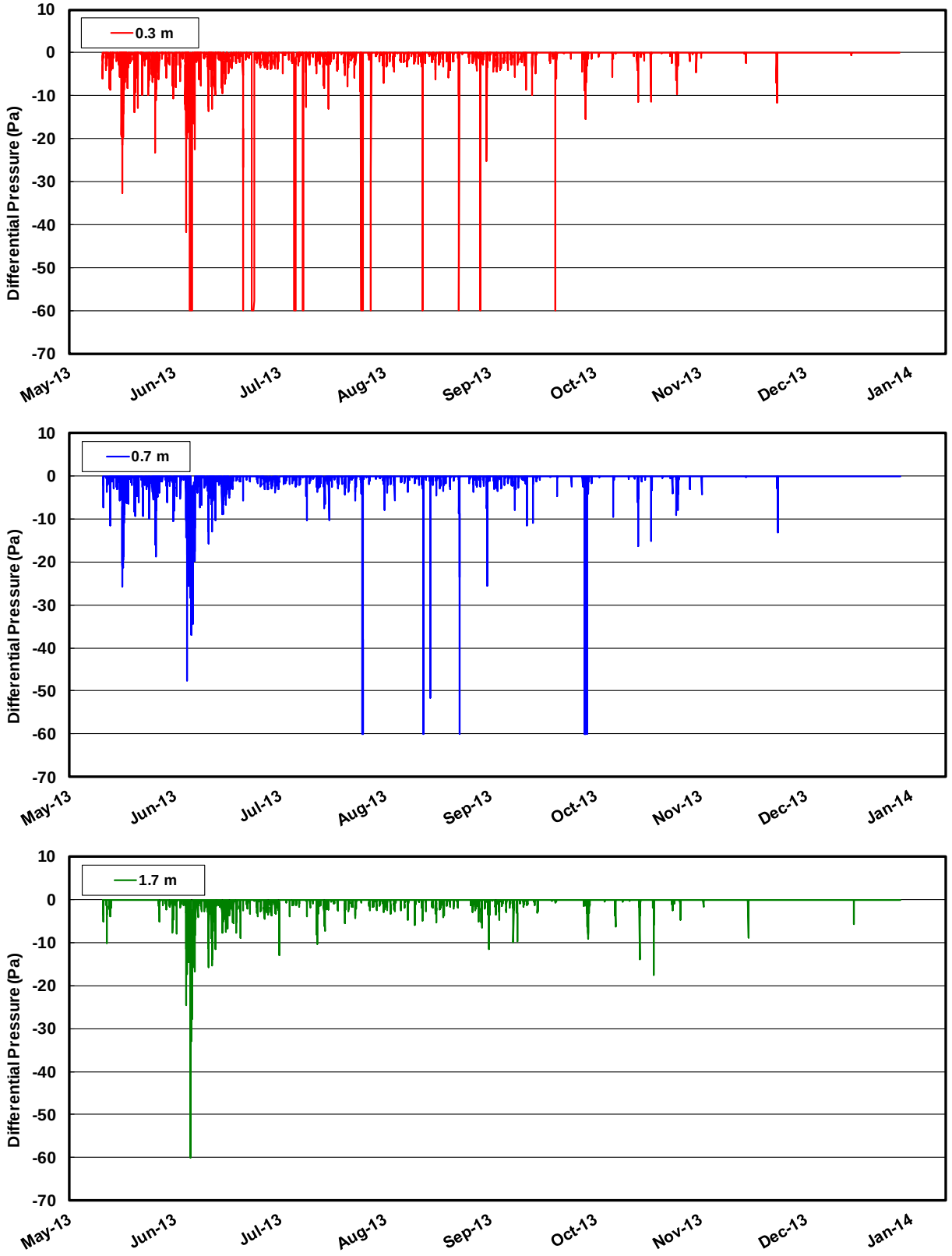

Figure 4.10 Differential pressure measured at D03 (2013).

From the presented results it can be seen that measured differential pressures at both cover systems vary throughout the season in 2013; however, the highest values generally occur in early spring and then gradually decrease over the summer. Generally speaking, the highest differential pressures occurred on days when the ambient temperature was substantially higher than the subsurface temperature, and highest differential pressures were noted in late morning and early afternoon. Most nighttime differential pressures were low or zero due to a thermal, or near thermal equilibrium condition between the ambient temperature and subsurface temperature. The higher differential pressures measured in spring do not necessarily mean that airflow was highest during that time since consideration also needs to be given to the air permeability at any given point in time. It should be noted that the deep sensors at S03 failed due to an unknown issue with the datalogger, resulting in no results shown in Figure 4.7.

The daily variations in differential pressure are difficult to extrapolate from Figures Figure 4.5 through Figure 4.10 due to the large volume of data. In order to illustrate the daily cycle in differential pressure, three dates were selected to represent spring to late summer conditions in 2013. The daily changes at both the shallow and the deep cover system are presented for May 16 to 18 (Figure 4.11 and Figure 4.12, respectively), June 16 to June 18 (Figure 4.13 and Figure 4.14, respectively), and August 16 to 18 (Figure 4.15 and Figure 4.16, respectively). These days show how the daily differential pressure gradients fluctuated throughout the monitoring season with respect to temperature gradients across the cover systems.

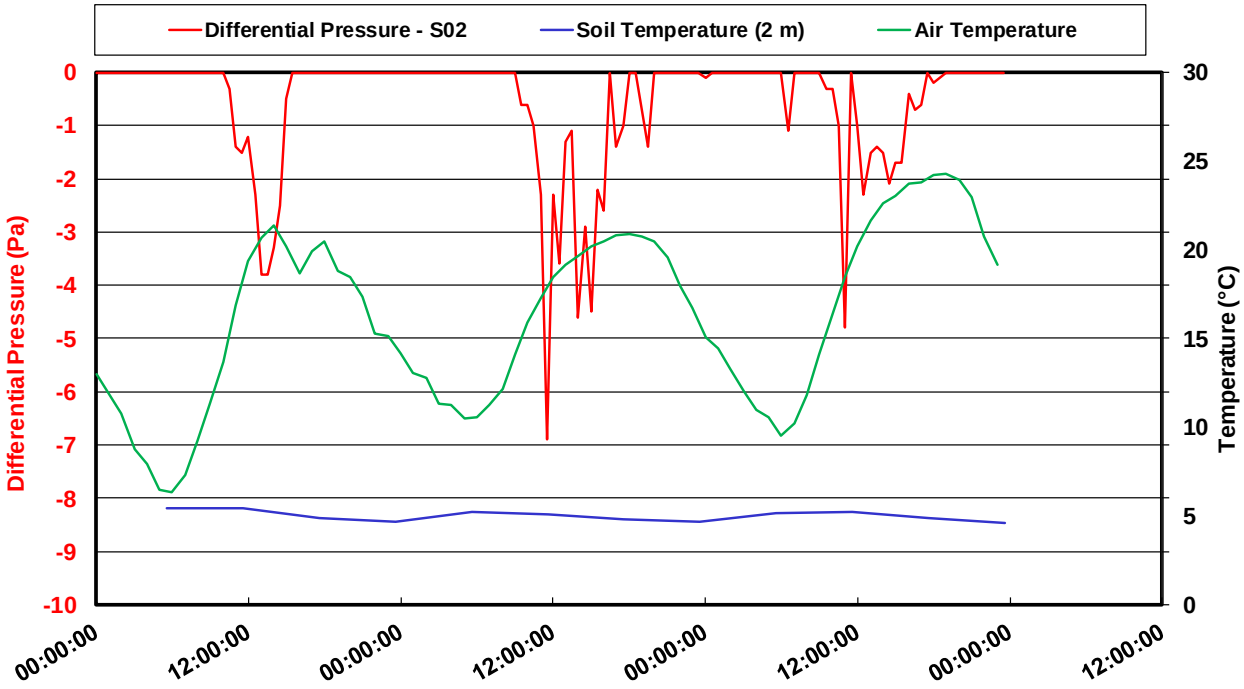

Figure 4.11 Daily variations in measured differential pressure at S02, May 16 to 18, 2013

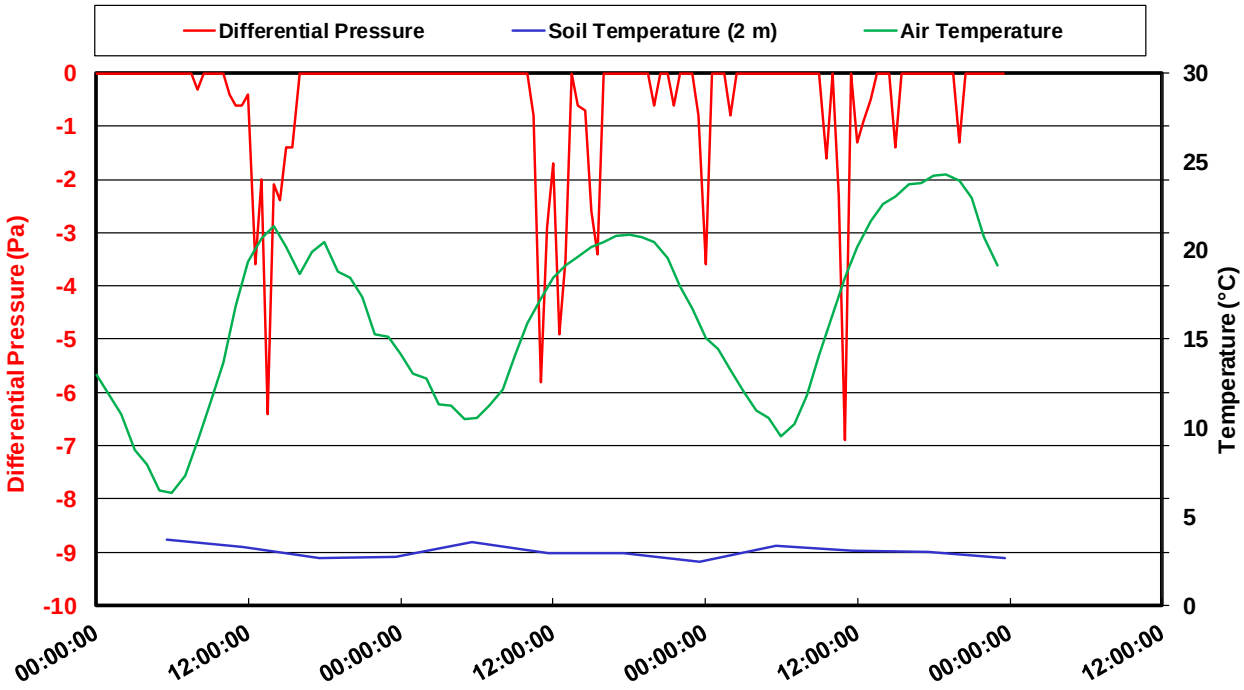

Figure 4.12 Daily variations in measured differential pressure at D02, May 16 to 18, 2013

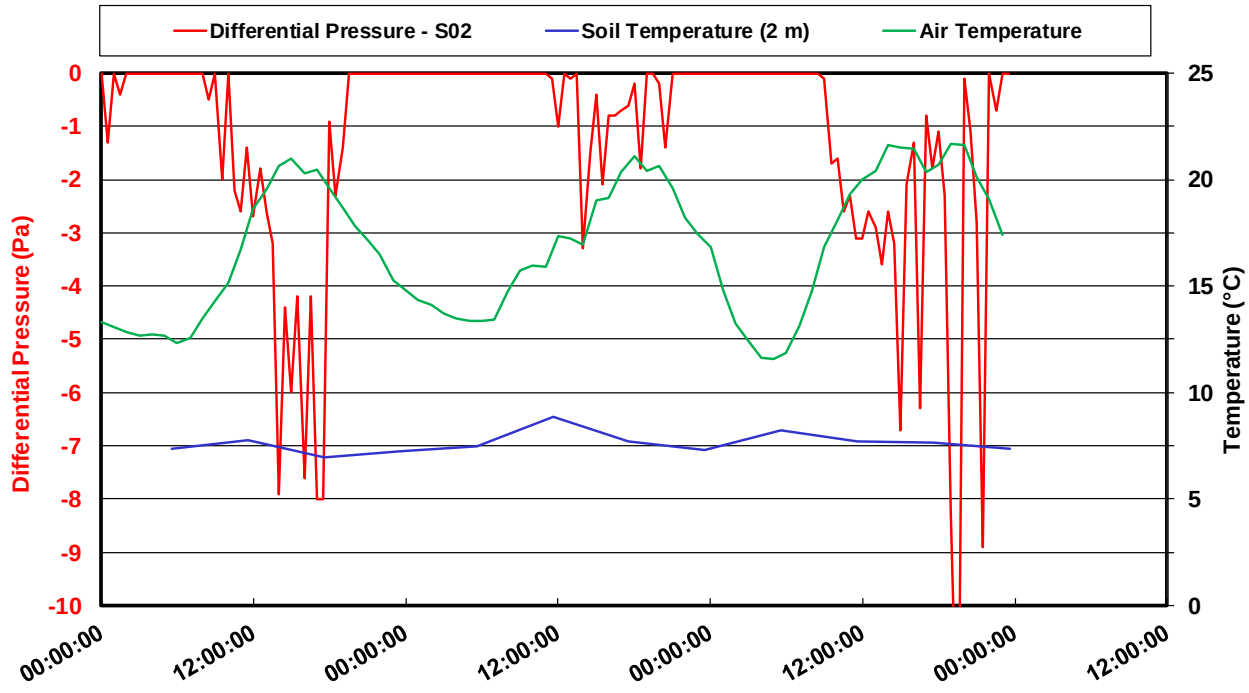

Figure 4.13 Daily variations in measured differential pressure at S02, June 16 to 18, 2013

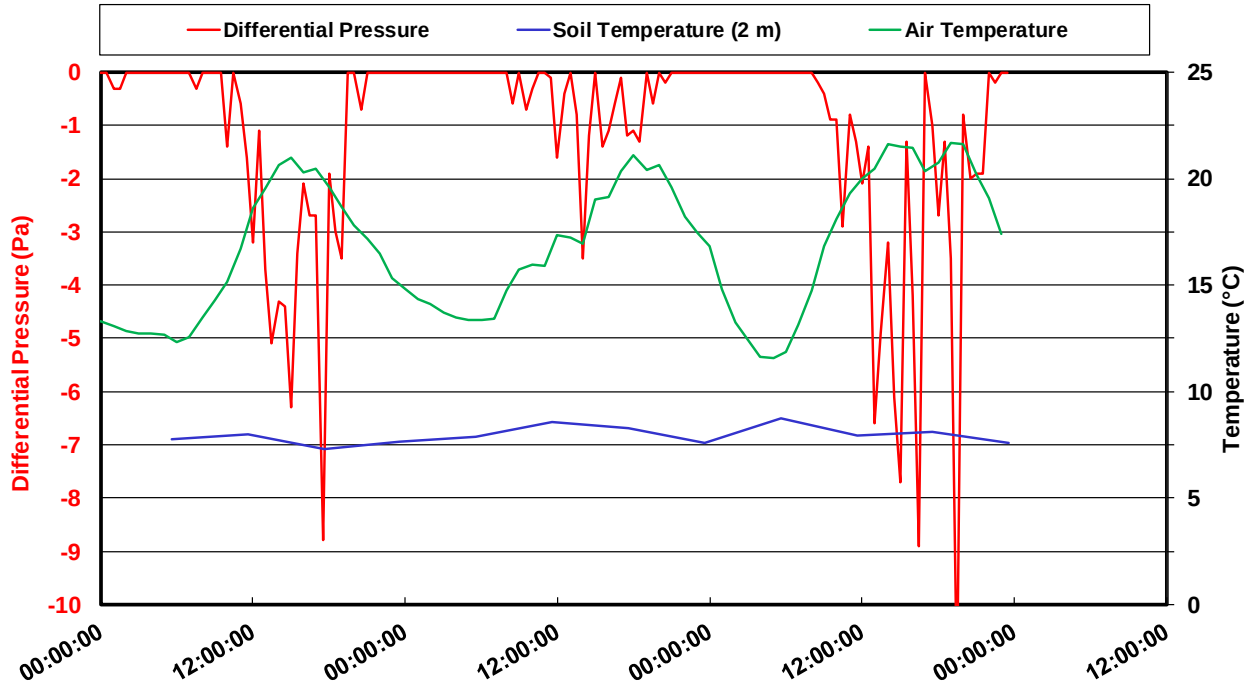

Figure 4.14 Daily variations in measured differential pressure at D02, June 16 to 18, 2013

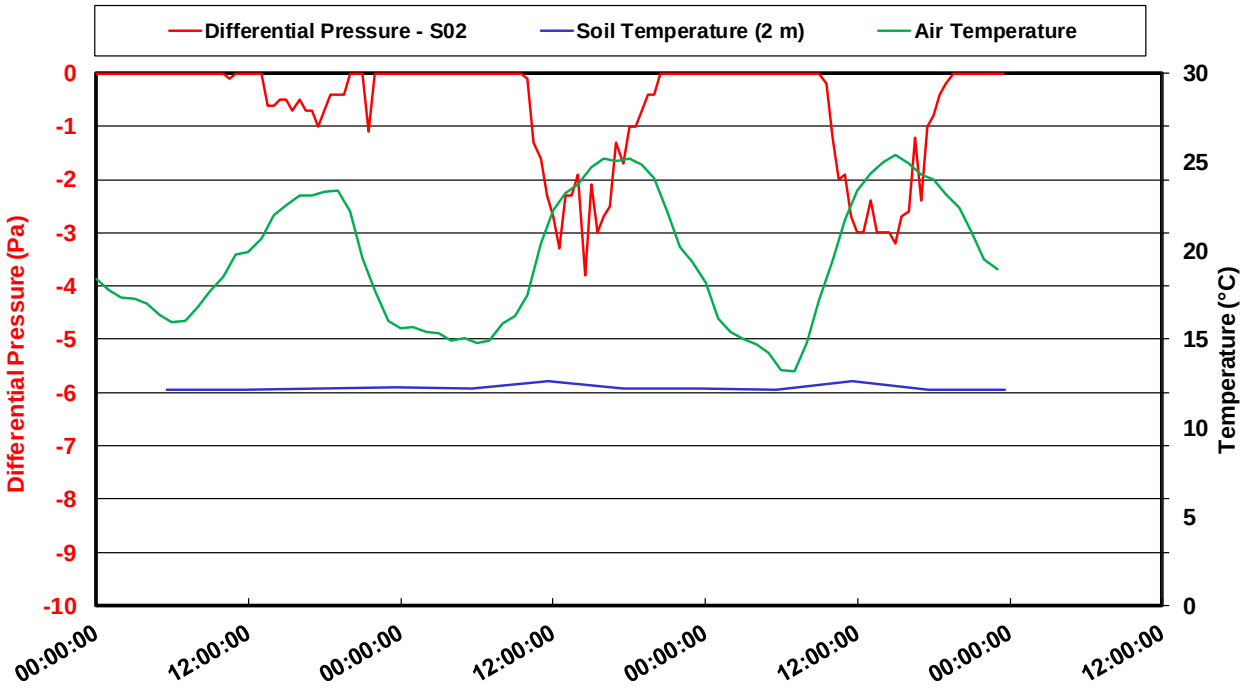

Figure 4.15 Daily variations in measured differential pressure at S02, August 16 to 18, 2013

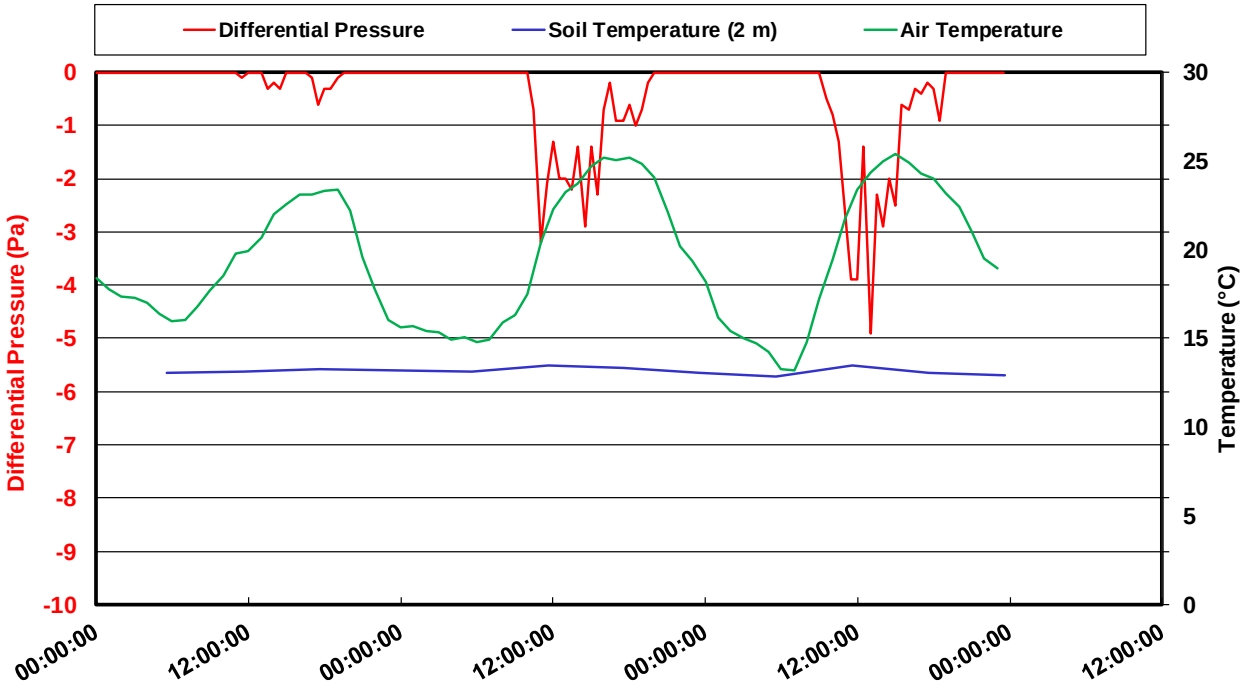

Figure 4.16 Daily variations in measured differential pressure at D02, August 16 to 18, 2013

It can be seen by Figure 4.12 through Figure 4.16 that the differential pressure consistently showed a downward pressure gradient consistently through the monitoring season in 2013. This gradient saw its highest value in June, 2013, and lowest at the end of the summer (August). Also shown in Figure 4.12 through Figure 4.16 is the difference in temperatures between the soil and the ambient atmosphere; these temperature gradients show a peak value in June alongside the same times that peak differential pressures are measured, while in August, the temperature gradient declines due to an increase in soil temperature, which is reflected in the lower values of differential pressure occurring during the day.

The predominant differential pressure measured at each cover system was between 0 and -10 Pa relative to atmospheric. Each monitoring location showed a different average differential pressure, when considering only non-zero measured differential pressures. The occurrence frequency, average, and standard deviation of non-zero differential pressures is presented in Figure 4.17 for the shallow cover system, and Figure 4.18 at the deep cover system.

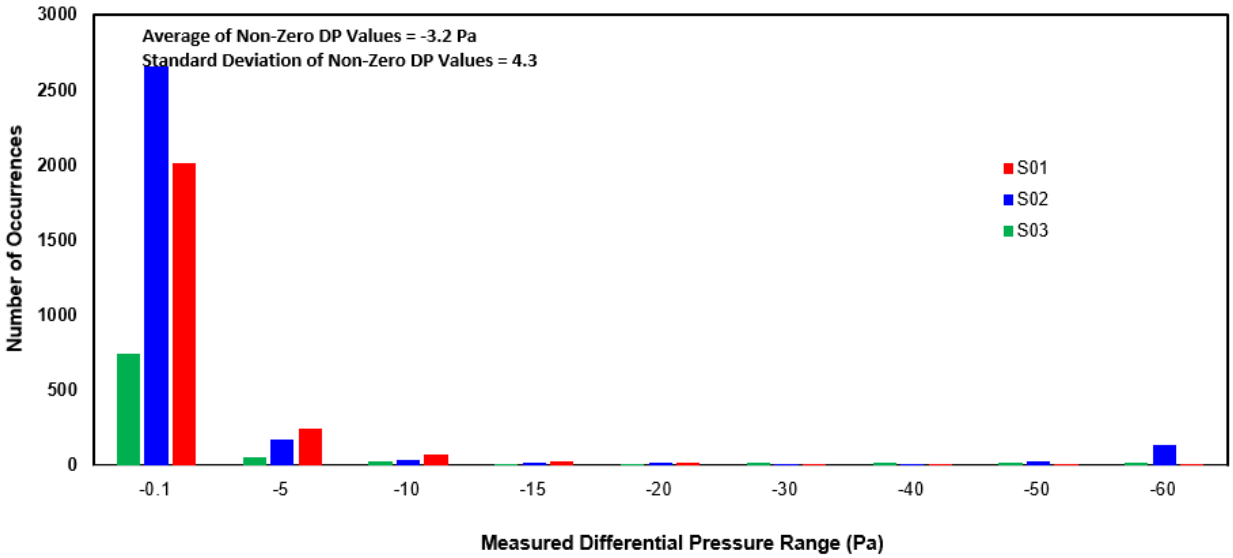

Figure 4.17 Histogram of measured non-zero DP values at Shallow Cover System

Table 4.1
Statistical Data of Measured Differential Pressures at Shallow Cover System

Monitoring Location	Average of Non-Zero DP Values	Standard Deviation of Non-Zero DP Values	Percentage of Values Non-Zero DP
S01	-3.2	4.3	23
S02	-5.6	12.9	33%
S03	-7.3	15.7	10%

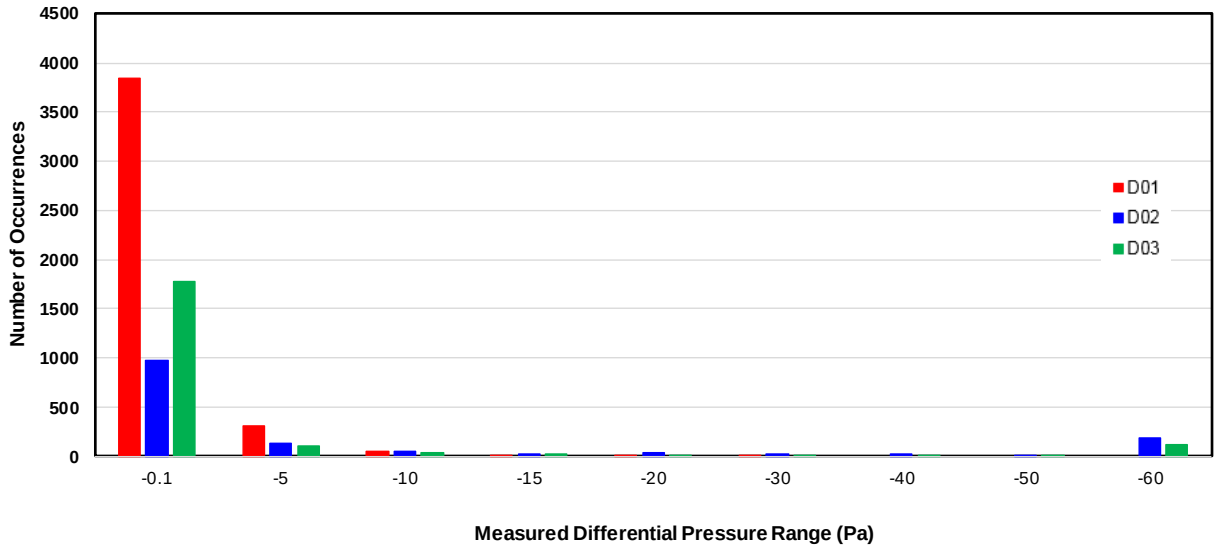

Figure 4.18 Histogram of measured non-zero DP values at deep cover system

Table 4.2
Statistical Data of Measured Differential Pressures at Deep Cover System

Monitoring Location	Average of Non-Zero DP Values	Standard Deviation of Non-Zero DP Values	Percentage of Values Non-Zero DP
D01	-2.4	2.4	44%
D02	-12.2	20.7	15%
D03	-3.1	14.1	22%

Both S01 and D01 showed a similar average measured DP when compared to each other, indicating that the pressure gradient across each cover system is comparable at these locations. However, D02 appeared anomalous as it showed an average differential pressure nearly double that of any other average differential pressure, while at D03 showed an average differential pressure nearly half that of its shallow cover system counterpart. These variations may be a result of localized surface cracking, variations in local soil moisture content, or variations in subsurface airflow patterns affecting pressure measurements across the cover system or variations in water content affecting local gas transmission rates through the soil cover systems.

The maximum pressure differentials at the shallow and deep cover systems (*e.g.* 60-70 pa) are greater than those reported in the waste rock case studies described by Phillips (2009) where large airflows were characterized utilizing a similar monitoring system. For example, Phillips (2009) observed that only small differential air pressures (<10 Pa) created by temperature differences were able to generate airflow across the surface of a waste rock dump in excess of 1 m/s. Although

the air permeability of a waste rock dump is likely to be much higher that the CBIW covers, the higher differential pressures measured as part of this study indicate there is a potential for convective airflow to occur, particularly through any high-permeability cracks which may appear at the surface of the cover system.

4.2.1 2014 Monitoring Year

In 2014 the differential pressure measurements represent the potential for upward flow. These results are shown in Figure 4.19 through Figure 4.24.

It can be seen that the differential air pressures (soil air pressure minus atmospheric pressure) are much lower than the results for 2013 (atmospheric minus soil air pressure). The highest potential for upward airflow is seen between June and July of 2014. Prior to May 2014, the differential pressure measurements showed predominantly downward pressure differentials at both D01 and S01, which indicate a high potential for downward flow; however, due to the freezing of the cover system, it is unlikely any significant airflow actually occurred during this time.

The measured DP at each cover system was reduced to shorter time intervals in order to show daily variations in DP alongside temperature differences across the cover system relative to ambient atmospheric temperature. The daily changes at both the shallow and the deep cover system in 2014 are presented for May 16 to 18 (Figure 4.11 and Figure 4.12, respectively), June 16 to18 (Figure 4.13 and Figure 4.14, respectively), and July 16 to 18 (

Figure 4.15 and Figure 4.16, respectively). No measurements are shown for August, 2014 as monitoring was ceased at the close of July, 2014.

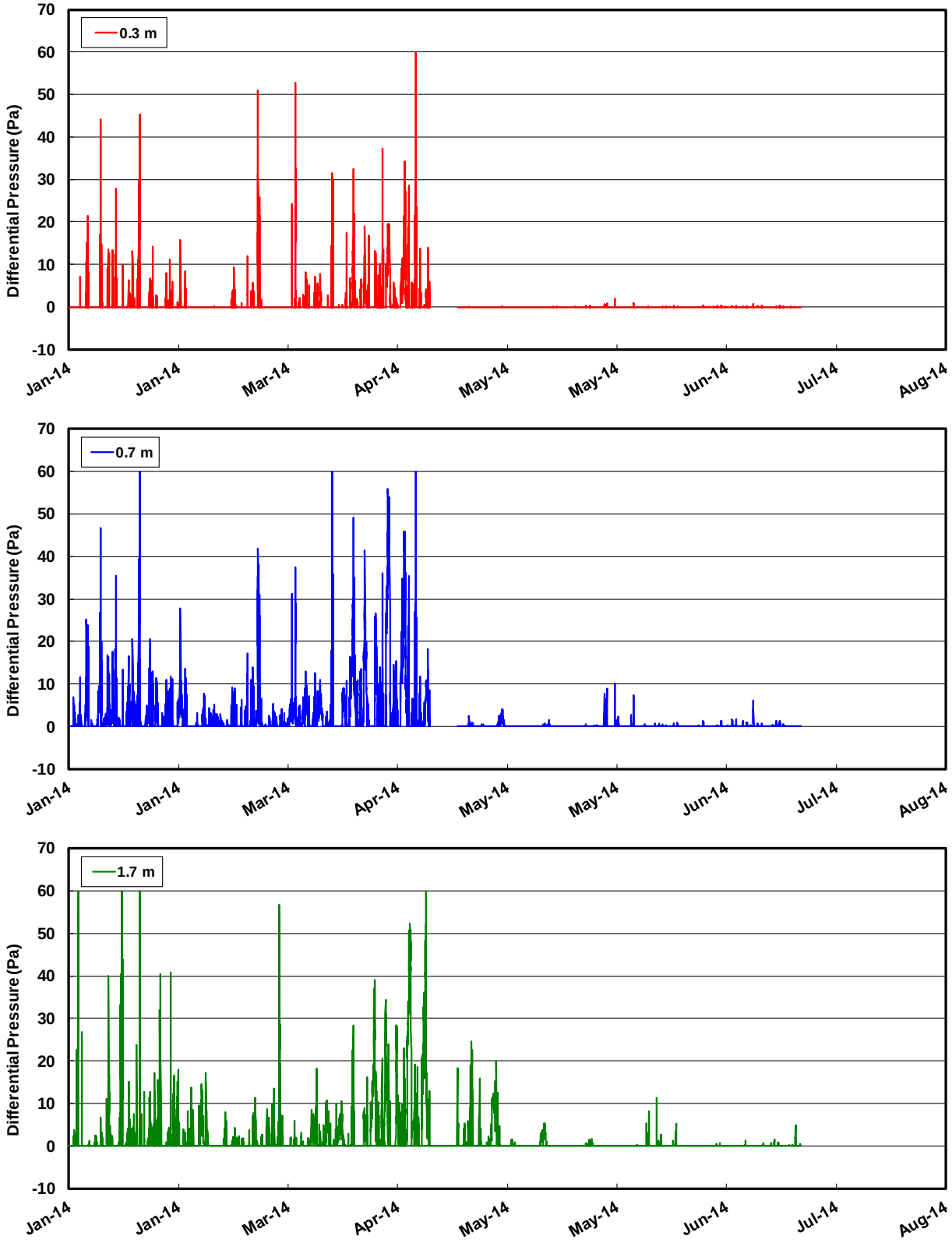

Figure 4.19 2014 Differential pressure for S01; sensor direction reversed May 15, 2014

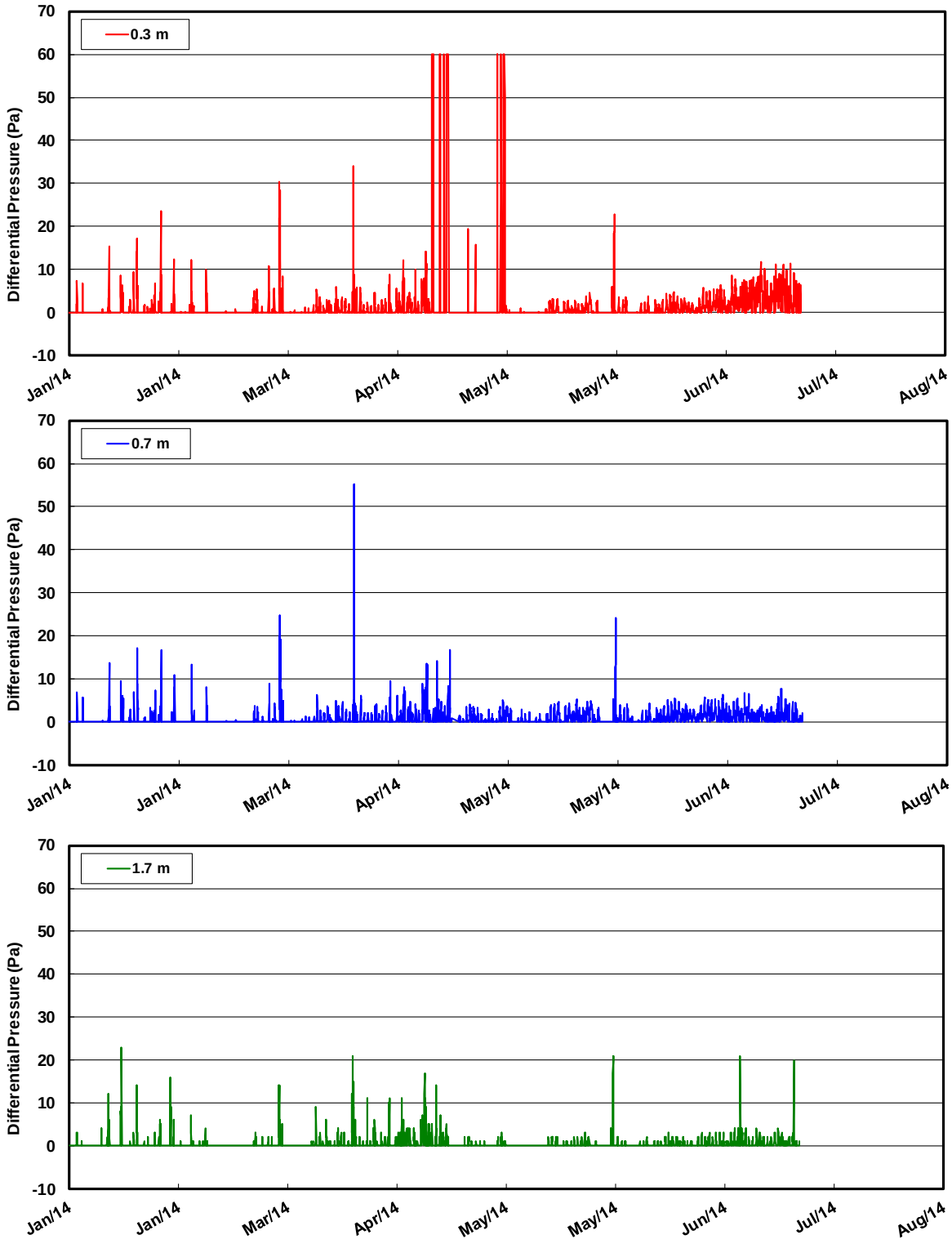

Figure 4.20 2014 Differential pressure for S02; sensor direction reversed May 15, 2014

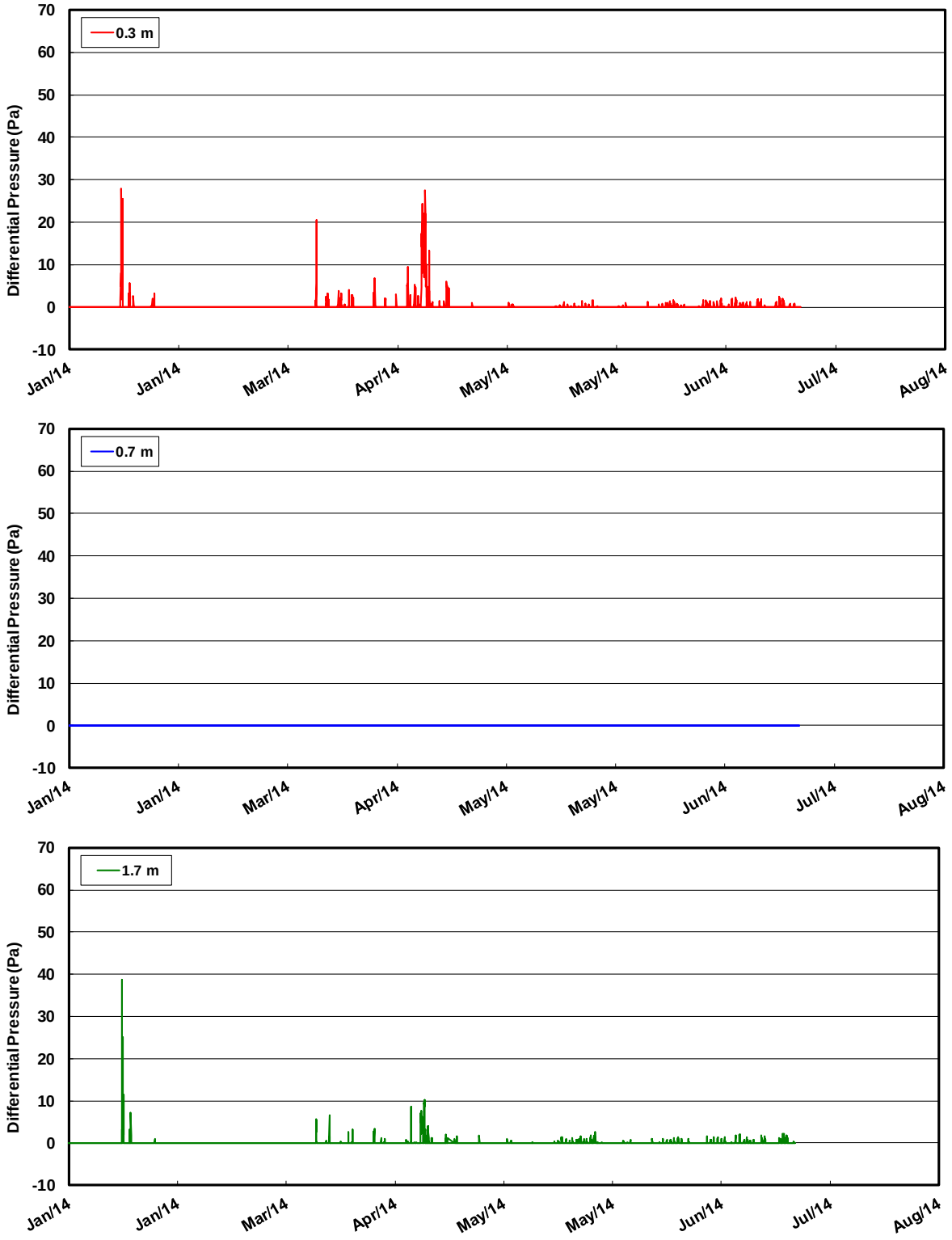

Figure 4.21 2014 Differential pressure for S03; sensor direction reversed May 15, 2014

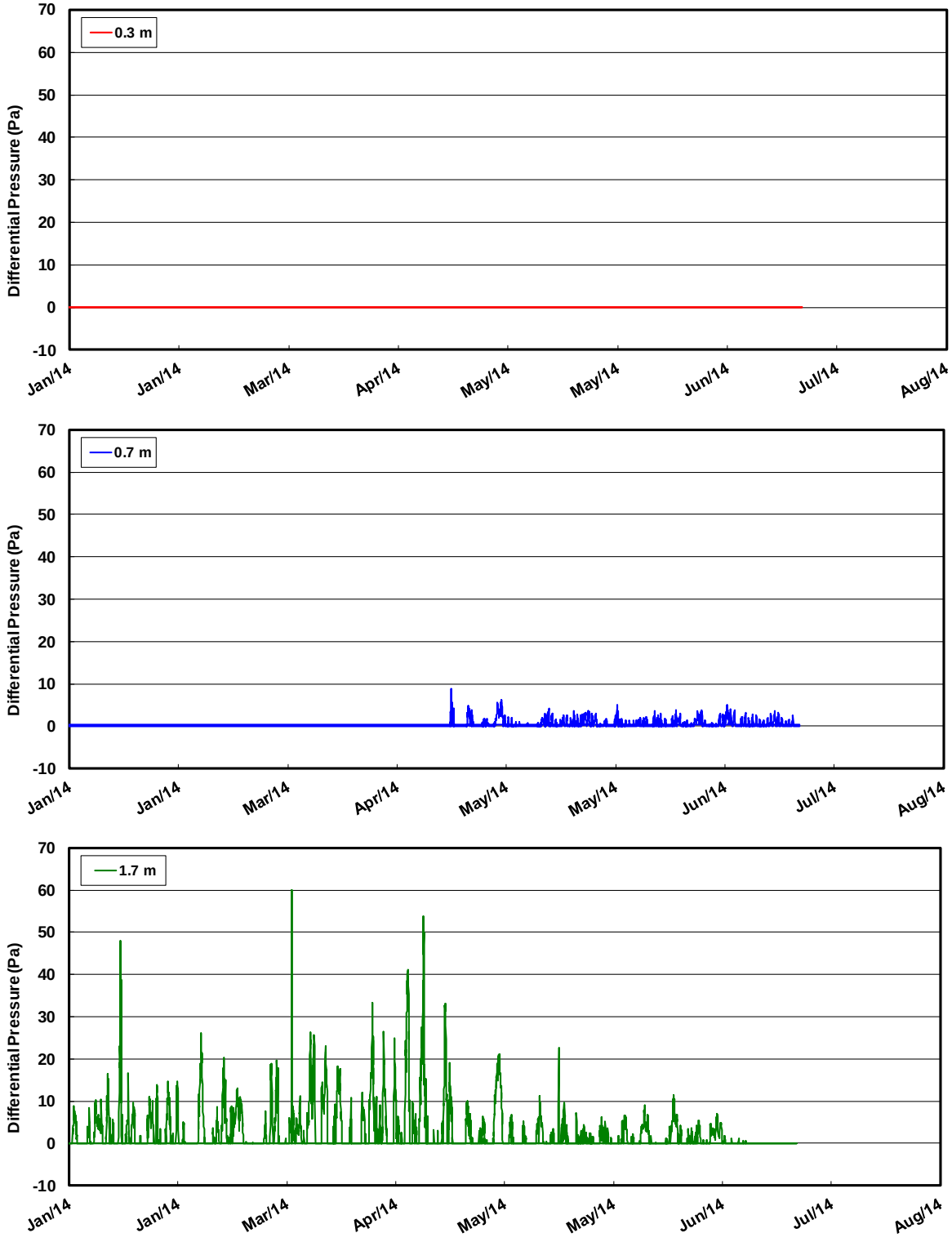

Figure 4.22 2014 Differential pressure for D01; sensor direction reversed May 15, 2014

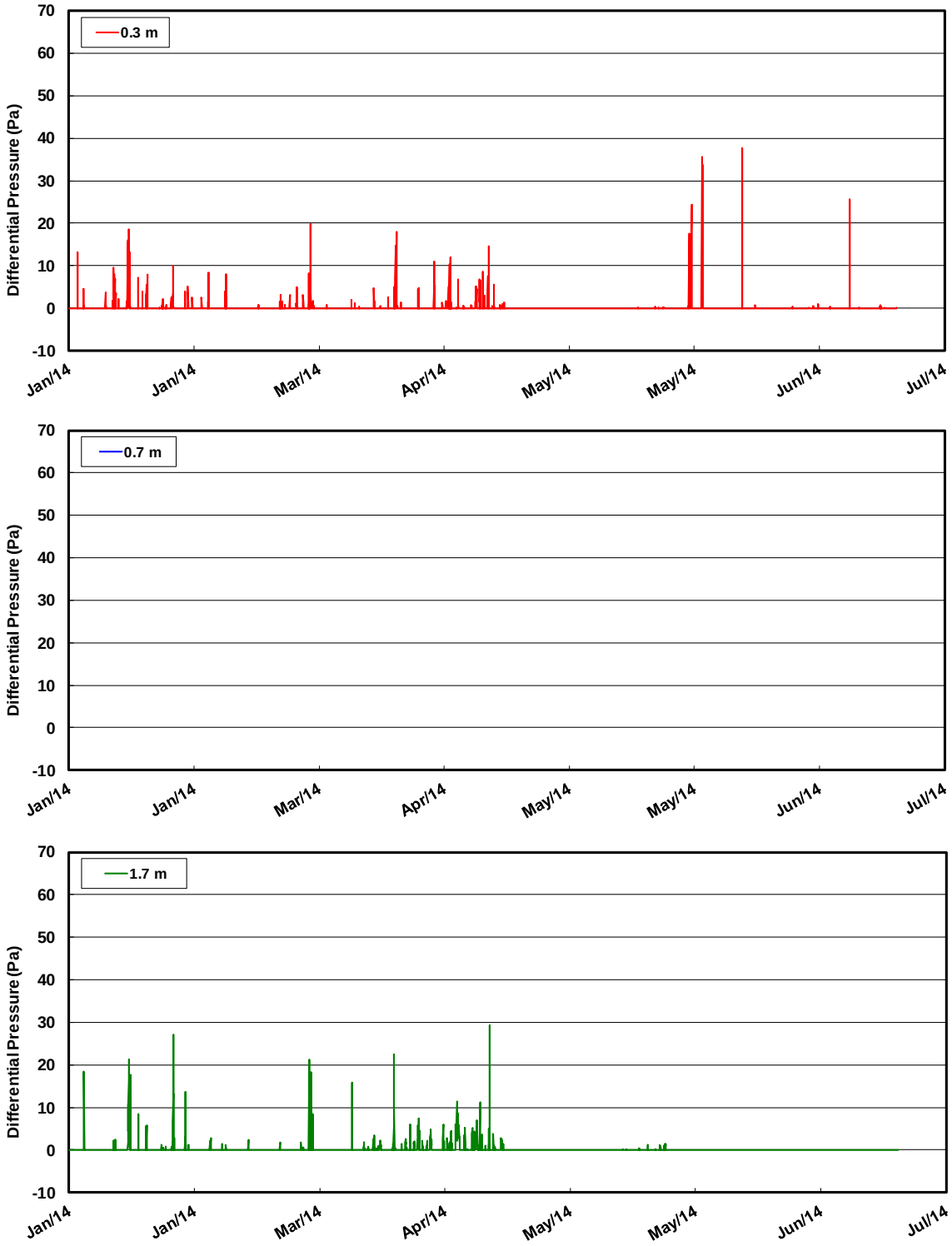

Figure 4.23 2014 Differential pressure for D02; sensor direction reversed May 15, 2014

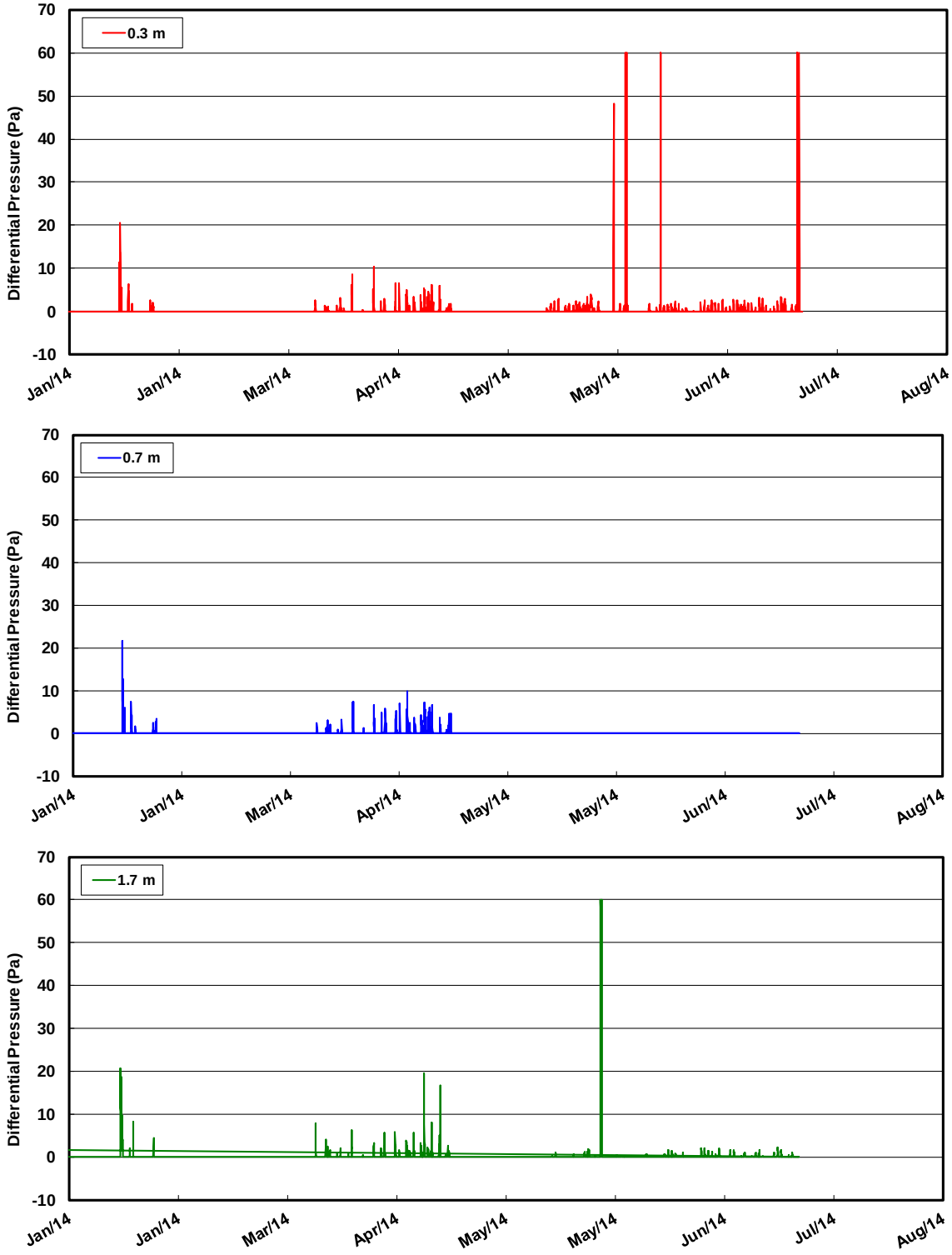

Figure 4.24 2014 Differential pressure for D02; sensor direction reversed May 15, 2014

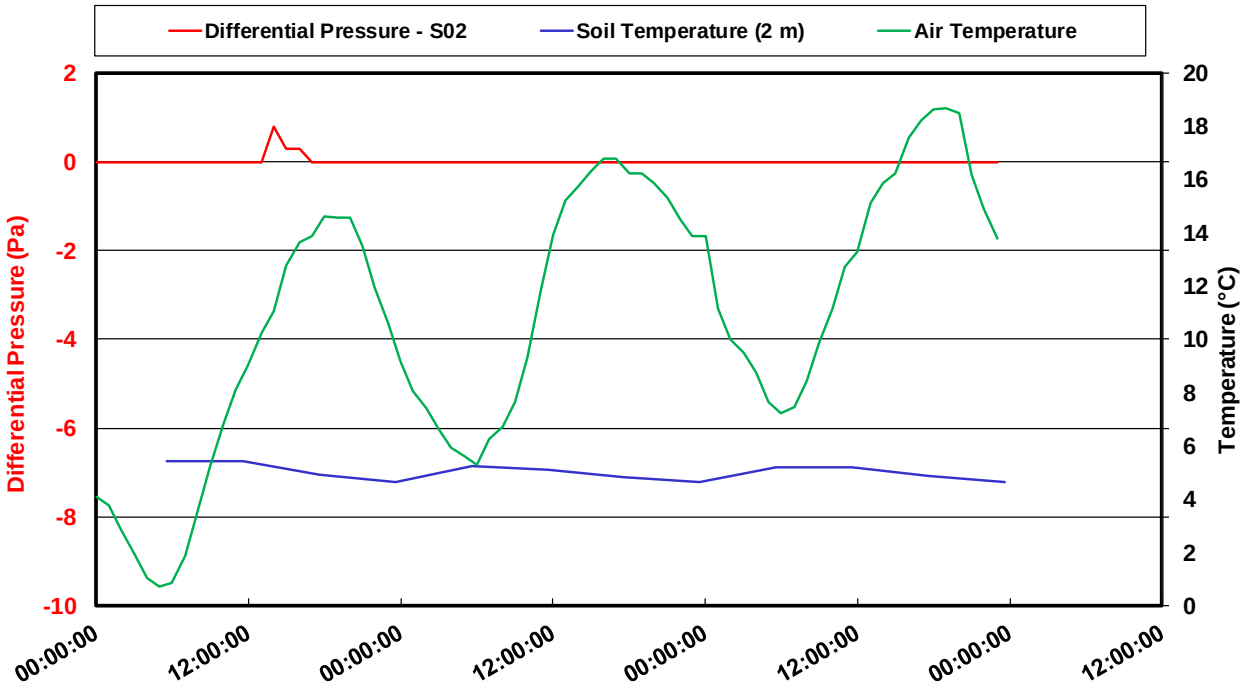

Figure 4.25 Daily variations in measured differential pressure at S02, May 16 to 18, 2014

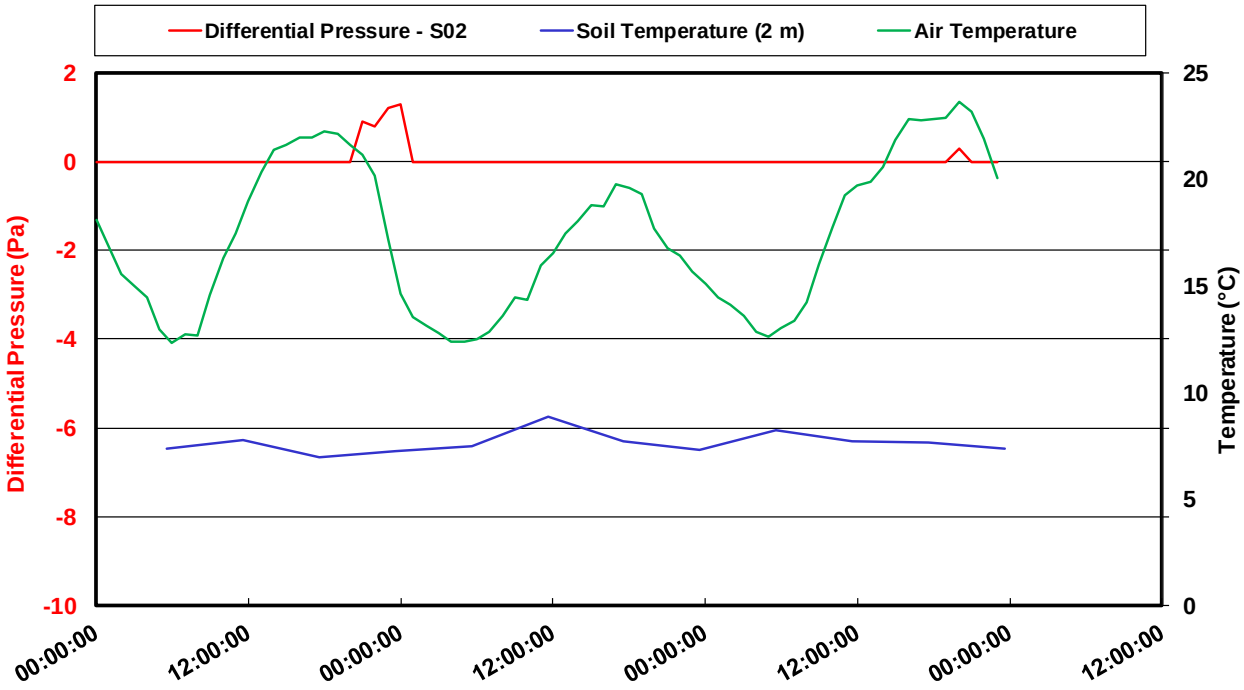

Figure 4.26 Daily variations in measured differential pressure at S02, June 16 to 18, 2014

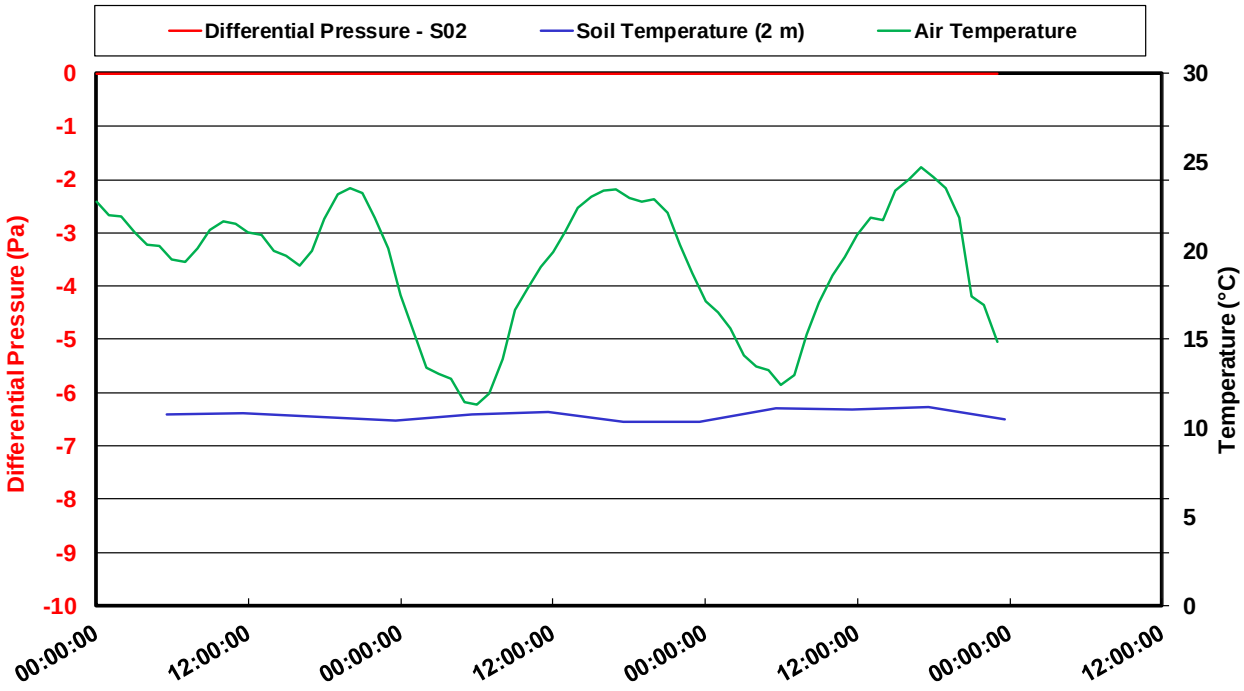

Figure 4.27 Daily variations in measured differential pressure at S02, July 16 to 18, 2014

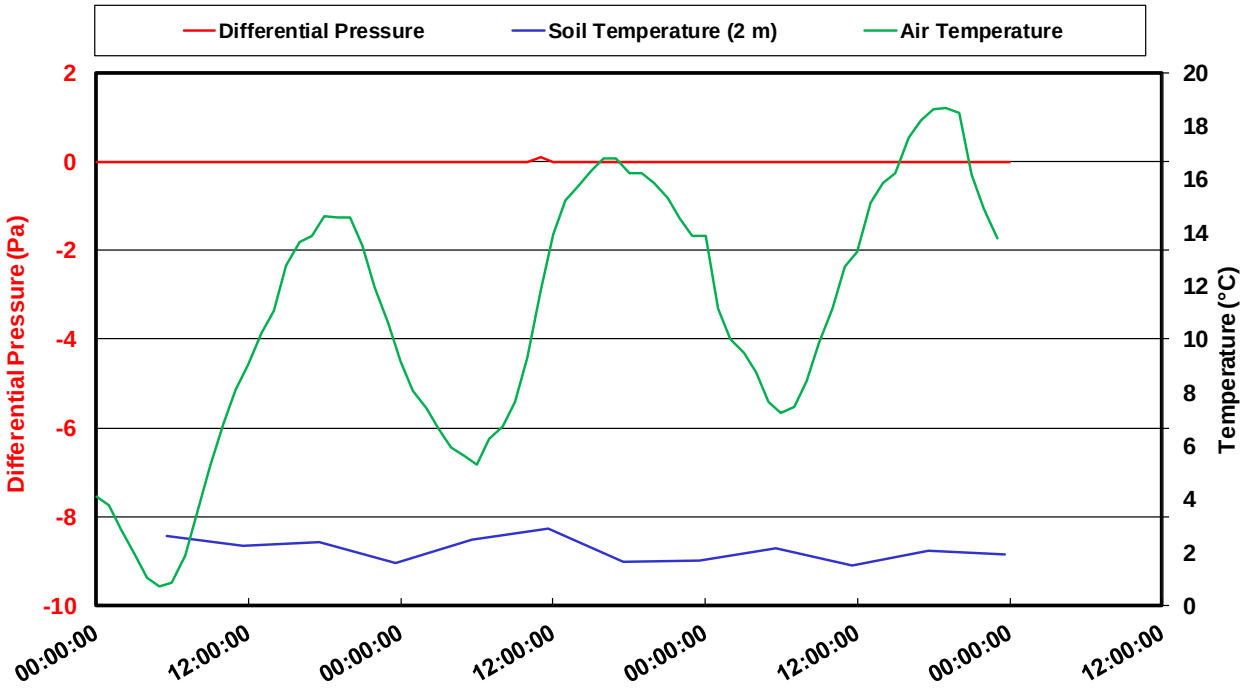

Figure 4.28 Daily variations in measured differential pressure at D02, May 16 to 18, 2014

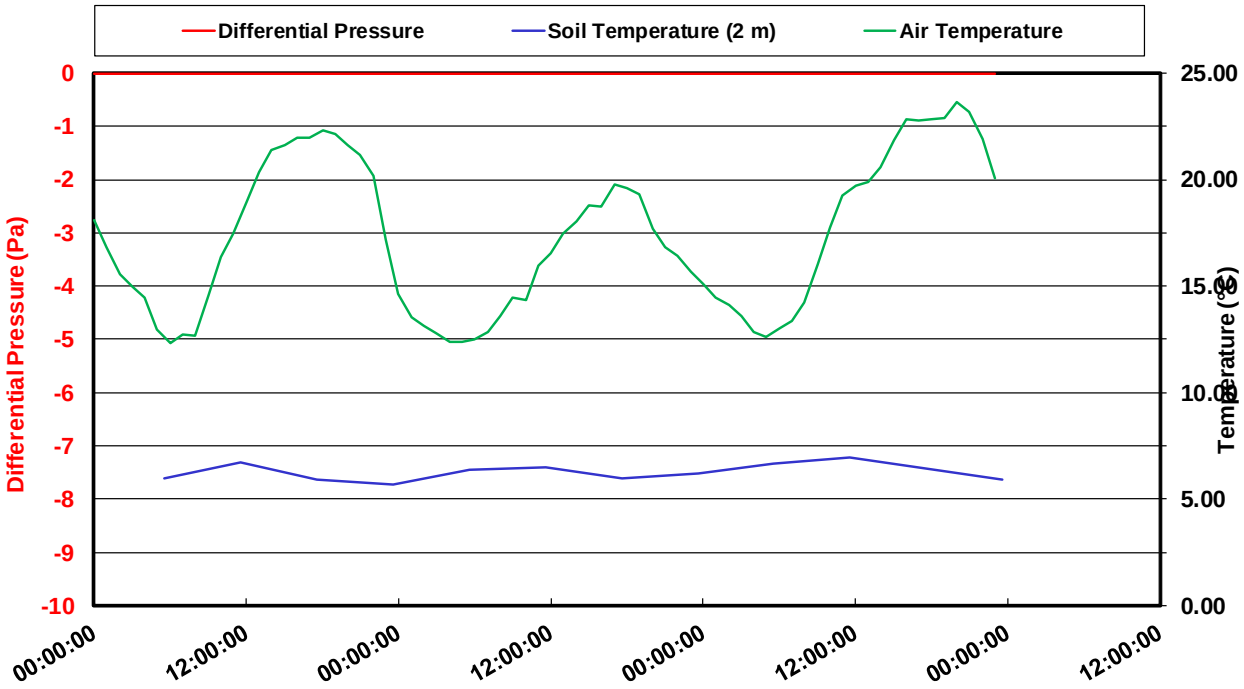

Figure 4.29 Daily variations in measured differential pressure at D02, June 16 to 18, 2014

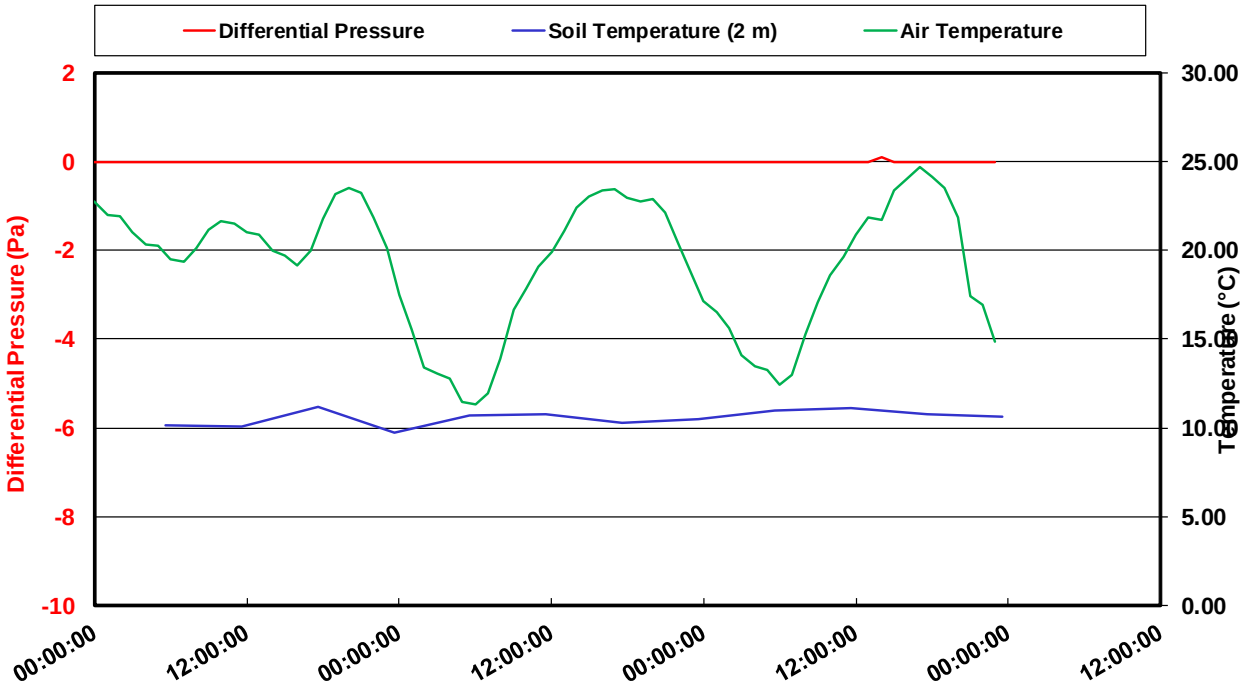

Figure 4.30 Daily variations in measured differential pressure at D02, July 16 to 18, 2014

As can be seen by the preceding figures, the temperature fluctuations did not have measurable effect on the upward movement of air in the system during the 2014 monitoring year (sensors

reversed to measure upward flow of air). This indicates that the differential pressures generated in the system are predominantly downward when influenced by temperature/density gradients.

4.2.2 MLSB Berm Differential Pressure Monitoring

The differential pressure systems installed on the berm were intended to determine the exit point of air entering the cover system across the surface of the berm. These were installed at 5 locations down slope from the shallow and deep cover systems. This line followed the centreline separating the two cover systems.

The differential pressure systems located on the berm did not show substantial changes to differential pressure over time. The results collected from the DP monitoring systems showed predominantly values of zero with only random occurrences of data points deviating from zero. A representative example of this is shown in Figure 4.31 below, as measured at B01 which was located at the base of the berm.

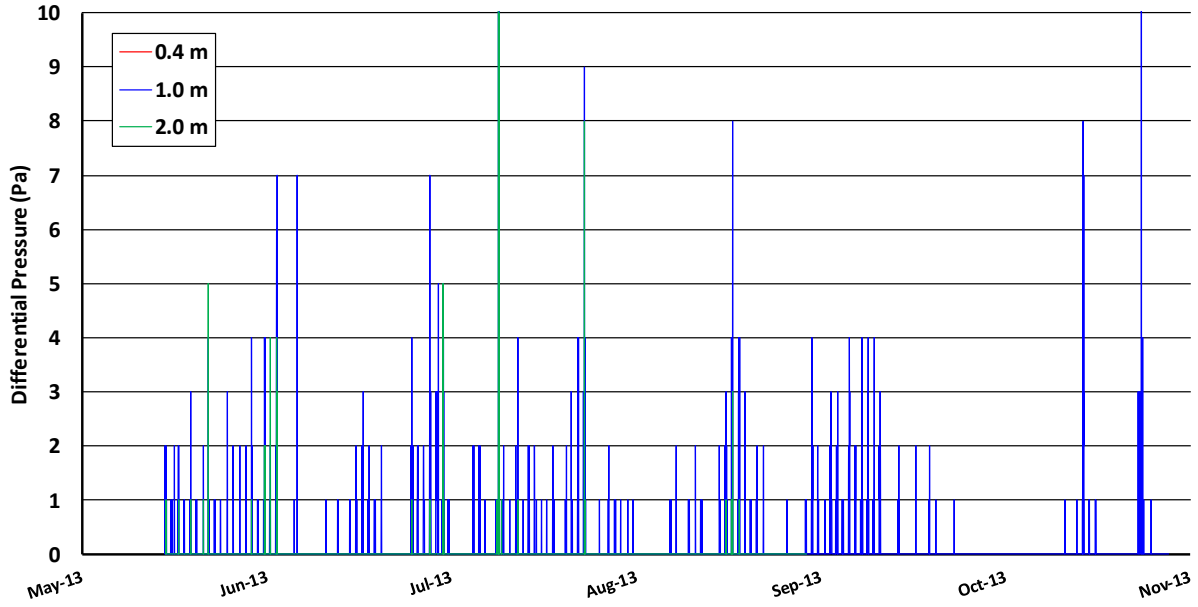

Figure 4.31 Measured differential pressures, B01 (base of berm)

The results showing negligible pressure gradients across the berm cover system may the result of large diffuse areas over which the airflow through the CBIW may be exiting, or may suggest alternative exit locations (such as buried drainage systems/sumps). As well, these results suggest

that for normal surfaces/constructions, the presence of convective airflow may not affect revegetation/reclamation efforts, and suggest that the presence of pressure gradients measured at the top of the CBIW are a result of the underlying material.

4.3 Air Permeability Testing

In situ air permeability testing was performed by the author with the assistance of Dyan Pratt of the University of Saskatchewan, using the method developed by Rodgers (2008). Results of the air permeability testing showed highly variable air permeability in the various material types of the cover systems at the time of sampling.

The first step in determining the air permeability using the modified air permeameter is to plot the flow rate against the measured change in pressure head to ensure a linear relationship. An example of this is presented in Figure 4.32, as measured during testing at S01 at a depth of 80 cm.

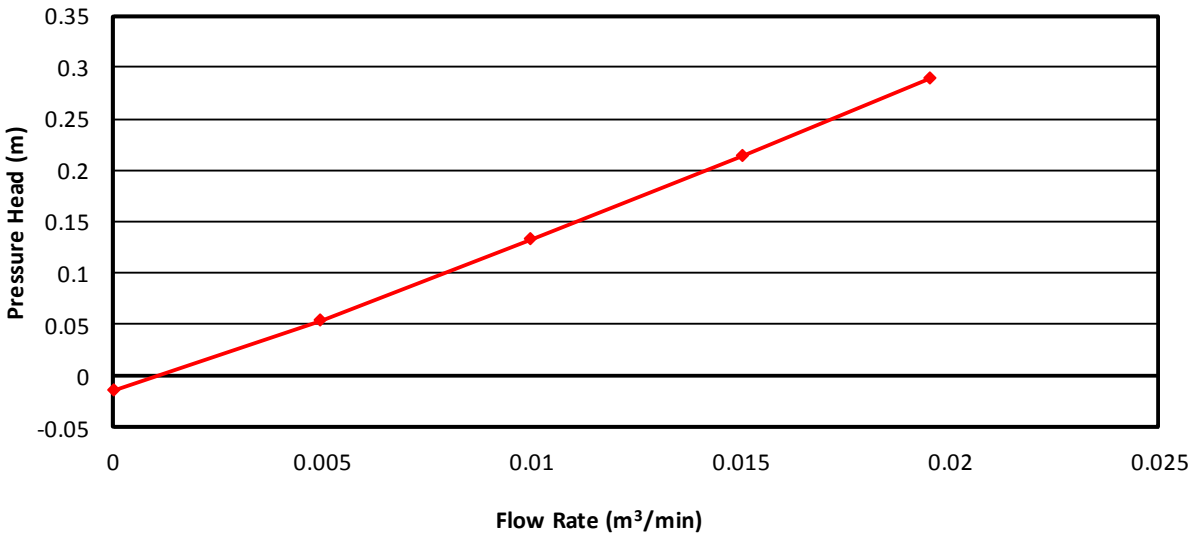

Figure 4.32 Flow rate – pressure head relationship during air permeameter testing

The linear relationship indicates a correlation between changes in flow rate and change in pressure head which is dependant on the soil properties; a non-linear relationship may indicate outside influencing factors (soil heterogeneity or other soil properties), or short circuiting under higher flow rates.

The results for all sampled locations and depths are summarized in Table 4.3.

Table 4.3
Measured Intrinsic Air Permeability by Author (Sept, 2012)

	Test Depth	Average Air Conductivity (m/s)	Average Intrinsic Permeability (m^2)
Shallow Cover System	30 cm	4.1×10^{-5}	7.1×10^{-11}
	80 cm	4.3×10^{-5}	6.7×10^{-11}
Deep Cover System	30 cm	2.3×10^{-4}	3.8×10^{-10}
	80 cm	3.9×10^{-4}	6.5×10^{-10}
	110 cm	9.1×10^{-5}	1.5×10^{-10}

The results in Table 4-1 are comparable to the average air permeability measurements made by Rodgers (2008), as shown in Table 4.4, although the intrinsic air permeability of the cover systems does appear to have decreased slightly since the testing carried out by Rodgers (2008). This decrease in intrinsic permeability may be due to variation in methods used to conduct the tests, or may be due to a change in the soil structure due to variable environmental conditions.

Table 4.4
Measured Air Permeability by Rodgers (2006)

Test Depth	Trial 1 (m^2)	Trial 2 (m^2)	Trial 3 (m^2)
10 cm	1.2×10^{-10}	1.8×10^{-10}	3.7×10^{-11}
20 cm	1.0×10^{-10}	2.5×10^{-10}	6.9×10^{-11}
30 cm	1.0×10^{-10}	2.8×10^{-10}	7.1×10^{-11}
40 cm	1.4×10^{-10}	3.6×10^{-10}	8.0×10^{-11}

The measured intrinsic permeability is independent of the VWC of the soil, however, the effective air conductivity is going to be heavily influenced by the water content of the soil, as water within the void space and higher effective saturation will limit the airflow in the system. If there is a high presence of macropores, then air conductivity is less affected by moisture in the soil. This presents a unique challenge when considering the air permeability and airflow potential of a reclamation cover system, as the relative air permeability will change with changes in water content. A combination of numerical modelling and intensive field investigation could determine a dynamic air permeability for the site, however, this was outside the scope of this thesis.

4.4 Visual Observations Noted in the Field

Visual observations of the condition of the covers were made and recorded during regular site visits were noted and recorded. One of the most striking observations was the presence of large and deep surface cracks in the cover system across both the deep and shallow cover systems;

however, these were more prevalent on the shallow cover system (Figure 4.33). In many cases, these surface cracks extended greater than 25 cm into the ground. The cracks would provide a preferential pathway by which infiltrating water might bypass the cover system and enter the underlying coke. If sufficient pathways exist at the cover systems, the result could be a water movement pathway not currently covered by the standard water balance approach, and thus, would affect the results. They would also provide high permeability flow paths for airflow. The effect of these cracks on potential air movements across the cover system was not monitored and represents a potential research opportunity.

Figure 4.33 Example of deep and wide surface cracking at the shallow cover system.

It was also noted that several areas of the cover system had begun to show loss of the surficial peat, resulting in exposure of the underlying, lower hydraulic conductivity till. This loss in peat may have been due to erosion by wind or water. In spite of this low hydraulic conductivity surface, little to no ponding on the cover surface was not observed following heavy rainfalls consisting of over 70 mm over four days in early June, 2013, and over 30 mm over two days at the end of May, 2013 and May 2014. This suggests that either runoff was occurring or that the surface cracks provided for rapid infiltration of water in and possibly through the covers.

Each of the cover systems showed a substantial decrease in thickness of the peat layer. The peat layer provides an important control on the water balance of the cover by allowing large precipitation events to infiltrate and be stored so that the water can be released more slowly to the underlying till layer.

Chapter 5
Analysis

The cover monitoring data, along with the field measurements of air-permeability and air pressure will be used in this chapter to develop more quantitative interpretations of the water balance for each of the covers as well as the magnitude of convective airflow. Daily and growing season water balances were calculated for both covers for 2006 to 2014. These water balances are used to identify if there is drying of the covers beyond that associated with normal evapotranspiration and/or drainage. Estimates of airflow across the cover system as a function of time are used to evaluate whether these airflow rates are sufficient to influence the water balance of the system.

5.1 Water Balances

5.1.1 Shallow Cover System

Actual evapotranspiration (AET) rates at the shallow cover system, calculated using the method outlined in Section 2.8, are presented in Figures 5-1 through 5-9 for the years 2006 through 2014. Included in each figure is a volume of water referred to as an "Additional Water Removal Process" (AWR). This is the volume of water that would have to be removed to close the water balance for the cover based on the conventional estimates of the water balance components. It will be used as a semi-quantitative measurement of additional water losses not accounted for in the water balance method outline in Section 2-5. In reality, visual observations of cracking suggest that the majority of AWR is likely a component of net percolation (NP) as a result of bypass flow, however, this could not be confirmed utilizing instrumentation in this thesis.

The AET/PET ratio was calculated using Equation 2.8 based on the measured volumetric water contents (VWC). The values of field capacity (FC) and wilting point (WP) were taken from published values as presented in Shurniak (2003) and summarized in Table 5.1.

Table 5.1
Summary of Cover System Material Properties

Cover System Component	FC (cm^3/cm^3)	WP (cm^3/cm^3)	AWHC (mm)
Shallow Cover Peat	0.3	0.20	20
Shallow Cover Till	0.35	0.21	28
Deep Cover Peat	0.30	0.20	25

Deep Cover Till	0.35	0.21	98

Similar studies were carried out at SCL 30-dump by Huang et al. (2015), using similar cover system materials. The field capacity and wilting point of the material used in their study were 0.37 and 0.178, respectively. This shows good correlation to those values measured by Shurniak (2003).

The calculated and measured changes in storage for 2006 (Fig. 5-1) are similar with only minor differences. This indicates that conventional estimates of AET and drainage are providing a reasonable description of the water balance for this cover. The average AET:PET ratio during the 2006 field season was found to be 0.4, with the ratio falling to 0 during an extended dry period when VWC dropped below the wilting point. It is interesting to note that the AWR for 2006 is relatively low (e.g. ~ 50 mm) and appears to develop when there is a large precipitation event (*e.g.* early spring or July 2006). This is likely water lost from storage as a result of drainage/bypass flow.

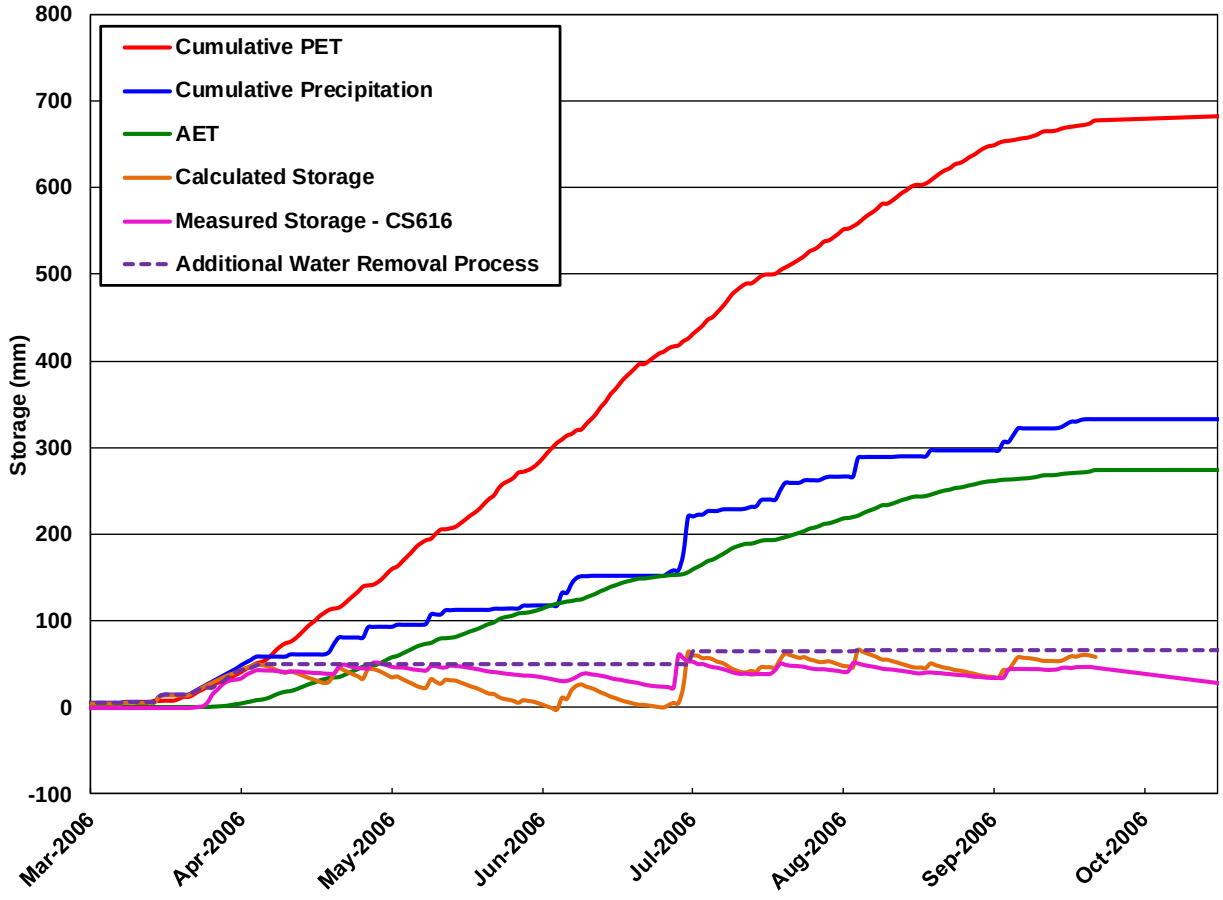

Figure 5.1 Water balance for Shallow Cover System, 2006 monitoring year.

In subsequent years (2007-2014) the calculated AET:PET ratios become much lower than in 2006 during key evaporation months of June through August (*e.g.* 0.1 – 0.2). This occurs because the VWC within the shallow cover remains near or below the wilting point through much of the growing season from 2007 to 2014. These lower values of AET require that higher AWR volumes are required to close the water balance increase. The increases in AWR during rapid increases in precipitation likely reflect losses from rapid drainage; however, there are still ongoing increases in AWR even during periods with smaller precipitation events. It is interesting to note that the volume of AWR over the growing season was generally between 200 – 300 mm/year, and was roughly 60-75% of the available precipitation. The volume of AWR for each monitoring year is presented in Table 5.2, while the water balances for each monitoring year (2007 through 2014) at the shallow cover system are shown in Figure 5.2 through Figure 5.9.

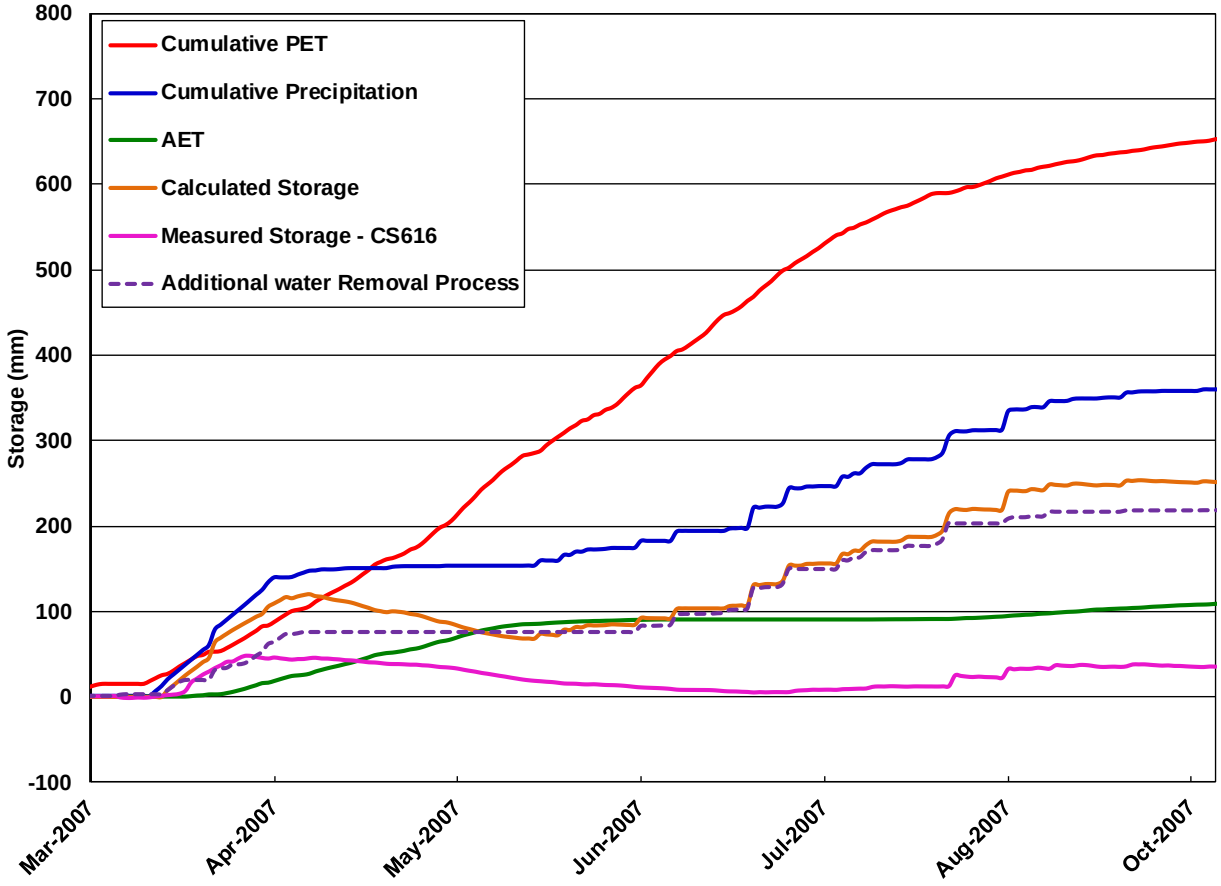

Figure 5.2 Water balance for Shallow Cover System, 2007 monitoring year.

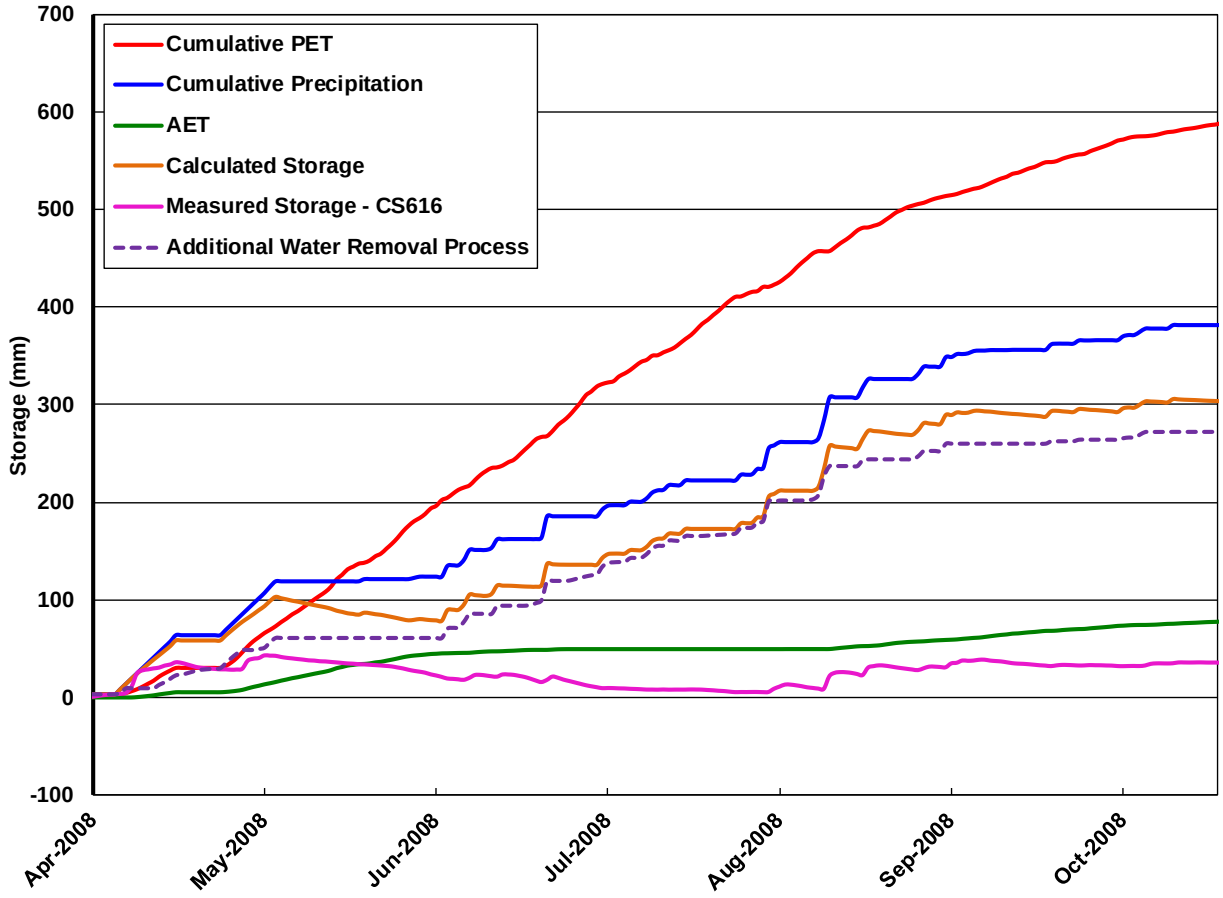

Figure 5.3 Water balance for Shallow Cover System, 2008 monitoring year.

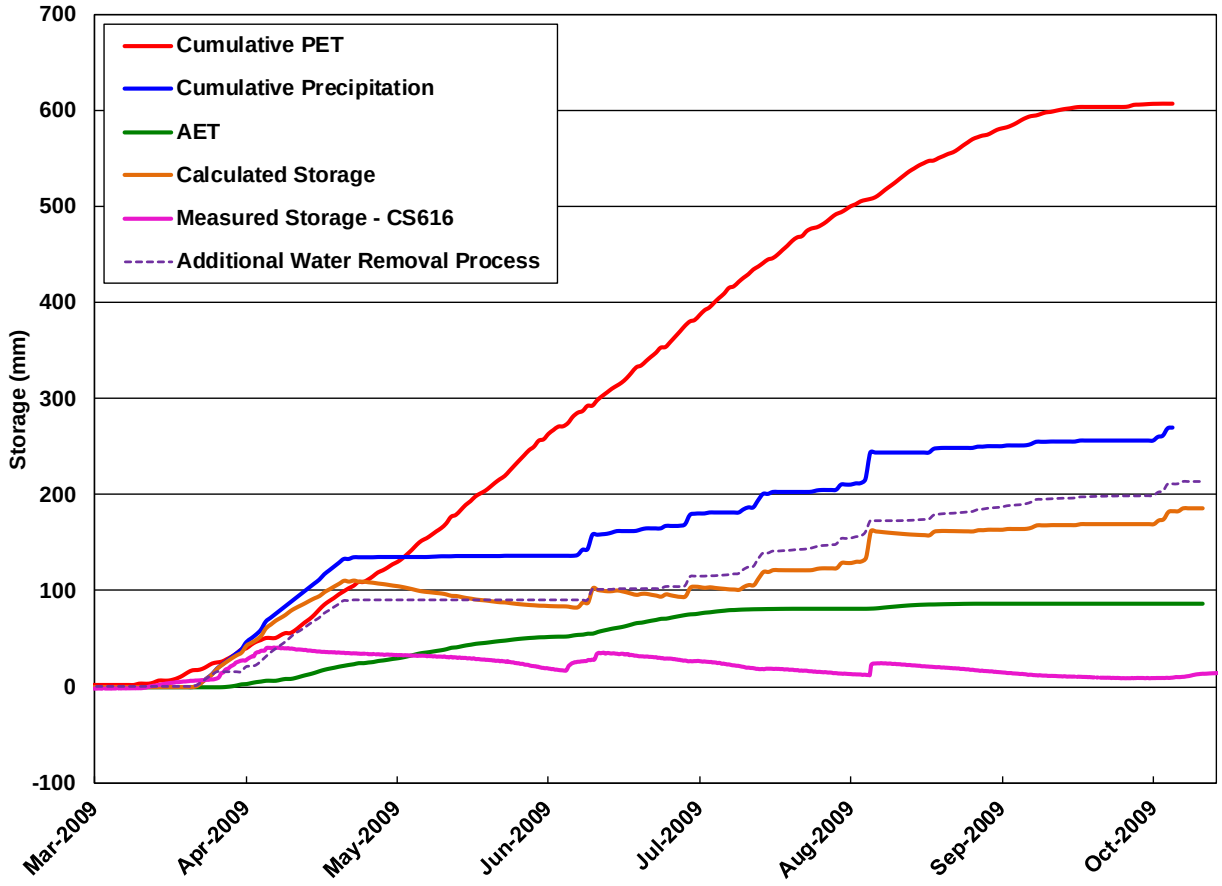

Figure 5.4 Water balance for Shallow Cover System, 2009 monitoring year.

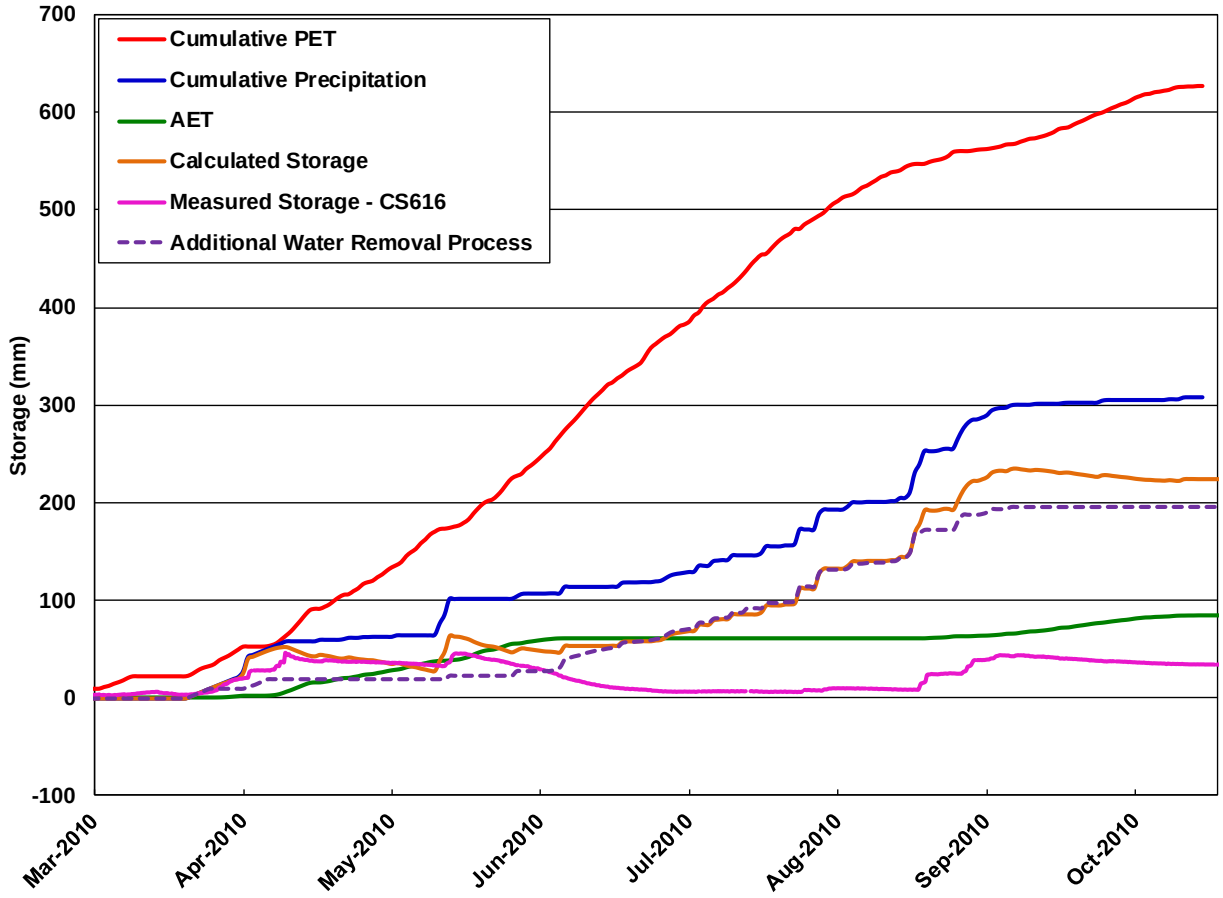

Figure 5.5 Water balance for Shallow Cover System, 2010 monitoring year.

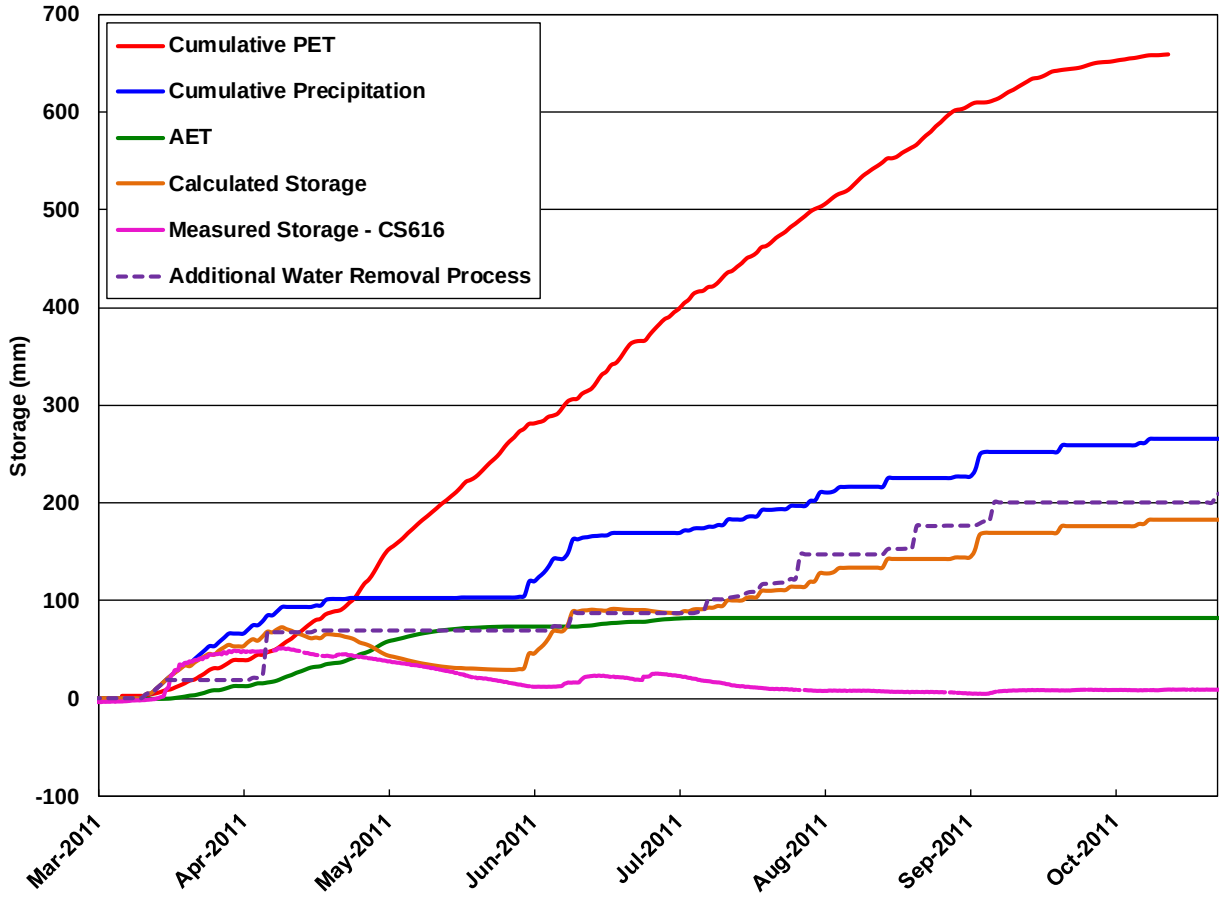

Figure 5.6 Water balance for Shallow Cover System, 2011 monitoring year.

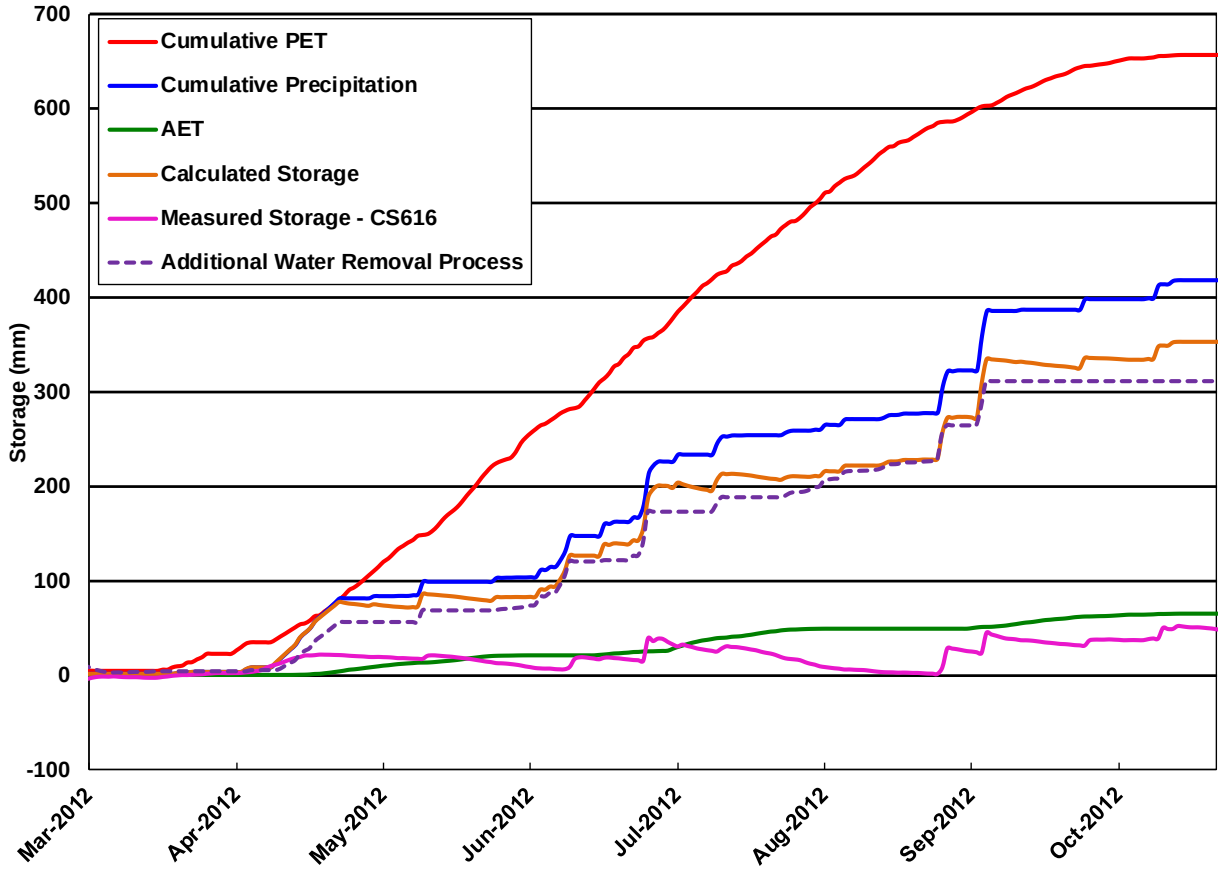

Figure 5.7 Water balance for Shallow Cover System, 2012 monitoring year.

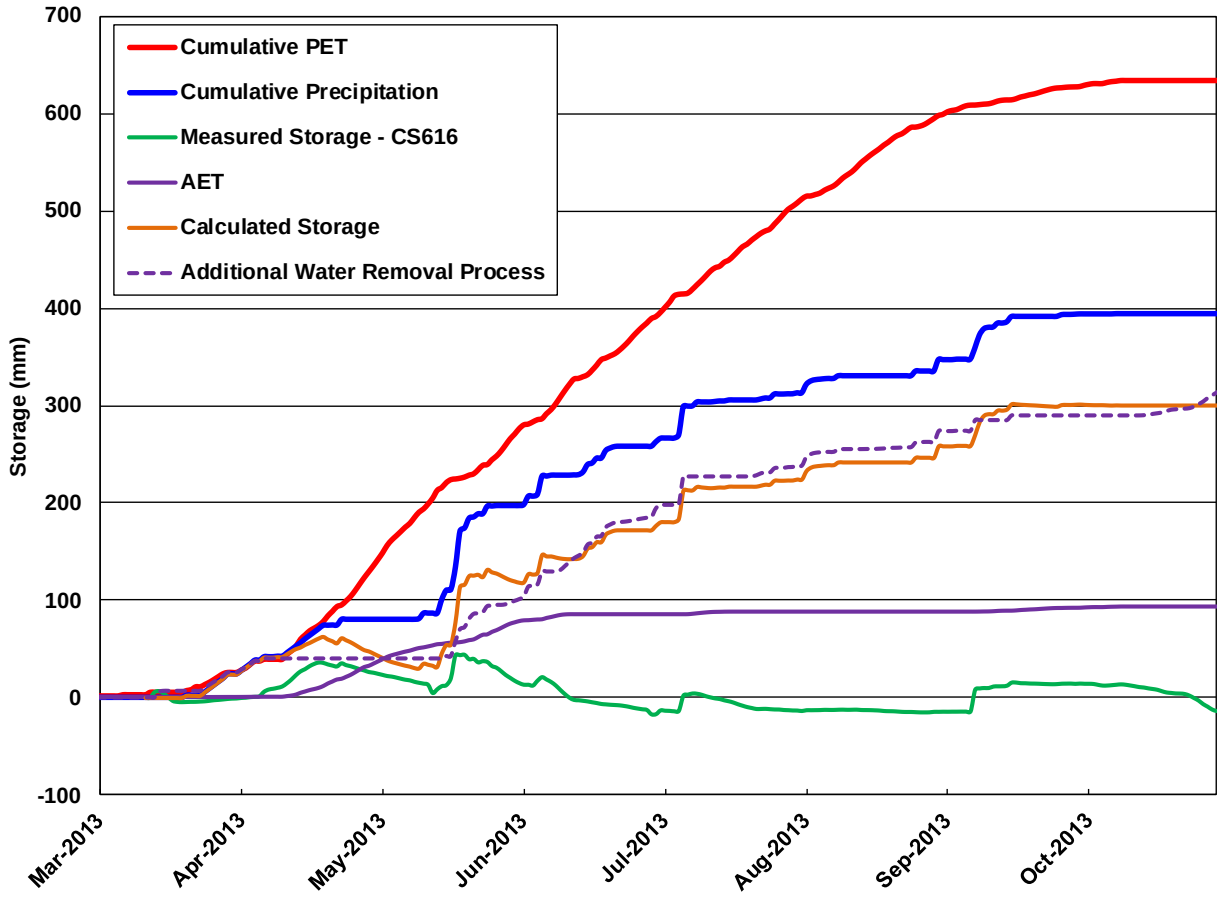

Figure 5.8 Water balance for Shallow Cover System, 2013 monitoring year.

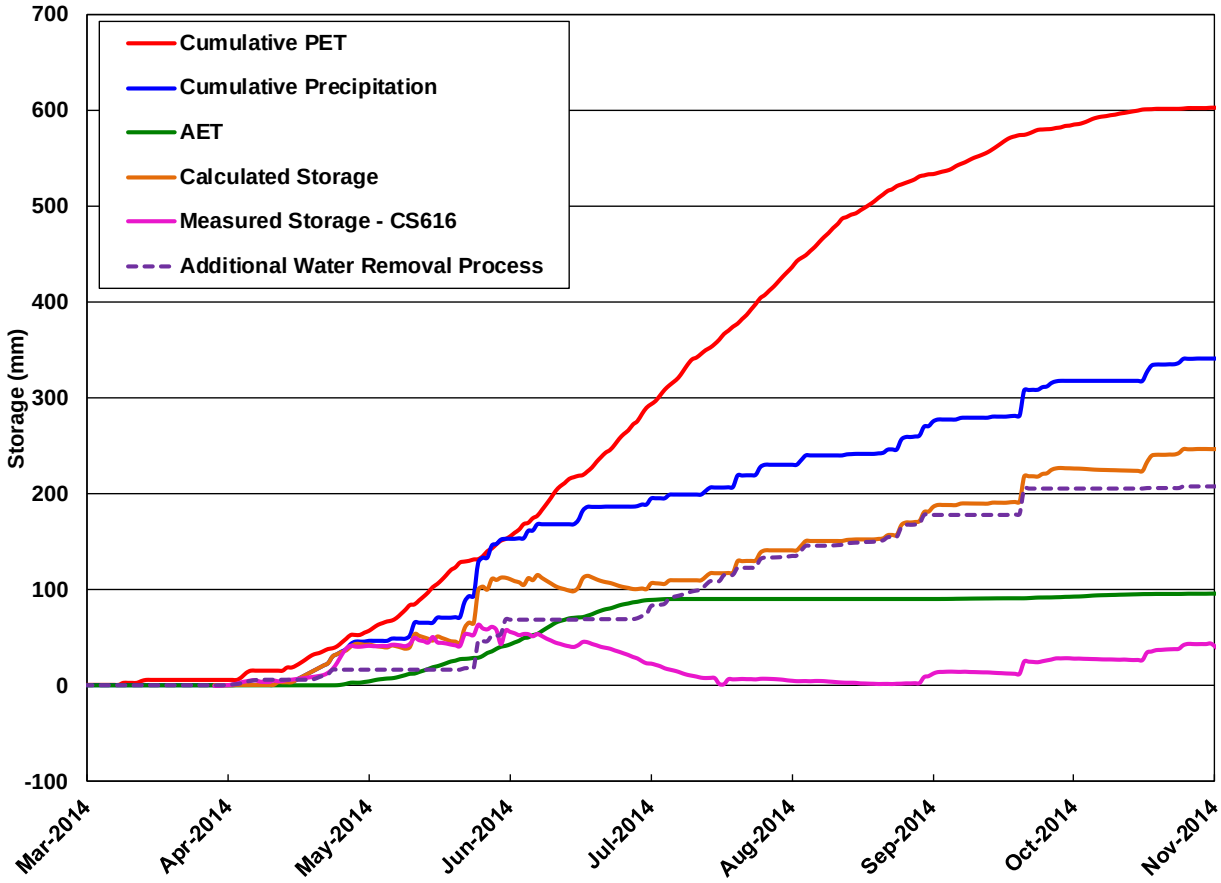

Figure 5.9 Water balance for Shallow Cover System, 2014 monitoring year.

Table 5.2 shows that the additional water removal (AWR) in the water balance formulation for the Shallow Cover System as a function of the PET and precipitation which occurred at the site.

Table 5.2
Moisture Loss Not Accounted by Water Balance – Shallow Cover System

Year	Total AWR (mm)	Total Precipitation (mm)	Total PET (mm)	AWR as Percentage of Precipitation (%)	AWR as Percentage of PET (%)
2006	106	332	692	32	15
2007	218	361	675	60	32
2008	271	392	596	69	45
2009	211	272	608	78	35
2010	195	307	632	64	31
2011	200	265	632	75	32
2012	305	422	613	72	50
2013	309	394	634	78	49
2014	205	341	603	60	34

The volume of AWR represents approximately 60-75% of precipitation in all monitoring years save for 2006. The possible causes of this water loss are runoff, net percolation (particularly that associated with preferential flow through fractures or macropores), or enhanced drying. The flat topography of the cover and the lack of evidence of ponded conditions suggests that runoff is unlikely. This suggests that the additional water loss is either the result of increased net percolation as a result of flow through the macropores or the result of enhanced drying or both.

5.1.2 Deep Cover System

Unlike the shallow cover system, the deep cover system never showed a monitoring year in which the calculated and measured storage were a good match without including a factor to account for AWR. Figures 5-10 through 5-18 present the water balances obtained for 2006 through 2014. The volume of AWR for each year as presented in Table 5-2 shows that the AWR for the deep cover ranged from 140 to 293 mm/year, which is somewhat less than the AWR for the shallow cover.

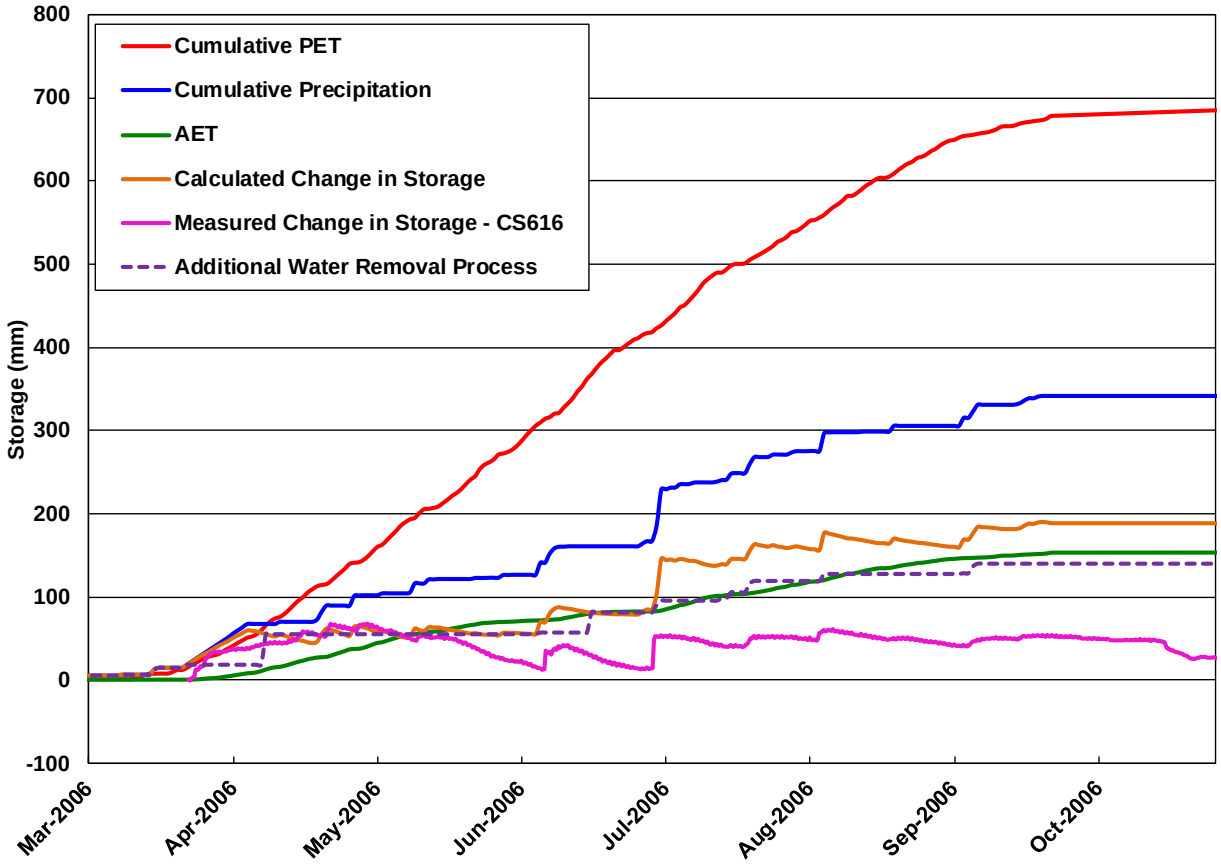

Figure 5.10 Water balance for Deep Cover System, 2006 monitoring year.

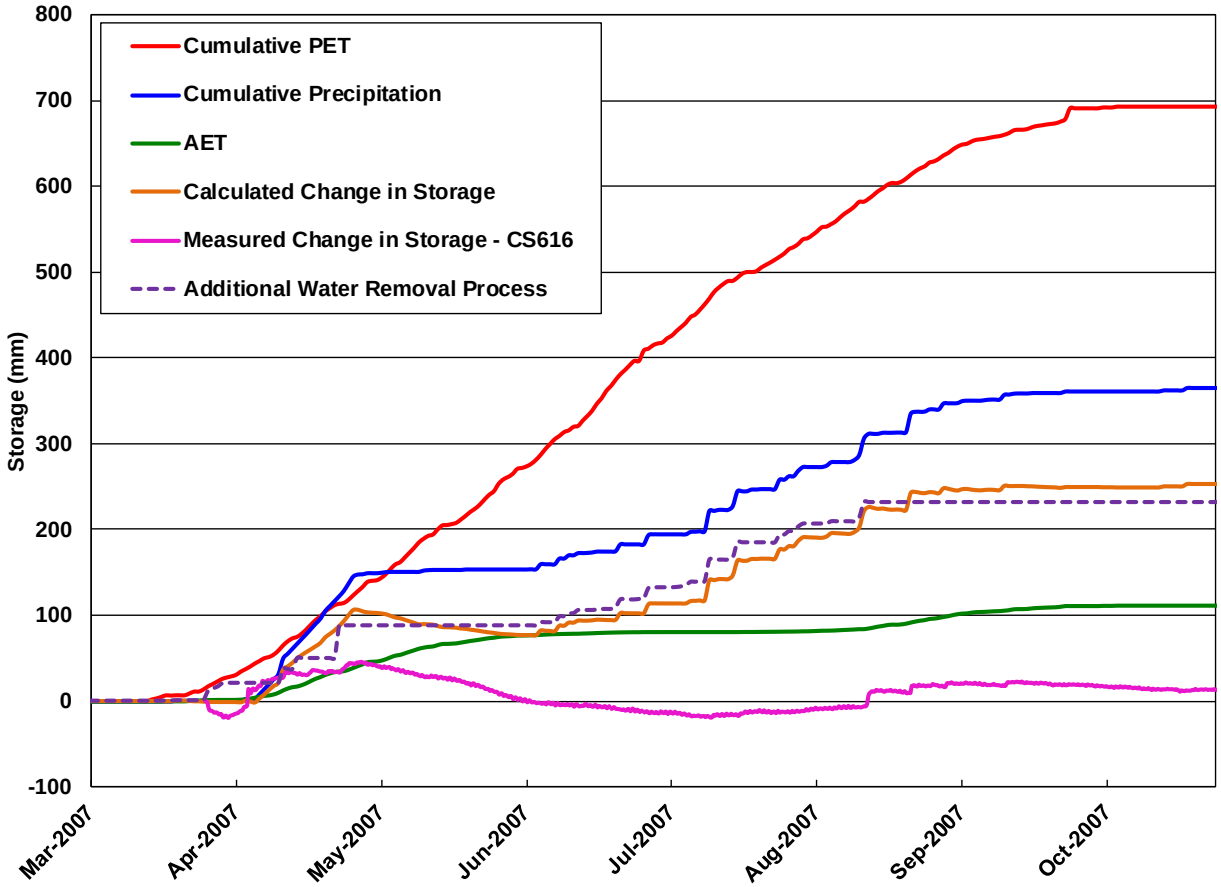

Figure 5.11 Water balance for Deep Cover System, 2007 monitoring year.

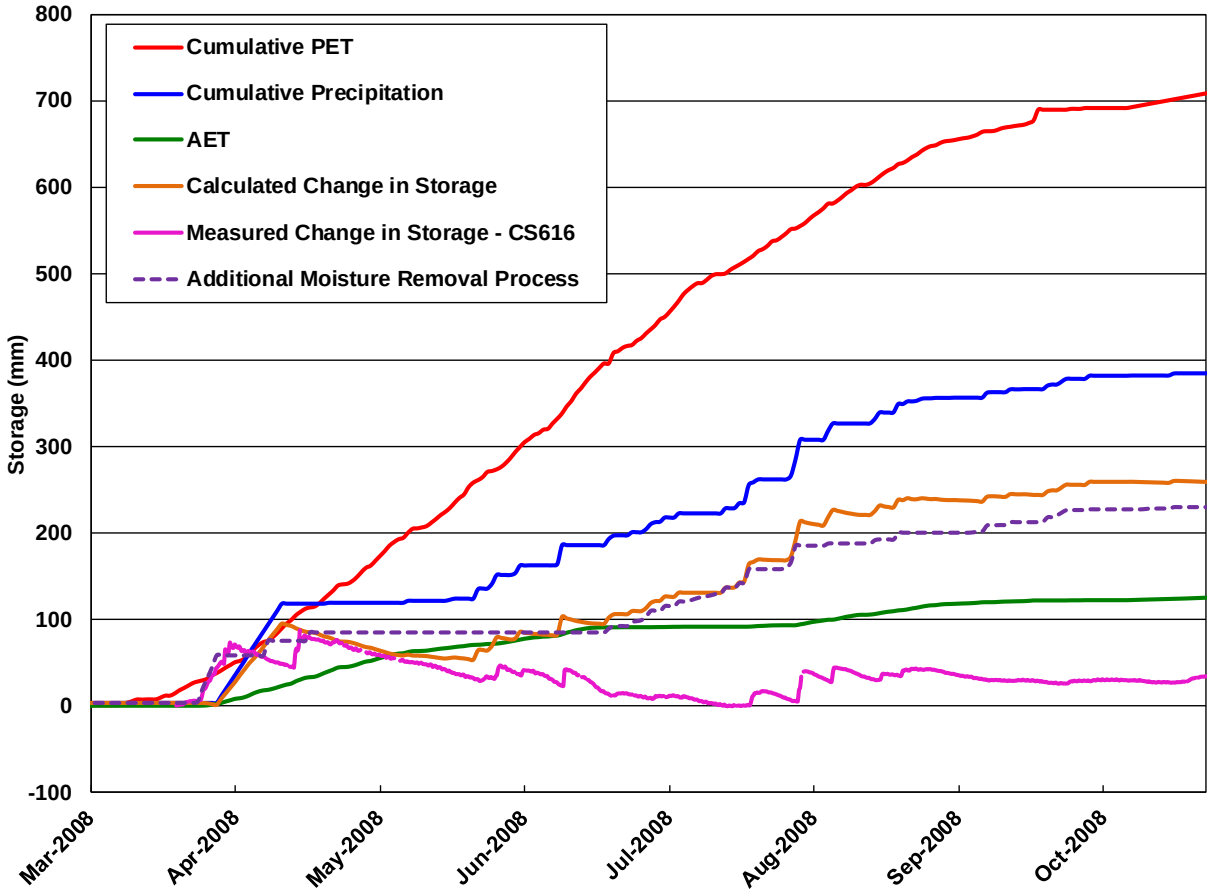

Figure 5.12 Water balance for Deep Cover System, 2008 monitoring year.

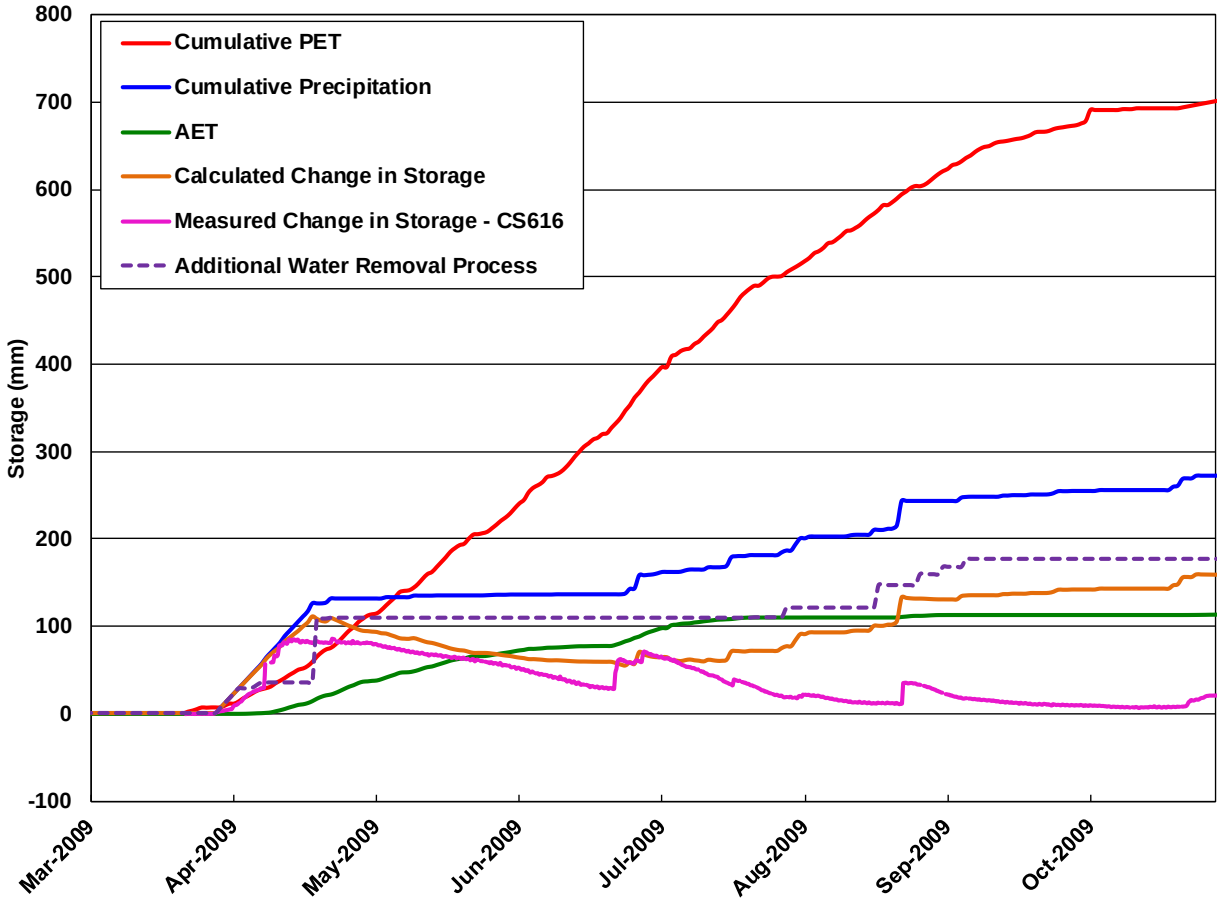

Figure 5.13 Water balance for Deep Cover System, 2009 monitoring year.

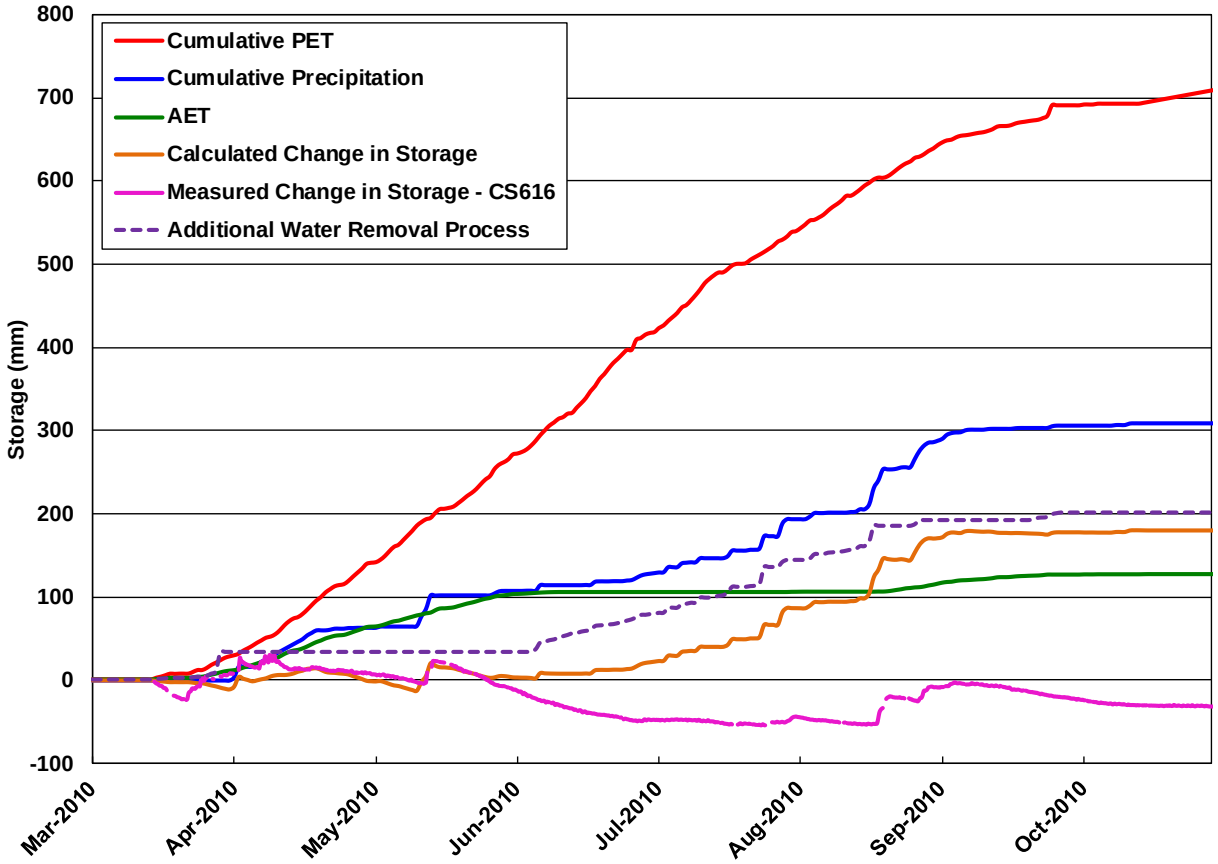

Figure 5.14 Water balance for Deep Cover System, 2010 monitoring year.

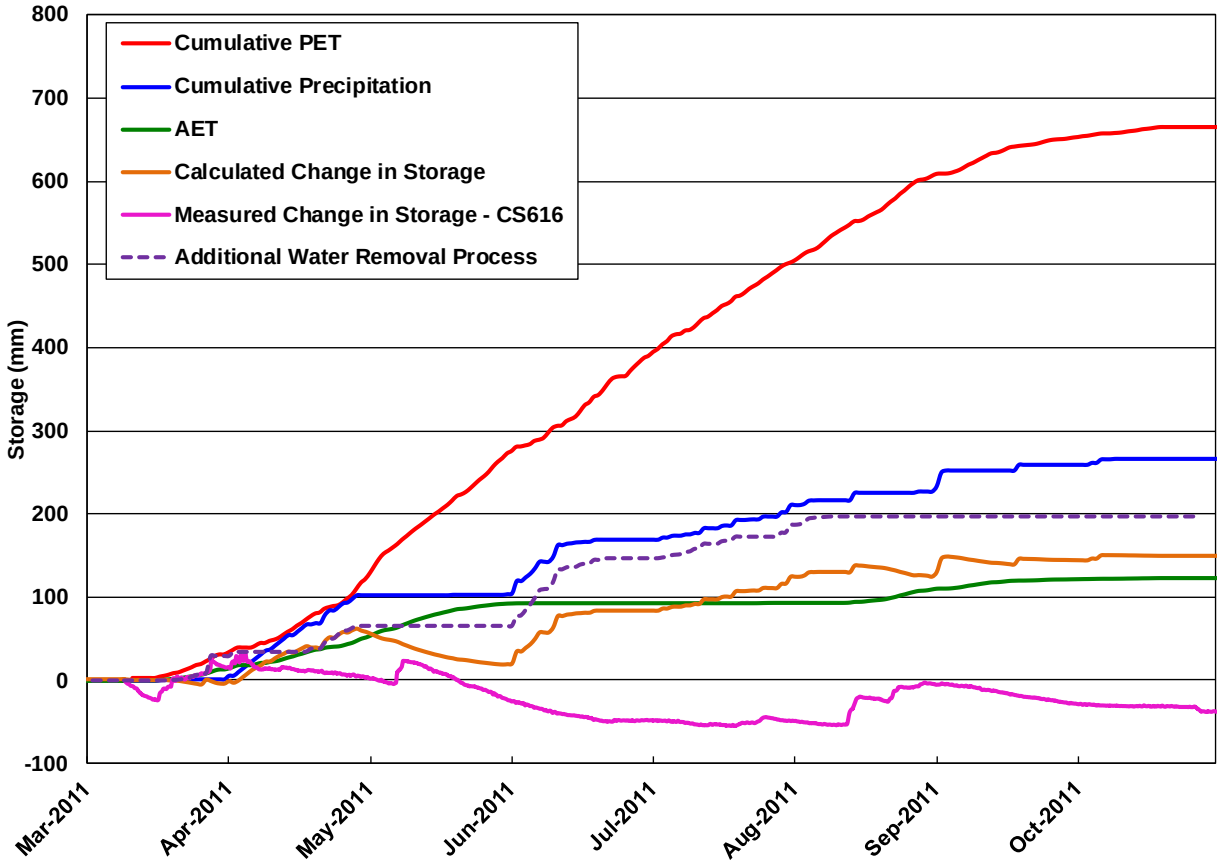

Figure 5.15 Water balance for Deep Cover System, 2011 monitoring year.

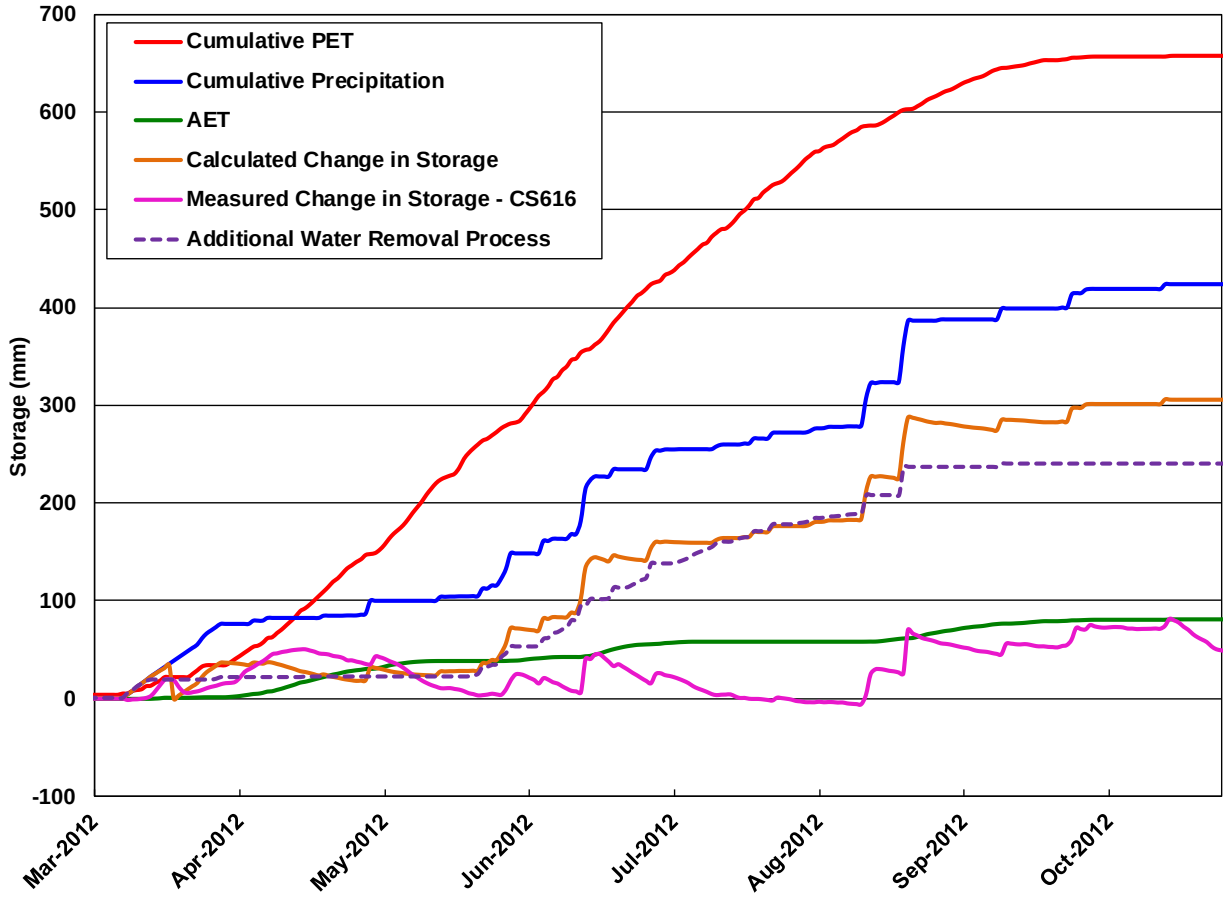

Figure 5.16 Water balance for Deep Cover System, 2012 monitoring year.

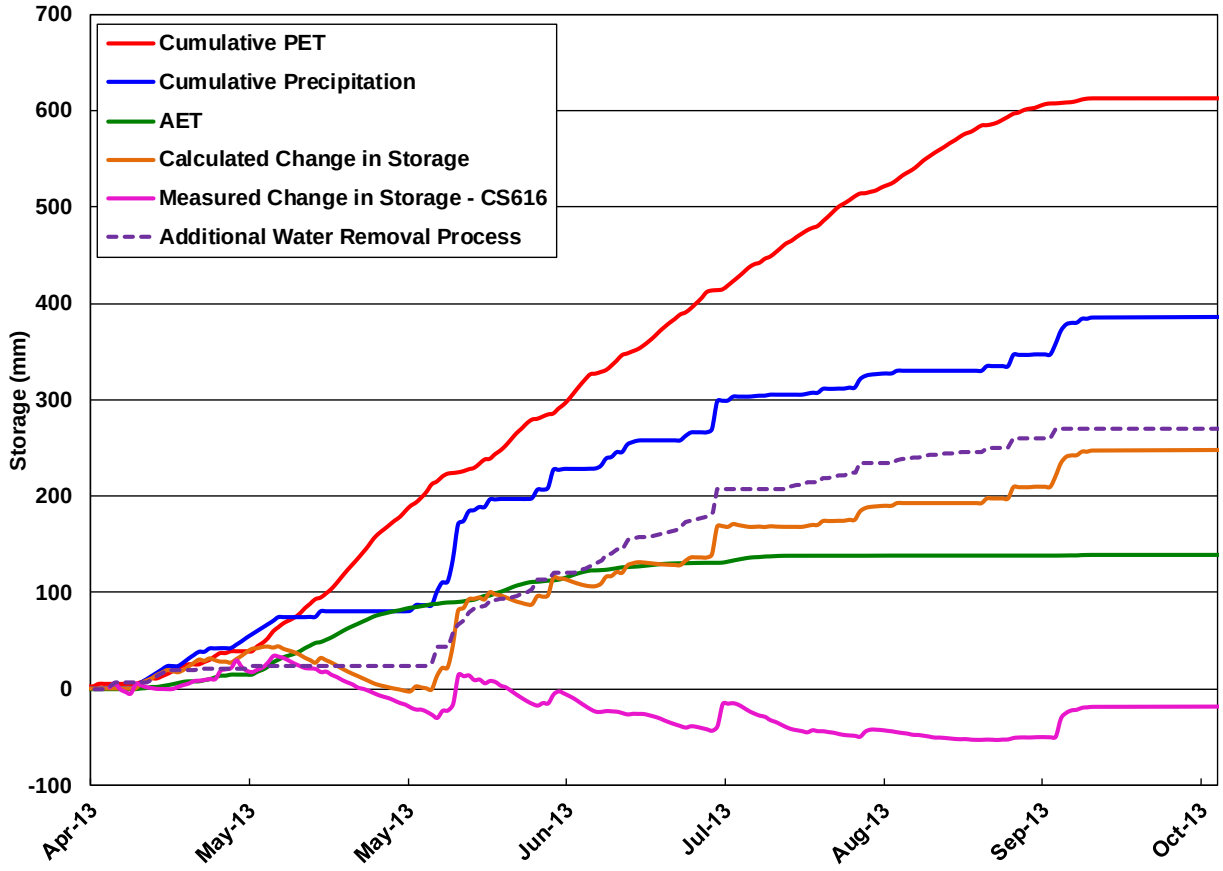

Figure 5.17 Water balance for Deep Cover System, 2013 monitoring year.

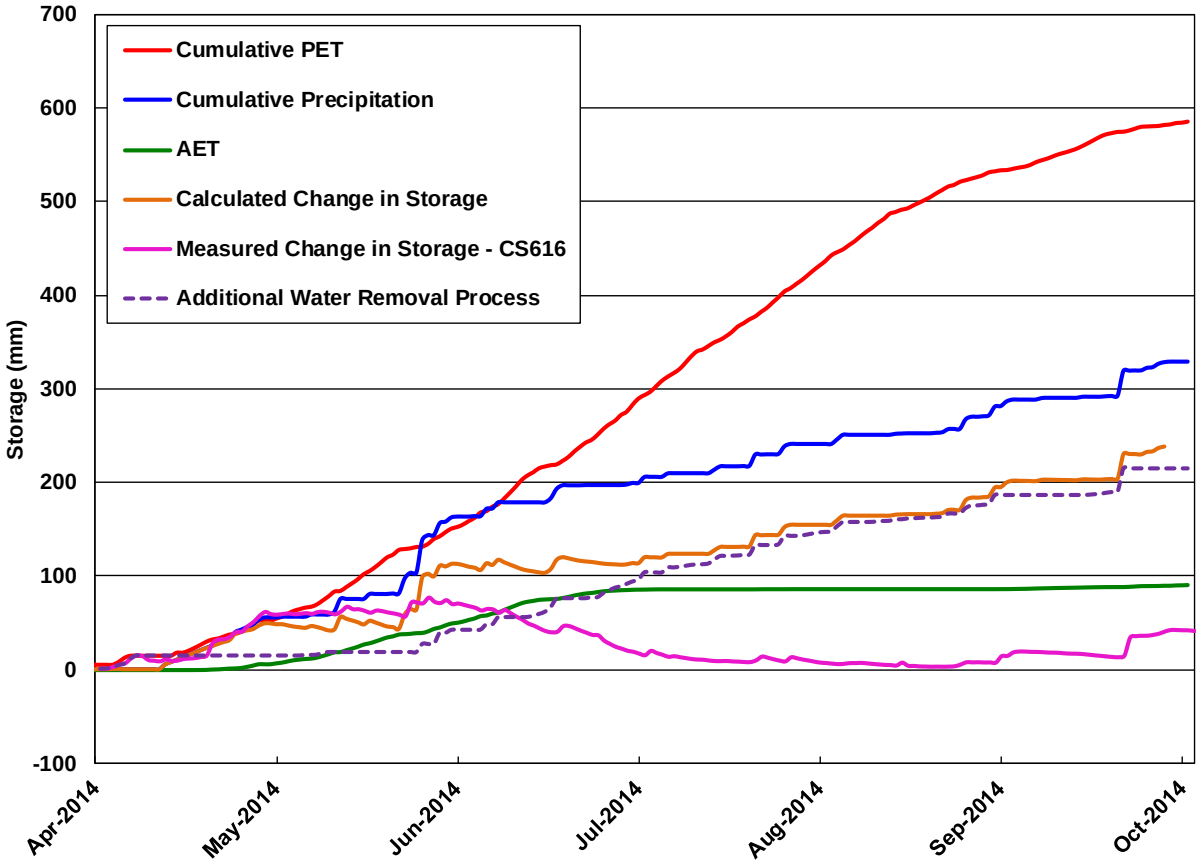

Figure 5.18 Water balance for Deep Cover System, 2014 monitoring year.

Table 5.3 shows that the additional water removal (AWR) in the water balance formulation for the Deep Cover System as a function of the PET and precipitation which occurred at the site.

Table 5.3
Moisture Loss Not Accounted by Water Balance – Deep Cover Sytem

Year	Total AWR (mm)	Total Precipitation (mm)	Total PET (mm)	AWR as Percentage of Precipitation (%)	AWR as Percentage of PET (%)
2006	140	341	692	41	20
2007	231	364	675	63	34
2008	293	392	596	75	49
2009	177	272	608	65	29
2010	201	307	632	65	32
2011	197	265	632	74	31
2012	239	424	613	56	39
2013	270	387	634	70	43
2014	215	328	603	60	36

Similar results comparing the AWR to the precipitation were observed at the Deep Cover System in that 60-75% of all precipitation is lost to the AWR process and is not captured in the water balance.

A comparison between the AWR measured at both the Shallow and Deep cover system is presented in Figure 5.19. Generally speaking, the Shallow Cover System showed higher values for AWR as compared to the Deep Cover System, however, both cover systems showed similar trends. It is hypothesized that a larger volume of bypass flow is occurring at the shallow cover since casual measurements of cracking was observed to occur to depths of 25 cm, which represents approximately half the depth of the cover system but less than a quarter the depth of the deep cover system. As a result, any excess water entering the crack system on the surface of the Shallow Cover System would percolate/infiltrate more rapidly through the remaining cover system profile than at the Deep Cover System. The observations of cracking at the surface of each cover system were performed on a casual basis, and a more extensive crack survey may reveal deeper cracks which penetrate the entirety of the Shallow Cover System. Other unaccounted moisture/water loss streams may include runoff and percolation, which would be reflected in the AWR and were not captured in the water balance monitoring equipment.

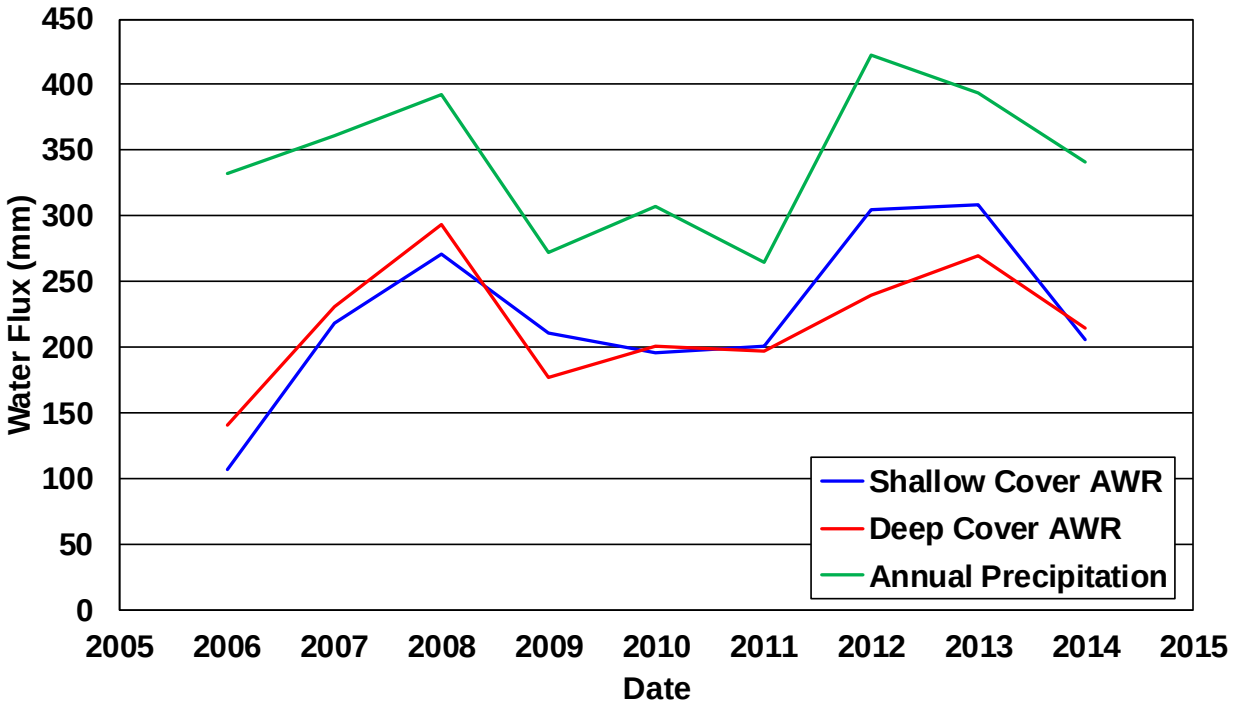

Figure 5.19 Comparison of AWR measured at Deep and Shallow Cover Systems

5.2 Bulk Air Permeability

A bulk air conductivity was determined used the equation presented by Freeze and Cherry (1979) was modified by substituting conductivity for permeability for use in this study and is reflected in Equation 2.5. The resulting bulk permeability values are presented in Table 5.4.

Table 5.4
Bulk Air Conductivity at Each Cover System

	Bulk Air Conductivity (m/s)
Shallow Cover System	3.7×10^{-5}
Deep Cover System	1.9×10^{-4}

It would be expected to see higher air conductivity at the Shallow Cover System as opposed to the Deep Cover System due to a smaller profile being more susceptible to evaporative drying; however, the results indicate that the air conductivity of the shallow system is actually lower than the Deep System. The reason for this is not known, as the tests were conducted during periods of similar moisture content and at similar depths but may be due to variations in soil properties on a small scale due to the nature of the permeameter tests being point investigations. Investigation of air conductivities across larger areas to determine a larger sample size may alleviate this discrepancy.

5.3 Air and Soil Water Content Profile

The saturation vapour pressure (P_{sat}) is only a function of temperature. The ratio the actual vapour pressure (P_{vap}) to P_{sat} is the relative humidity (RH). The maximum amount of water that could be removed for a volume of dry air entering the cover would be the mass of water (per unit volume of air) required to bring that initial dry air up to a saturated vapour pressure (*i.e.* RH=100%). Once the air entering the soil was at vapour saturation then any further drop in temperature would result in condensation. Generally speaking, the pore air within soil profiles are assumed to be at a RH of 100%. Reducing the RH below 100% would require that the suction exceed levels capable of being measured accurately by the suction sensors based on the Lord Kelvin equation (Wilson et al.,

1997). Representative values of saturation and actual vapour pressure can be calculated from the *in situ* monitoring sensors (temperature and suction) from each cover system. Both cover systems show development of suctions in the rooting zone which indicate moisture content falls below the wilting point of the respective soil materials.

5.3.1 Ambient Air and Soil Air Moisture Availability

The ambient air properties were used in order to estimate the saturated vapour pressures using Equation 3.1. This same method was used in combination with soil temperature profiles from automated monitoring sensors to calculate the saturation vapour pressure in the soil voids.

The vapour pressure of the ambient air was determined using available temperature and RH data, averaged on a daily basis. Relative humidity of the air in the soil voids was assumed to be 100% due to measured suction values indicating lower than wilting point for the duration of the field period. Using this information to determine RH, the actual vapour pressure of the soil can be determined using Equation 3.2.

The moisture removal potential of a parcel of air passing through the cover system is dependent on the difference between the saturated and actual vapour pressures of said parcel of air. Working with these assumptions, the soil moisture availability for the shallow cover system and deep cover system through the 2013 monitoring year was calculated by determining the difference between the P_{sat} of the air in soil voids, and the P_{vap} of the ambient air. The value for P_{sat} in the cover systems was calculated at the base of each cover system based on the measured temperature; this location and method was selected due to uncertainty with calculation of RH from the soil suction sensors, and to remove uncertainty with non-uniformity of the cover system moisture profile. This difference represents the additional moisture required to bring the moisture conditions of the ambient air to equilibrium with the air in the soil voids.

For example, on June 5, 2013 the average air temperature was 15.6^{o}C with an average RH of 0.77, which when used in conjunction with Equations 3.1 and Equation 3.2 results in a vapour concentration in the air of 8.99 g/m^3. In addition, the average soil temperature as measured by the CS229 sensors was 18^{o}C. The soil moisture availability at this temperature, calculated using Equation 3.3 with the average soil temperature, showed that the water concentration in the air

within the soil voids was an average of 9.5 g/m^3. The maximum available moisture for removal is the difference between the ambient air vapour concentration and the saturated soil vapour concentration; this would bring the two values into equilibrium. As such, in this example the difference between the soil vapour concentration and ambient air concentration is approximately 0.5 g/m^3.

The resulting moisture availability coupled with calculations of airflow presented in Section 5.5 can be used to determine the total moisture loss due to airflow across the system. The moisture availability for the shallow and deep cover systems are presented in Figure 5.20 and Figure 5.21 for the 2013 monitoring years, respectively.

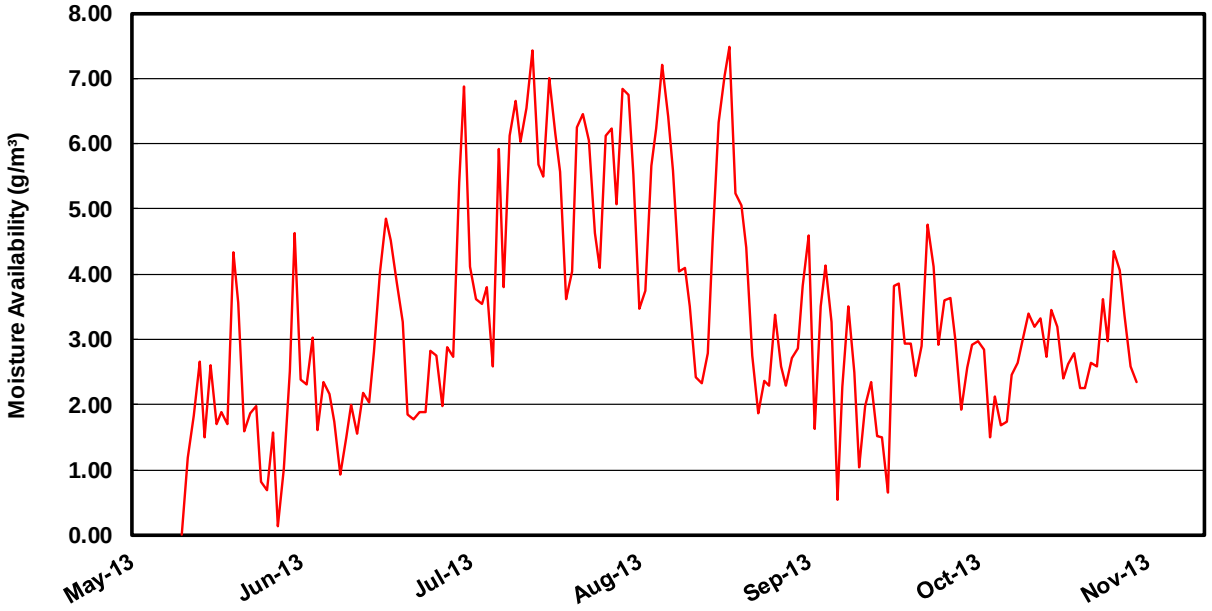

Figure 5.20 Shallow cover system moisture removal potential during 2013.

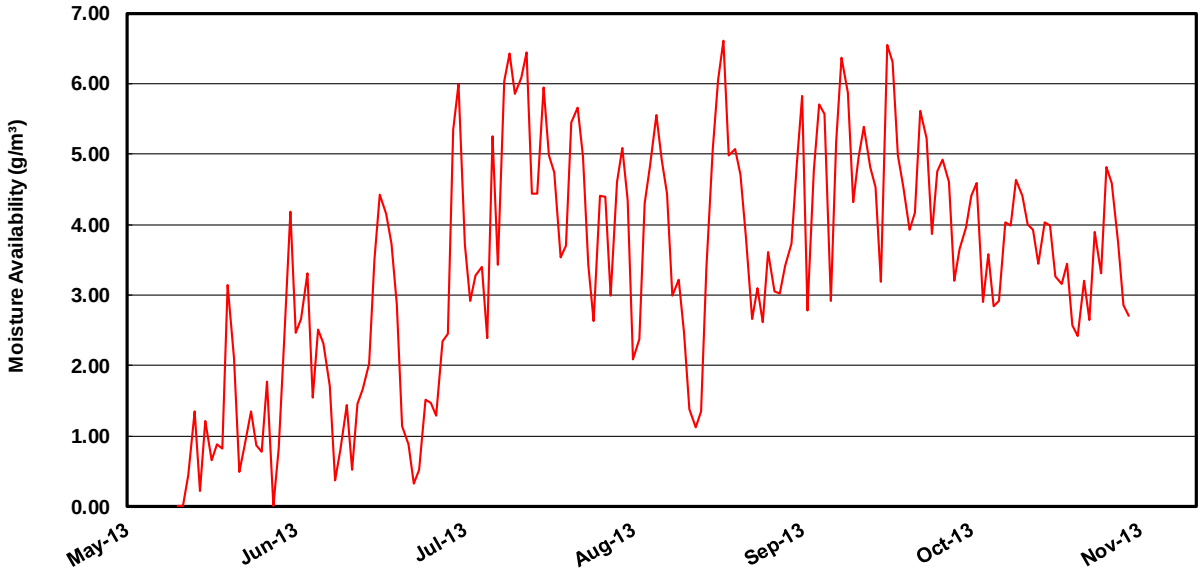

Figure 5.21 Deep cover system moisture removal potential during 2013.

The Shallow Cover system was consistently warmer than the Deep Cover system throughout the majority of the summer. Therefore, the shallow cover system inherently presents a better opportunity for moisture removal via airflow than the deep cover system when experiencing the same airflow rates.

5.4 Convective Airflow System Conceptual Model

In this study it is hypothesized that convective airflow from the atmosphere into and through the covers may be the cause of the observed AWR calculated from the water balance. The mechanism driving this airflow is not defined but two potential mechanisms include both free convection as well as forced convection. Free convection could be occurring due to the density contrasts between the cooler air within the coke and the warmer atmospheric air combined with the steep sand dyke slope. Forced convection would be caused by a loss in the volume of air in the coke below the covers as a result of the reaction between oxygen from the atmosphere and methane released by the underlying tailings. In order to undertake an evaluation of the potential airflow, only the vertical flow through the lower permeability cover system within the CBIW is interpreted quantitatively. A full exploration of whether the airflow is due to free or forced convection is outside the scope of this thesis and will be left to future research.

Due to the fact that the differential pressure cycles coincide with the temperature cycle, it suggests that the differential pressures and resultant airflow are linked to the temperature variations (advective airflow) rather than chemical reactions (forced airflow). However, this does not discredit the potential for forced airflow entirely, and also does not eliminate the possibility that the temperature of the stored coke was unaffected by chemical reactions in the subsurface, and further investigation is still warranted.

5.5 Calculation of Convective Airflow

The presence of actual airflow versus the theoretical presence based on temperature and density gradients is heavily reliant on the soil air permeability. The permeability of the soil to air is lowest in early summer due to a high soil VWC, and is greatest in late summer due to a low VWC as a result of continual drying throughout the summer months. Due to the difficulties in determining changes in the density profile within the column of air due to dynamic temperature and pressure changes, the analysis of airflow was simplified as a preliminary evaluation for the potential for airflow drying. The analysis is based on the measured values of differential pressure presented in Section 4.2, which is taken at a constant elevation assuming that the density profile between the measurement points (surface and subsurface) is not affecting flow.

5.5.1 Estimate of Airflow Rates

Using the differential pressure data shown in Section 4.2 in conjunction with the average bulk air permeability determined in Section 4.3, an estimate of airflow rates through the cover system can be calculated for each differential pressure monitoring location using Equation 2.3. It should be noted that the soil VWC is measured at the centre of each cover system (S02 and D02), whereas the differential pressure is measured at three locations. For the purposes of this calculation, it is assumed that the measured VWC at the centre of the cover systems represent the water content distribution across the entire cover system. It is likely that the moisture conditions varied in space across the cover system, and as such, the air permeability may not have been accurately represented at the outlying S01, S03, D01, and D03 monitoring locations.

For example, using 2.3, an assumed bulk air conductivity for the shallow cover system of 3.7×10^{-5} m^2, a density of air of 1.19 kg/m^3, a barometric pressure of 97.0 kPa, ambient temperature of

20ºC, ambient RH of 70%, a vertical distance of 0.3 m, and a differential pressure of 10 Pa as follows:

$$f_g = 3.7\ x\ 10^{-5}\frac{m}{s} * \left(\frac{10\ Pa}{0.3\ \text{m} * 9.81\frac{\text{m}}{s^2} * 1.19\frac{\text{kg}}{m^3}}\right) = 1.07\ x\ 10^{-4}\frac{m}{s}$$

results in a calculated airflow rate of 1.07 x 10^{-4} m/s, or when applied over an area of 1 m^2, 9.21 m^3/day.

The results for the 2013 monitoring year are shown in Figure 5.22 and Figure 5.23 for the shallow cover system and deep cover system, respectively.

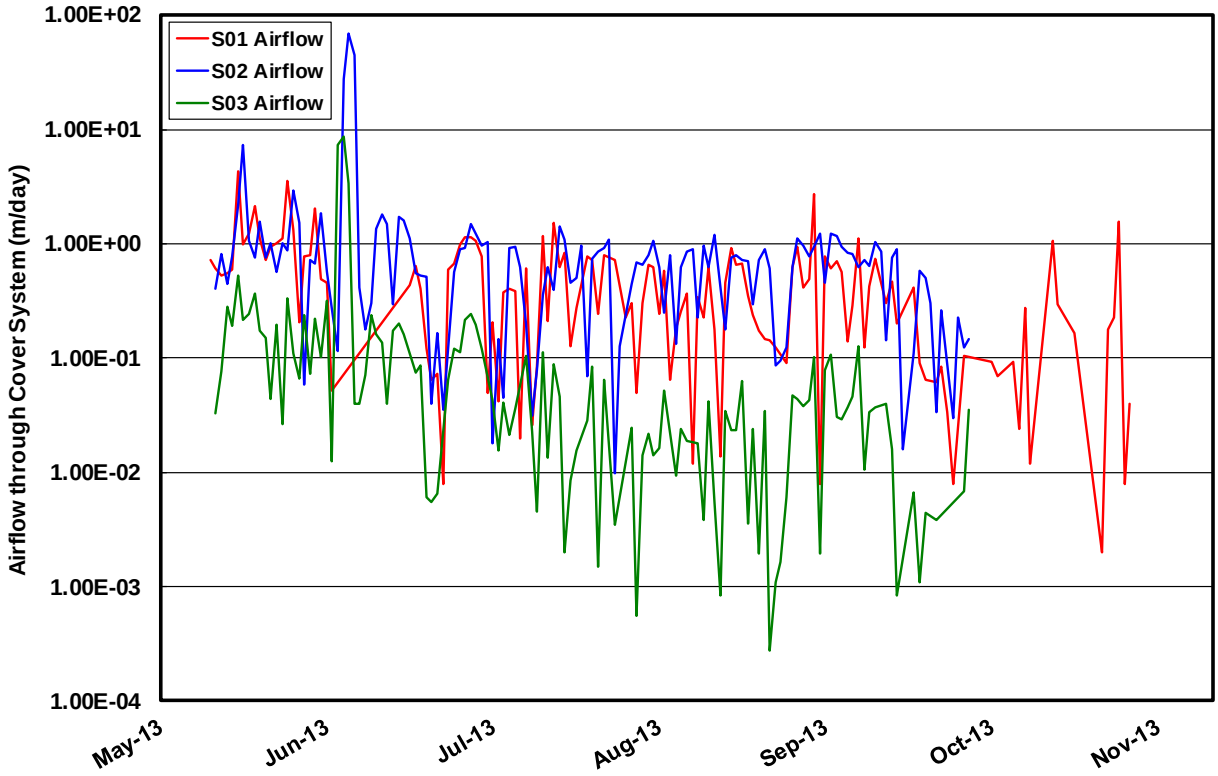

Figure 5.22 Calculated shallow cover system downward airflow rates, 2013

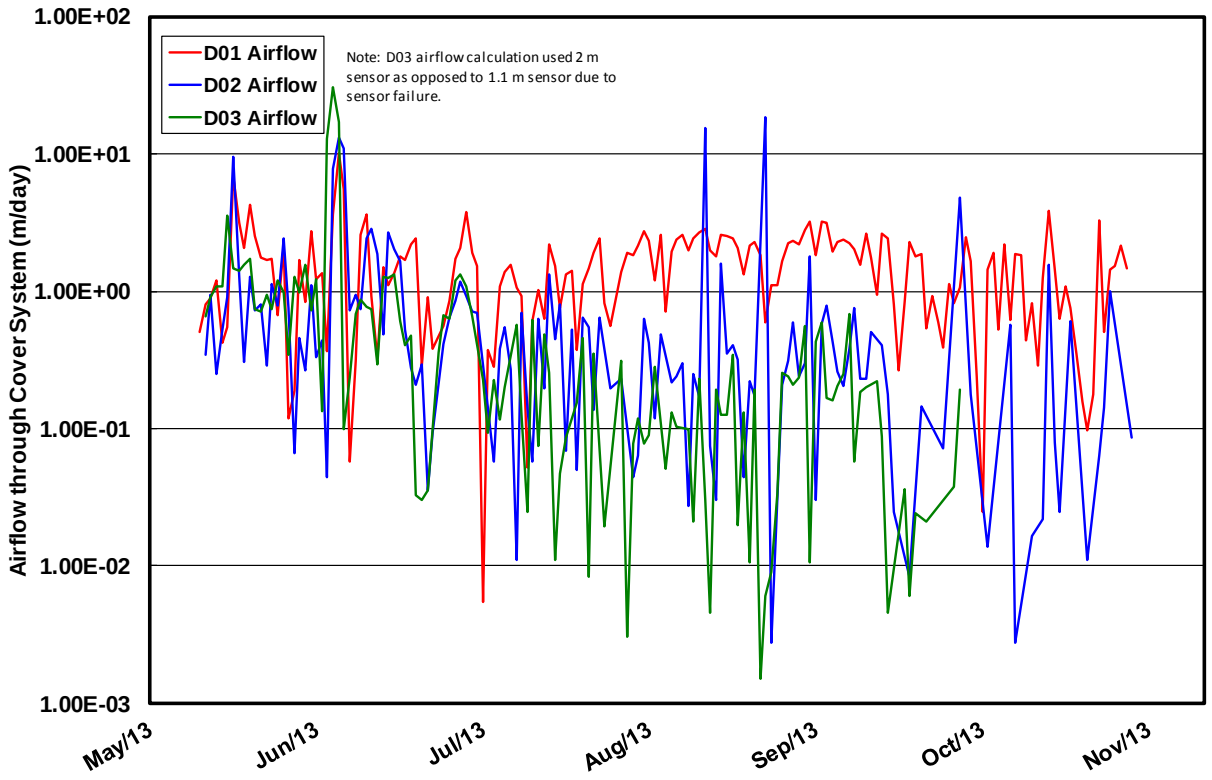

Figure 5.23 Calculated deep cover system downward airflow rates, 2013

Under similar differential pressures/permeabilities relative to their monitored depths, the calculated airflow rates at both the deep and shallow cover systems should be similar. However, the Deep Cover System showed a higher calculated airflow rate due to a higher bulk permeability than the Shallow Cover System. A sensitivity analysis is presented in Section 5.6 to investigate the effects of higher air conductivities on both cover systems and to determine the effects on potential moisture removal under variable conditions.

5.5.2 Airflow Induced Moisture Removal

In order to calculate the potential moisture removal via airflow, it was necessary to assume instantaneous equilibrium of soil moisture to air moisture within the soil voids, and that a downward moving parcel of air was unsaturated at the point of entering the cover system, and was saturated following departure from the voids of the cover system (difference between saturated vapour pressure and actual vapour pressure is representative of soil moisture removal). This

assumption, although potentially not truly representative of field conditions, would allow for estimation of the maximum moisture removal due to airflow across the cover systems.

The calculated maximum potential moisture removal rates were based on the calculated airflow and the moisture removal potential previously discussed in Sections 5.5.1 and 5.3.1, respectively. These values are calculated based on the assumed conditions within the cover system and the assumed properties of the air used in calculating the airflow and moisture removal potential and can be found in Figure 5.24. The estimated moisture removal rate is calculated as shown in Equation 3.3. The results are converted into units of millimetres following the calculation to maintain consistency with the units in the water balances. The results are presented in Figure 5.24 and Figure 5.25 for the 2013 monitoring year for the shallow cover system and deep cover system, receptively.

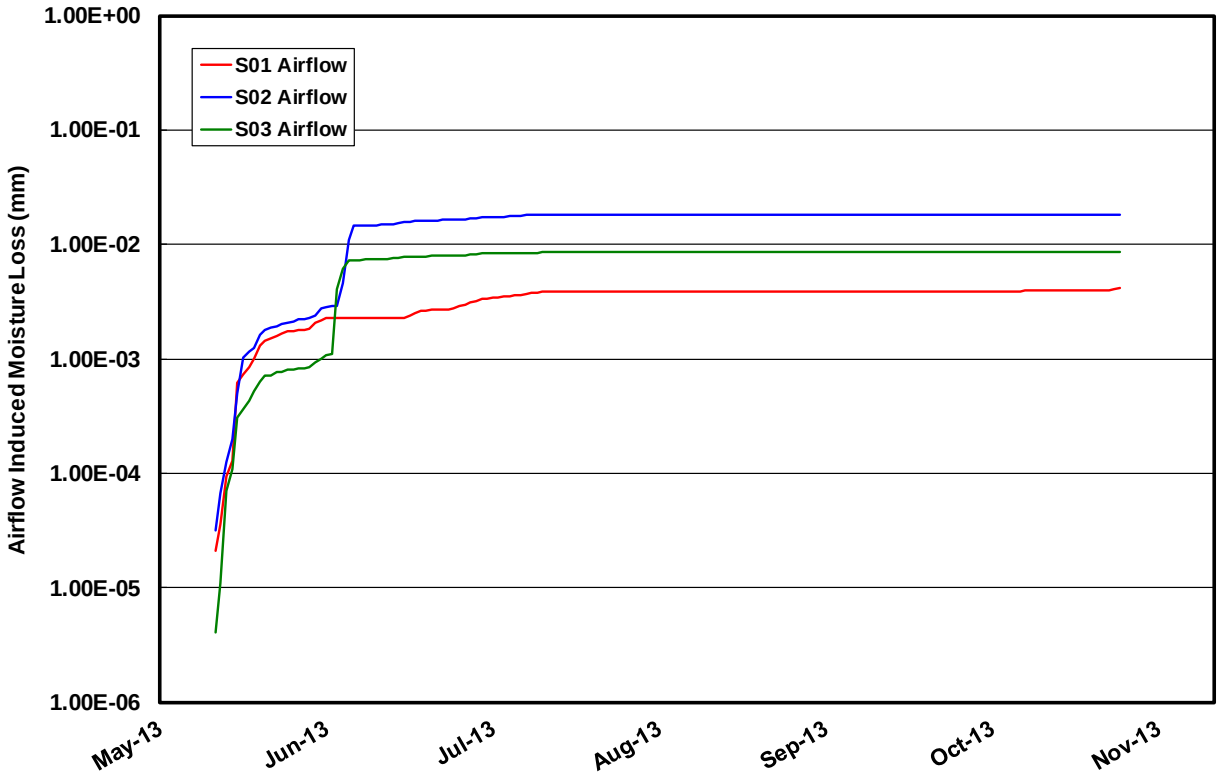

Figure 5.24 Calculated cumulative maximum moisture removal potential using calculated airflow and moisture removal potential – shallow cover system

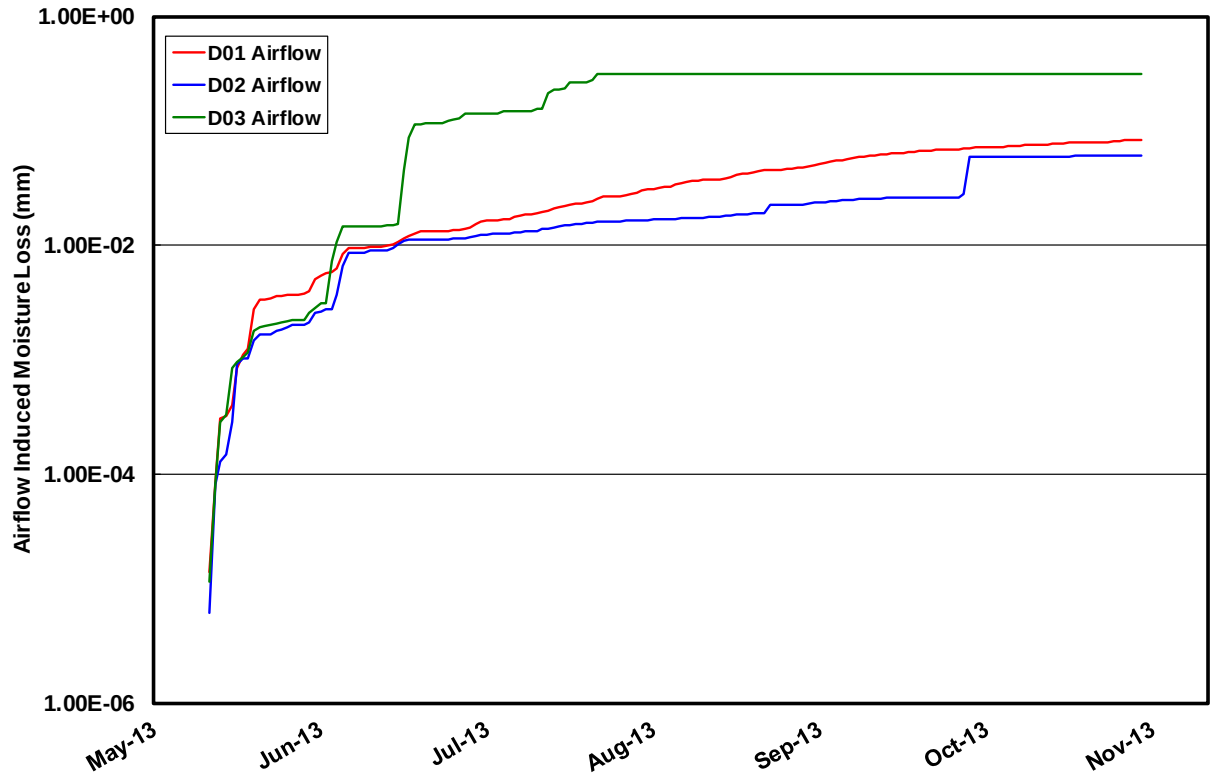

Figure 5.25 Calculated cumulative maximum moisture removal potential using calculated airflow and moisture removal potential – deep cover system

As can be seen, the majority of moisture removal from both the shallow and deep cover systems occurs in June/July, while at the deep cover system it occurs in August/September. However, due to the low permeability of the cover system resulting in low airflow rates, the overall moisture removal rates were several orders of magnitude lower than the overall moisture availability in the system. The overall low airflow rates and low potential for moisture losses associated with the airflow across each cover system indicate that the hypothesis that convective airflow is the primary cause of the enhanced drying of the cover systems is proven false, and the unaccounted moisture loss in each system is likely attributed to another outside influencing factor. Alternatively, the convection rates may be underestimated as a result of limited permeability data.

5.6 Convective Drying Sensitivity Study

An analysis was performed which increased the measured permeability by two orders of magnitude (100 multiplication factor) and three orders of magnitude (1000 multiplication factor) to determine the effect on the moisture removal rates as they pertained to the water balance. This allows us to

determine what airflow rates would be required to cause the increase in moisture removal observed at each cover system.

In both cases of the shallow cover system and deep cover system, an increase in permeability of three orders of magnitude is unlikely and represents a large deviation from the conditions observed during field observations; however, the analysis is intended to represent what is required for convective moisture removal to have a significant effect on the cover system moisture conditions. Given the highly variable moisture content of the cover system, a variable permeability is highly likely throughout the summer, and may result in additional losses from the cover system depending on local weather conditions. These additional losses when considering a variable permeability, coupled with increase percolation due to macro-pore formation, or additional runoff not accounted for in the water balance may contribute to a more accurate water balance formulation.

The results of the water balance formulation considering the increase in average permeability are shown in Figure 5.26 and Figure 5.27 for the shallow cover system and deep cover system respectively.

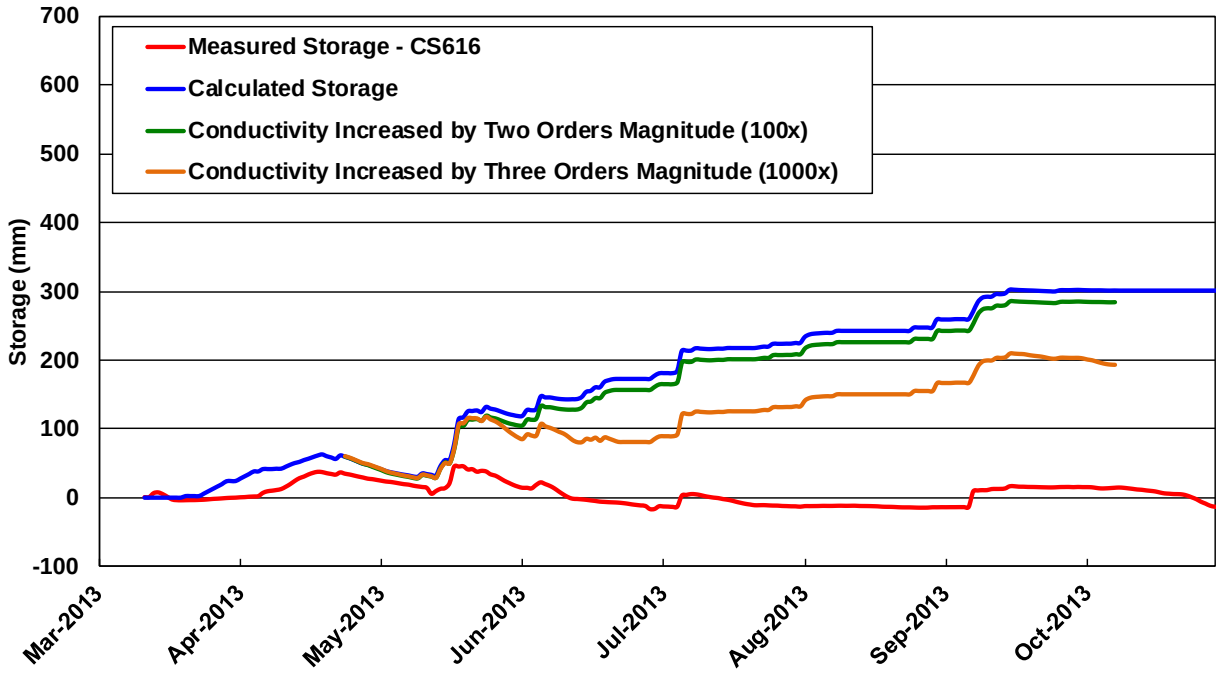

Figure 5.26 Water Storage assuming increased permeability at shallow cover system, 2013 monitoring year

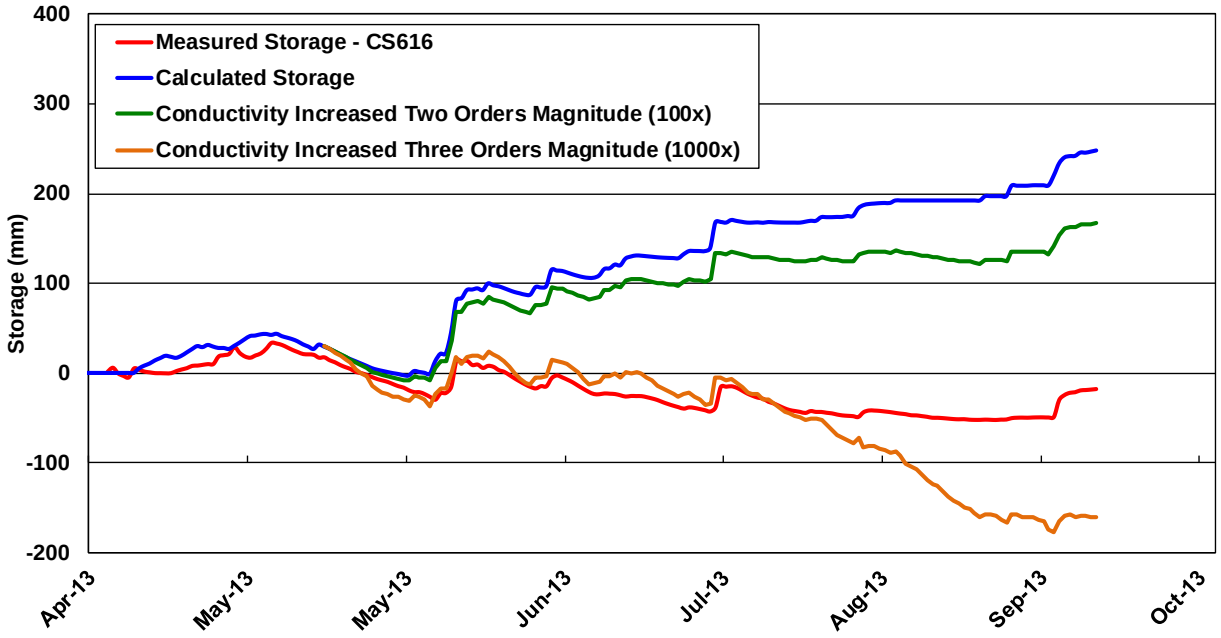

Figure 5.27 Water storage assuming increased permeability at deep cover system, 2013 monitoring year

Increasing the hypothetical permeability of each cover system by two orders of magnitude did not increase airflow rates sufficiently to have a substantial impact on moisture removal rates, and thus did little to affect the water balance.

At the shallow cover system, an increase of three orders of magnitude, or equivalent to increasing the permeability by 1,000 started to show calculated storage values decrease towards the measured storage values, indicating that further increases in permeability would be required to further calibrate the water balance. The general shape and trends of the calculated storage using a three order of magnitude increase on the permeability value matches that of the calculated storage curve, and it is likely that if the hypothetical permeability were increased by another 1,000, convergence of the two curves would be likely.

At the deep cover system, a three order of magnitude increase to the measured permeability value resulted in a near match of the calculated storage and measured storage values until the end of July. At this point, the increased permeability resulted in airflow rates which removed more moisture than was required to allow for convergence of the measured and calculated storage values.

The broad application of a standard increase in permeability does not represent true conditions in the field and does not account for changes in rainfall and soil moisture throughout the summer. In addition, daily permeability values will change as a result of changes in moisture conditions, thus further complicating the analysis.

A sensitivity analysis on the bypass/runoff during major storm events was carried out in order to investigate the effect the potential increased infiltration/bypass flow may have on the water balance formulation. Included in this sensitivity analysis was an increase in the permeability of the cover system by a factor of 400 to determine what airflow rates would be required in order to remove sufficient moisture to "close" the water balance formulation.

It was noted that changes in soil VWC coincided with major storm events (*i.e.* those exceeding 5 mm in a 24-hour period), however, minor storm events (*i.e.* those less than 5 mm in a 24-hour period) had minor to zero impact on the VWC in the upper 30 cm of the soil profile. This is shown by the comparison of changes in soil moisture content to precipitation events (Figure 5.28).

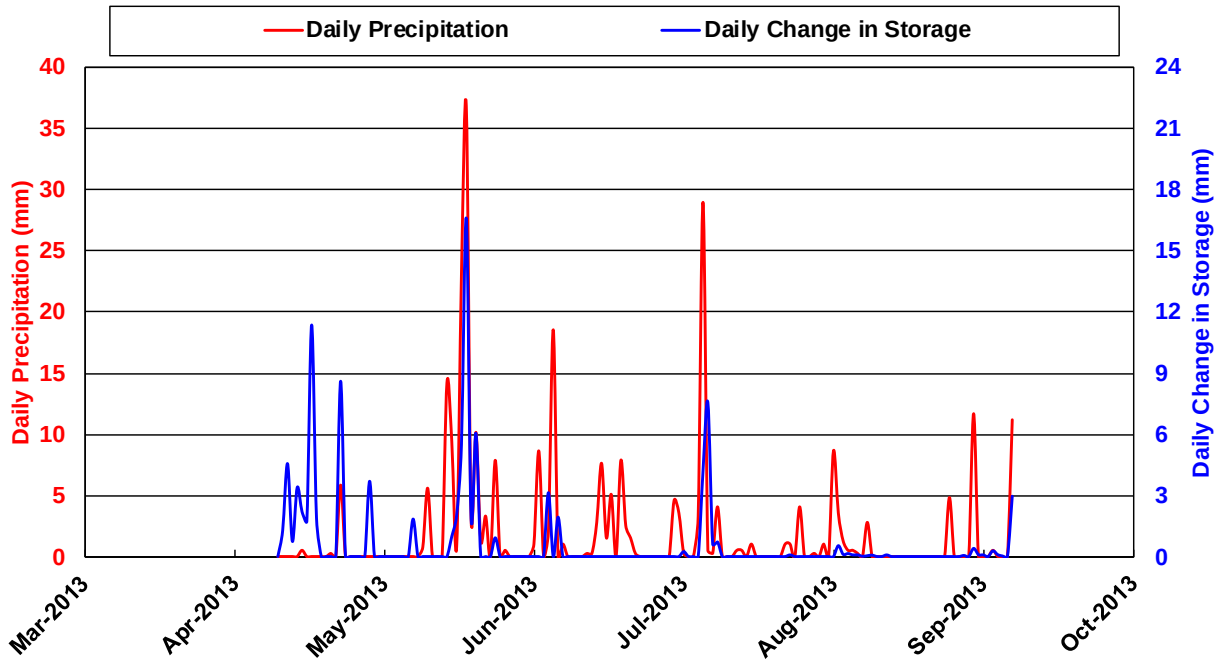

Figure 5.28 Precipitation effects on soil moisture in Shallow Cover System rooting zone.

The major storm events were analyzed on a case by case basis, and the relative changes to soil VWC as a percentage of total rainfall are presented in Table 5.5.

Table 5.5
Comparison of Change in Storage to Precipitation at the Shallow Cover System

Storm Event Date Range	Change in VWC versus Precipitation (%)
June 5 through June 13, 2013	32.3
June 26 through June 28, 2013	15.2
July 4 through July 14, 2013	0
July 27 through July 31, 2013	35.3
August 25 through September 1, 2013	11.9

Based on the above information, the sensitivity analysis was carried out assuming that for all storm events aside from those listed above, any precipitation in excess of that already accounted for in the water balance will bypass the cover system through other processes (macropore flow or runoff), while for those storm events listed above the bypass rate will be calculated using the fractions listed in Table 5.4.

The resulting water balance formulation including the increased airflow capacity is presented in Figure 5.29.

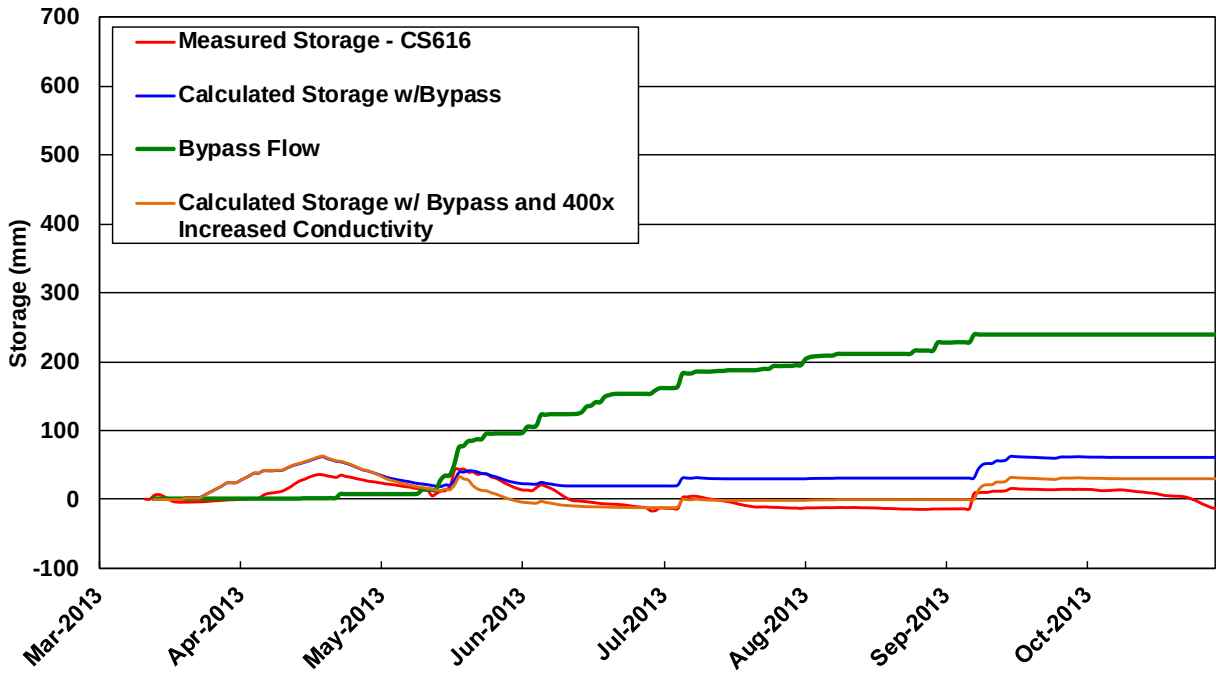

Figure 5.29 Increased infiltration and airflow rates sensitivity analysis – shallow cover system.

The results seen in Figure 5.29 show that the large rainfall events had a substantial impact on the overall water balance; the blue line representing the newly calculated storage minus the bypass

flow shows a much better correlation with the measured storage. In addition, by increasing the permeability of the cover system by a factor of 400 in conjunction with the new consideration for bypass water flow, it allows for a good correlation of calculated storage with the measured storage, indicating that the airflow at this permeability condition would be sufficient enough to have an impact on the moisture condition of the cover system. An increase in permeability of this level is not entirely unfeasible, as the cracking observed in the cover system would allow for such an increase; in addition, variations in cover system moisture content may allow for increased permeability throughout the summer season; a detailed permeability monitoring system would be able to verify this hypothesis.

Chapter 6
Summary and Recommendations

Soil covers at Syncrude Canada's Coke Beach Instrumented Watershed have appeared to undergo greater water losses than can be accounted for from calculations of AET since cover construction in 2004. These additional water losses appear to also be linked to drying of the cover to levels below water contents associated with wilting point. Preliminary investigations hypothesized that the enhanced drying effect was a result of convective airflow of dry atmospheric air in through the covers, causing enhanced evaporation. As outlined in Chapter 1, the purpose of this investigation was to

- Design and implement a field monitoring system to determine the presence, or lack there-of, of this downward airflow cycle and to account for the changes in the internal moisture storage of the cover system.
- Design and install additional field instrumentation to identify the presence and magnitude of airflow through the cover profiles at the CBIW. This instrumentation is to include differential air pressure and barometric pressure monitoring.

The field data was subsequently analyzed using a variety of analytical methods to assess the potential for convective airflow and subsequent enhanced water removal from the cover systems.

6.1 Cover System Instrumentation.

Watershed monitoring instrumentation was installed by O'Kane Consultants Inc. in 2004 as part of the initial cover system construction. This included:

- Meteorological monitoring instrumentation which measured precipitation (rainfall), relative humidity, temperature, wind speed, and net radiation. This data was compared and verified with the Fort McMurray International Airport data.
- Soil moisture content using CS616 time domain reflectometry probes. Water contents measured in the soil cover systems were measured adequately during the field observation period, and there was a sufficient amount of data to verify the moisture conditions in each of the cover systems. The water content sensors proved to be a valuable tool to assess the

water balance and in-system moisture transfer processes. Using the moisture content sensors in conjunction with meteorological sensors, a detailed water balance was generated, the moisture removal potential of migrating airflow was calculated, and the impact of the enhanced evaporation from was pinpointed throughout all monitoring years.

- Soil suction and temperature was measured using CS229 thermal conductivity sensors. The soil matric potentials measured by these sensors were utilized to calculate soil RH which proved to be a vital component of calculating the moisture removal potential of air moving across the cover system. In addition, the temperatures measured provided a valuable tool to present a conceptual understanding of airflow dynamics in the subsurface and contributed to calculating the density of air in the subsurface which was utilized to calculate a density gradient across the cover system and thus relative direction of airflow movement.

In order to quantify the potential for airflow across the cover system, the author of this thesis installed the following additional instrumentation:

- The barometric pressure monitor installed by the author recorded data on a regular basis and was successfully used in the investigation. The sensor proved to be a valuable tool to benchmark the ambient and subsurface air densities.
- Differential pressure sensors and dataloggers which tracked the difference in pressure gradients from the ambient atmosphere relative to the subsurface. In total, 18 sensors were installed at the cover system; however, in reviewing the data the most valuable results proved to be from the sensors installed at 2 m below the surface of the cover systems. It was this sensor which coincided with the air mass representative of the deep temperature gradients and thus driving force behind any air temperature driven movement in the system. When using this sensor coupled with the soil monitoring stations installed by OKC the airflow across the cover system was determined successfully and applied to the water balance via moisture transfer processes.
- Despite being successful at measuring uni-directional differential pressure, the differential pressure monitoring system was limited in that it could not measure upward movement (bi-directional) airflow. In order to investigate the potential for bi-directional flow, the differential pressure sensors were reversed in 2014, and were only capable of measuring

upward airflow gradients. During this period, minimal pressure gradients indicated upward airflow, and as such, it is not likely that reversal of flow conditions occurred frequently. However, in order to improve similar monitoring systems in the future, bi-directional sensors would be ideal, and would allow for continuous monitoring of flow in both directions.

- Measured differential pressures in 2013 generally showed diurnal trends, with little to no differential pressure measured at night (DP=0 Pa), while during the day, negative differential pressures varied from as low as 0 Pa to over 60 Pa.
- Measured differential pressures in 2014 were limited to only a few instances of values not equivalent to 0; however, several of these values did reach differential pressures of 60 Pa at instantaneous points in time. That is rather than a gradual increase, point measurements of high differential pressures were measured. These may be attributed to sensor error due to the lack of correlation with preceding measurements.
- Air permeability testing was successfully performed with results comparing to previously measured values determined at the point of development of the air permeameter. The method developed by Rodgers (2008) was successfully adapted to the AMS International sampling system in conjunction with measurements from the differential pressure sensors to measure air permeability's at both cover systems. When coupling the measured data with known VWC values at the time of measurement, a broad, full scale volumetric air content/permeability function was calculated and applied to airflow calculations. This allowed for dynamic calculations of airflow throughout the 2013 monitoring season and contributed to the successful determination of airflow enhanced moisture removal from the cover system.
- Air permeability measured as part of this thesis correlate with previous measurements made by Rodgers (2008) at the same cover system. Measured permeabilities at the shallow and deep cover system were found to be in the range of 10^{-10} to 10^{-11} m^2. The permeability measured at a depth of 30 cm in the shallow cover was approximately 1 order of magnitude lower than the other measurements made at the same time at other locations, as well as when compared to Rodgers (2008). This result may have been due to differences in soil water content at the time of measurement, but also shows the wide range of permeabilities

across the cover system. A detailed investigation of variable permeabilities would allow for the convective airflow model to be refined and more accurately calculate airflow rates.

6.2 Field Measurements Assessing Airflow across Cover Systems

The differential pressure sensors installed on the cover systems were successfully used to measure pressure gradients across the cover system and were vital in measuring field air permeability. Compared to published papers and case studies, the measured differential pressures at both cover systems indicated a high potential for a convective airflow system to exist due to the presence of high differential pressures across a relatively small vertical distance.

Airflow rates across the cover system were then calculated using a modified version of Darcy's law combined with a dynamic cover system permeability calculated from field testing and field measurements. Airflow rates occurred across the cover system throughout the year at both cover systems, however, when combined with moisture availability in the soil it was shown that the airflow rates were insufficient to cause any effective enhanced moisture removal which would explain excess moisture losses in either cover system. The measured airflow rates at the shallow cover system and the deep cover system showed similarities, in that daily airflow rates varied between 0 m^3/day to approximately 50 m^3/day at peak flow periods; however average airflow rates at each cover system and at all monitoring points was between 1 m^3/day and 2 m^3/day. The low average airflow rates proved to be insufficient to remove water from the cover system when using the constant air conductivity value measured for each cover system. However, application of a dynamic air conductivity based on measured suctions and VWC may affect calculated airflow rates substantially and would be more representative of the dynamic water content within the cover system throughout the year.

The lack of evidence for convective airflow affecting moisture in the cover systems suggests that there is an alternative process occurring within the systems which is affecting the moisture availability in the soil. This is proven by the fact that the water balances for the systems do not account for a large portion of moisture removal required to match calculated storage and measured storage values.

Based on this conclusion, there may be another process occurring which is causing the enhanced drying of each cover system. The presence of forced convection via the occurrence of chemical reactions of the underlying coke with oxygen rich atmospheric air may be contributing to the enhanced drying being observed. Although temperature/density gradient data indicates that the advective airflow process is possible, it does not fully discredit the presence of forced convection. Further research at the site will be required to determine the cause of this enhanced drying.

6.3 Research Refinements and Future Research Potential

The water balance in both cases of the shallow and deep cover systems could be further refined to be more inclusive of runoff, however, the purpose of this thesis is to prove the presence of convective airflow. It was proven that convective airflow within the system is likely not a contributing factor to moisture losses unless a more thorough study of cover system permeability rates indicates that a larger permeability is present than those which were measured during this thesis. This was determined effectively using *in situ* differential pressure sensors. With very low instrumentation costs, the differential pressure was measured and combined with standard cover system monitoring equipment to provide a more comprehensive understanding of water flow processes in an otherwise complex system. The lack of evidence for convective airflow enhanced moisture removal can be used to remove one possibly cause of the enhanced moisture removal processes seen at the cover systems. The system can be used effectively at other locations to perform similar analyses and may be used to measure moisture removal as a result of airflow processes effectively at locations where cover systems are constructed with more permeable materials such as sand or gravel. In future usage, the airflow monitoring system can be further refined with the inclusion of more research opportunities:

- Other contributing processes to the airflow in the system, such as chemical reactions with the stored coke (oxygen consumption processes). This may be performed by measuring gas chemistry profiles in the subsurface to determine oxidation/degradation rates of various known constituents (*e.g.* Methane, oxygen) and use the variable concentrations to determine potential for convective cycles via density gradients.

- Inclusion of bi-directional differential pressure sensors at multiple locations across the cover system to account for the potential of air rising through the cover systems as well as the potential for downward migration simultaneously.
- Monitoring of RH in soil voids continuously using sensors specific to that purpose; this would alleviate issues with the current suction sensors and the limited range available using these sensors for determination of RH.
- Development of a numerical modelling program to determine a daily change in permeability due to soil moisture content affecting permeability of the soil to air will further refine the conceptual model of convective airflow at the CBIW. Numerical modelling will allow for inclusion of regular changes to soil VWC and the ability to compare these changes to measured changes in the field. In addition, numerical modelling will allow for variations in permeability as a function of VWC, more accurately representing the true variable nature both spatially and temporally of soil cover system conditions. Drier periods would show higher permeability to soil, while periods seeing more rainfall would show lower permeabilities.
- Measurements and regular monitoring of bulk air permeability across more locations on the cover system to assess variable air conductivities as a function of spatial location and the effect on potential airflow based on variable air conductivities. If a higher permeability is measured across the cover system, this would lead support to the original hypothesis as the pressure gradients are substantial enough to indicate the presence of airflow rates to induce enhanced drying under higher permeability conditions.

The overall water balance method still shows a process for moisture removal that is not being accounted for in using the current field instrumentation, inclusive of the now installed differential pressure monitoring system. In order to more effectively monitor water movement in the system, the following changes to field measurements can be made, and will assist with further research at the project location:

- Inclusion of system to quantify runoff, interflow, and net percolation/flow bypass across the cover systems to further refine water balance and capture moisture losses more accurately, especially in the case of the deep cover system; and

- Vegetation surveys of the trees planted on the cover system to identify the extent of impact the enhanced drying has had on the overall reclamation efforts.

REFERENCES

Amos, R., Ulrich Mayer, K., Bekins, B. Delin, G., Williams, R. (2005). Use of dissolved and vapor-phase gases to investigate methanogenic degradation of petroleum hydrocarbon contamination in the subsurface. Published in Water Resources Research, Vol. 41.

Arenson, L. U., Chen, J. F., Pham, H., & Sego, D. C. (2007). Laboratory Investigations On Air Convection In Porous Media, (2006), 1836–1843.

Ball, B. C., & Schjønning, P. (2002). *Methods of Soils Analysis Part 4* (pp. 1141 – 1158). Madison, Al: Soil Science Society of America.

Barbour, S. (1998). The soil-water characteristic curve: a historical perspective. *Canadian Geotechnical Journal*.

Bauters, T. W. ., Steenhuis, T. ., DiCarlo, D. ., Nieber, J. ., Dekker, L. ., Ritsema, C. Haverkamp, R. (2000). Physics of water repellent soils. *Journal of Hydrology*, *231-232*, 233–243. doi:10.1016/S0022-1694(00)00197-9

Birkham, T. K., M. J. Hendry, and S. L. Barbour. "Advective and diffusive gas transport through fractured sulfur blocks." Vadose Zone Journal 9.2 (2010): 451-461.

Birkham, T. K., Hendry, M. J., Barbour, S. L., & Lawrence, J. R. (2010). Controls and rates of acid production in commercial-scale sulfur blocks. Journal of environmental quality, 39(3), 834-844.

Birkham, T. K., Hendry, M. J., Barbour, S. L., Carey, S. K., Lawrence, J. R., & Lewko, R. (2011). Water flow and storage in fractured, unsaturated sulphur blocks. Canadian Geotechnical Journal, 48(5), 810-825.

Brooks, K., Folliott, P. F., & Magner, P. A. (2013). *Hydrology and the Management of Watersheds* (4e ed.). Ames, Iowa: Wiley-Blackwell Publishing.

Chin, D. A. (2006). *Water Resources Engineering* (2nd ed.). New Jersey: Pearson - Prentice Hall.

Cumulative Environmental Land Management Association. (2006). *Land Capability Classification System for Forest Ecosystems* (Vol. 1).

Doerr, S. H., Shakesby, R. a., & Walsh, R. P. D. (2000). Soil water repellency: its causes, characteristics and hydro-geomorphological significance. *Earth-Science Reviews*, *51*(1-4), 33–65. doi:10.1016/S0012-8252(00)00011-8

da Silva, C., Vargas, E., Sracek, O. 2009. Modeling Multiphase REactive Transport in a Waste Rock Pile with Convective Oxygen Supply. Vadoze Zone Journal 8:1038-1050.

Dunbar, R. B. (2009). Canada ' s Oil Sands - A World-Scale Hydrocarbon Resource, (February).

Fenske, D. (2012). *A study to evaluate the performance of reclamation soil covers placed over an oil sands fluid coke deposit*. Masters Thesis, University of Saskatchewan.

Fetter, C. W. (1994). *Applied Hydrogeology* (3e ed.). Eaglewood Cliffs, NJ: Prentice-Hall Publishing Co.

Fredlund, D.G, & Rahardjo, H. (1993). *Soil Mechanics for Unsaturated Soils*. New York, NY.: John Wiley & Sons Inc.

Fredlund, D.G., Rahardjo, H., & Fredlund, M. D. (2012). *Unsaturated Soil Mechanics in Engineering Practice*. New Jersey: John Wiley & Sons INc. Freeze, R.A., and Cherry, J.A. 1979. *Groundwater*. Prentice-Hall, Inc., Englewood Cliffs, N.J.

Goering, D. J., & Kumar, P. (1996). Winter-time convection in open-graded embankments. *Cold Regions Science and Technology*, *24*(1), 57–74. doi:10.1016/0165-232X(95)00011-Y

He, Q., Wang, R., Wang, W., Xu, R., & Hu, B. (2011). Effect of particle size distribution of PEroleum coke on the properties of PEroleum coke–oil slurry. *Fuel*, *90*(9), 2896–2901. doi:10.1016/j.fuel.2011.03.029

Hockley, D., Kuit, W., & Phillip, M. (2009). Sullivan Mine Fatalities Incident : Key Conclusions and Implications for Other Sites 1, 1–11.

Hu, Y., Vu, H., Hubble, D. 2006. Water content measurement in highly plastic clay using dielectric based probes. NRC Research press NRCC-49260.

Huang, M., Zettl, J., Barbour, S.L., Pratt, D. (2016). "Characterizing the spatial variability of the hydraulic conductivity of reclamation soils using air permeability", Geoderma, doi: 0.1016/j.geoderma.2015.08.014, 262: 285-293

Huang, M., Rodgers, H., Barbour, S.L. (2014). "An Evaluation of Air Permeability Measurements to Characterize the Hydraulic Conductivity of Soil Reclamation Covers", Cdn. J. Soil Sci., doi: 0.4141/CJSS-2014-072, 95(1): 15-26.

Huang, M.B., Barbour, S.L., and Zettl, J. 2010. Draft report: Summary of Cover Performance and Hydrology – Mildred Lake Coke Watershed. A report prepared for Tara Penner, Environmental Research, Edmonton Research & Development, Syncrude Canada Ltd. November 25, 2010.

Johnson, E. a, & Miyanishi, K. (2008). Creating new landscapes and ecosystems: the Alberta Oil Sands. *Annals of the New York Academy of Sciences*, *1134*, 120–45.doi:10.1196/annals.1439.007

Keshta, N., Elshorbagy, A., & Barbour, L. (2010). Comparative probabilistic assessment of the hydrological performance of reconstructed and natural watersheds. *Hydrological Processes*, *1342*(February), doi:10.1002/hyp.7596

Lu, N. (2001). An analytical assessment on the impact of covers on the onset of air convection in mine wastes. *Conference for numerical and analytical methods in geomechanics*, (August 1999), 347–364.

McKenna, G. (2004). *Sustainable mine reclamation and landscape engineering*. Doctoral Thesis, University of Alberta.

Monteith, J.L. (1965) Evaporation and Environment. Symposia of the Society for Experimental Biology, 1965, Vol. 19, pp.205-34

Massman, J.W. (1989) Applying Groundwater Flow Models in Vapor Extraction System Design. Journal of Environmental Engineering, Vol. 115, No. 1.

Ning, L., & Zhang, Y. (1997). Onset of thermally induced gas convection in mine wastes. *International Journal of Heat and Mass Transfer*, *40*(11), 2621–2636. doi:10.1016/S0017-9310(96)00281-5

O'Kane Consultants Inc. (2004). As-Built Report for the Meteorological Station and Net Percolation Monitoring System Installed at the Mildred Lake Coke Watershed, (690).

O'Kane, M., & Wels, C. (2003). Mine waste cover system design—linking predicted performance to groundwater and surface water impacts. *Sixth International Conference on Acid Rock Drainage*, (July), 12–18.

Olson, M. S., Tillman, F. D., Choi, J. W., & Smith, J. a. (2001). Comparison of three techniques to measure unsaturated-zone air permeability at Picatinny Arsenal, NJ. *Journal of contaminant hydrology*, *53*(1-2), 1–19.

Penman, H. (1948). Natural evaporation from open water, bare soil and grass. *Proceedings of the Royal Society of London*, A(194), S. 120-145.

Phillip, M., Hockley, D., Donald, B., Kuit, W., & Kane, M. O. (2010). Sullivan Mine Fatalities Technical Investigation and Subsequent Risk Management Monitoring.

Phillip, M., Hockley, D., Donald, B., Kuit, W., & Kane, M. O. (2010). Sullivan Mine Fatalities Technical Investigation and Findings. Presented at the 8th International ICARD.

Ritchie, A.I.M., 2003. Oxidation and gas transport in piles of sulfidic material, Environmental Aspects of Mine Wastes, Mineralogical Association of Canada. Vol. 31 73-94.

Rodgers, Heather Alecia. 2008. Tracking changes in hydraulic conductivity of soil reclamation covers with the use of air permeability measurements. A thesis submitted to the College of Graduate Studies and Research. University of Saskatchewan. Saskatoon, Canada

Savenjie, H. H. G. (1997). Determination of evaporation from a catchment water balance at a monthly time scale. Hydrology and Earth System Sciences, 1, 000-000.

Saravanathiiban D.S., Kutay M.E., Khire M.V., 2014. Effect of Macropore tortuosity and morphology on preferential flow through saturated soil: A Lattice boltzmann study. Journal of Computers and Geotechnics 59: 44-52.

Topp, G., Davis, J. L., & Annan, A. P. (1980). Electromagnetic determination of soil water content: Measurements in coaxial transmission lines. *Water Resources Research*, *16*(3), 574–582.

Wallach, R., & Jortzick, C. (2008). Unstable finger-like flow in water-repellent soils during wetting and redistribution – The case of a point water source. *Journal of Hydrology*, *351*(1-2), 26–41.

Wilson, G.W., Fredlund, D.G., and Barbour, S.L. 1997. The effect of soil suction on evaporative fluxes from soil surfaces. *Canadian Geotechnical Journal, 34(1): 145–155. doi:10.1139/t96-078.*

Appendix A

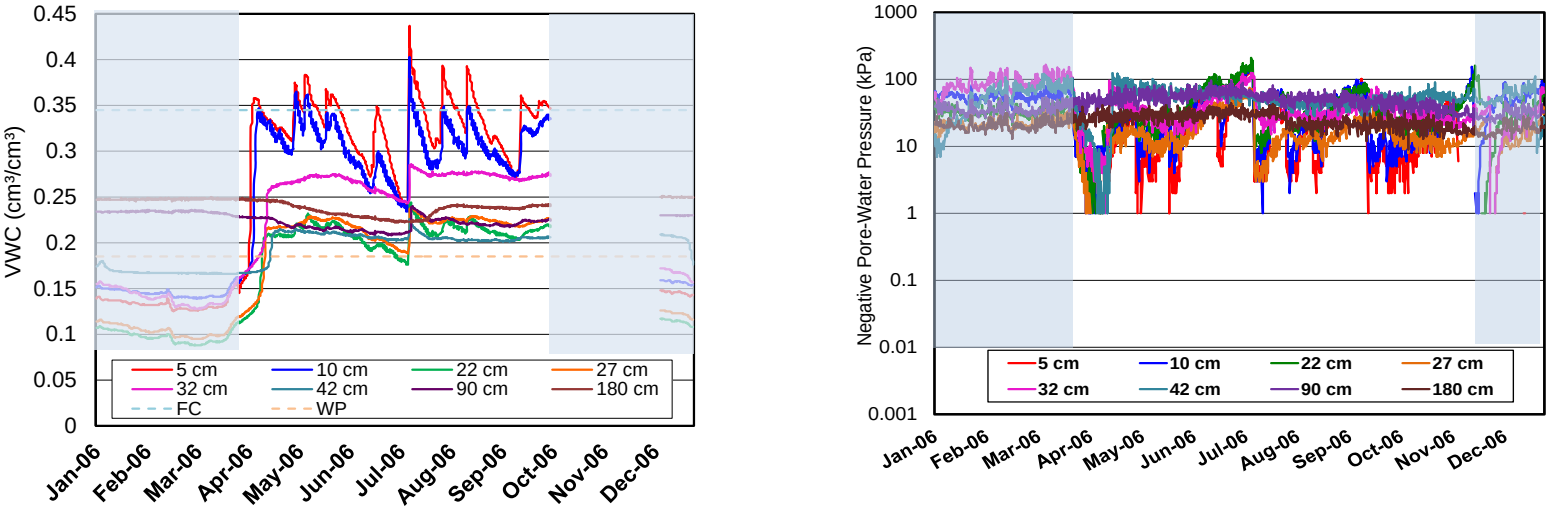

Figure A.1 Soil moisture (VWC [A] and matric suction [B]) in shallow cover system for 2006 monitoring year.

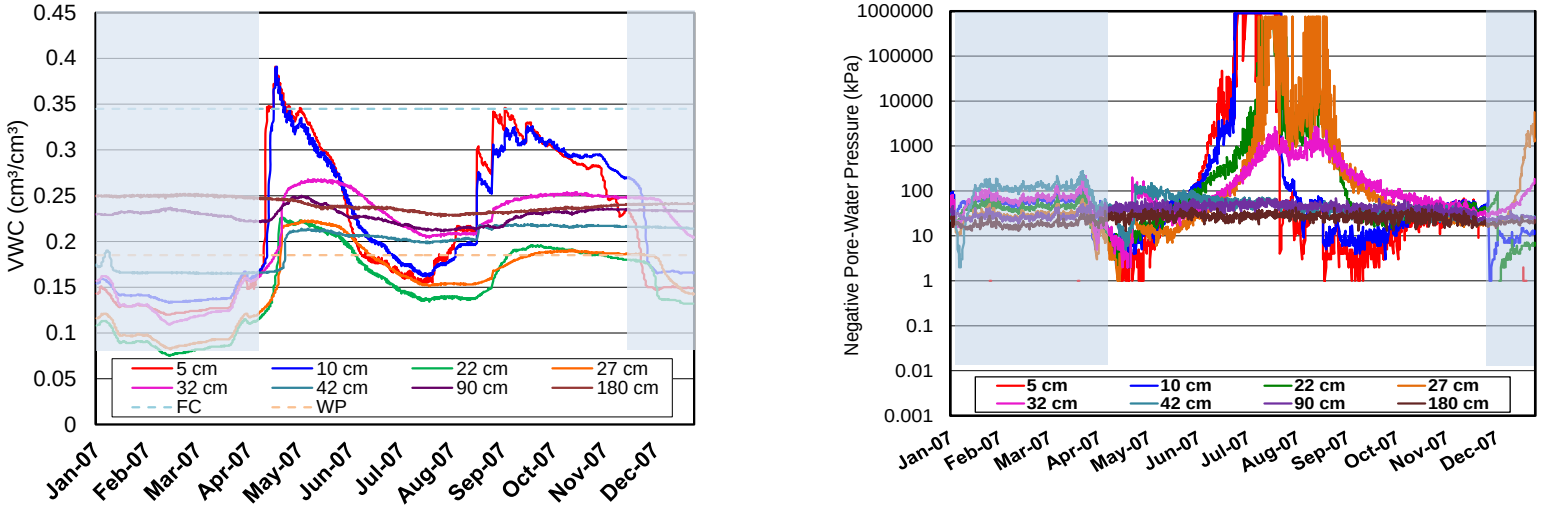

Figure A.2 Soil moisture (VWC [A] and matric suction [B]) in shallow cover system for 2007 monitoring year.

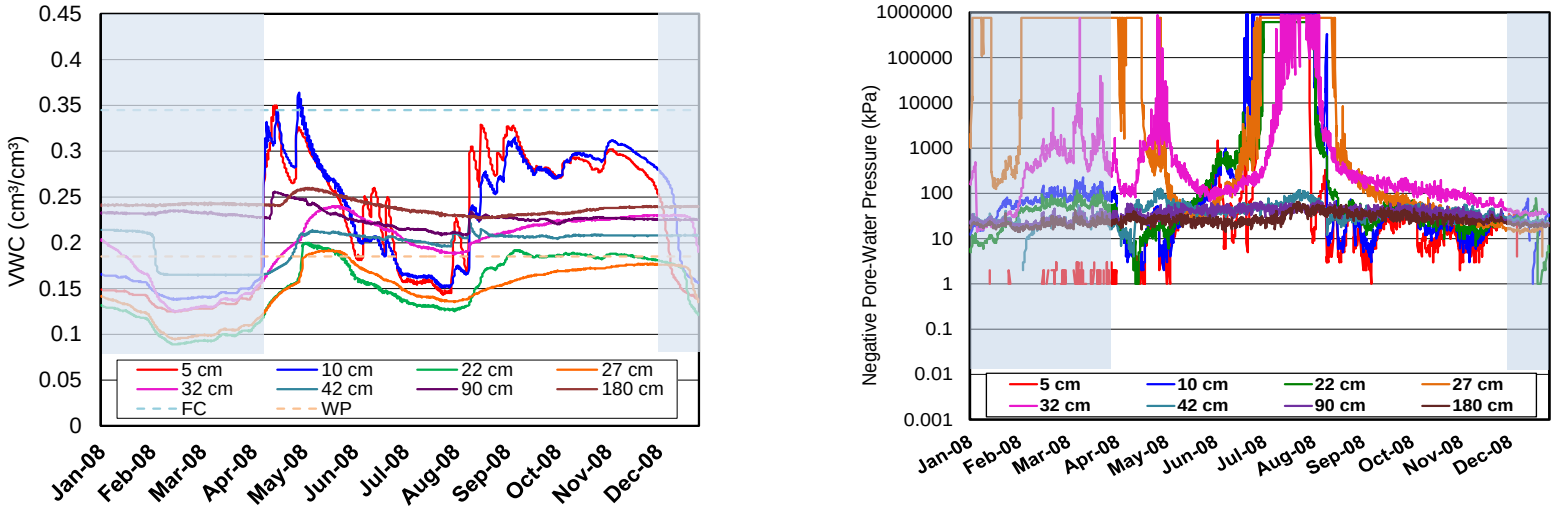

Figure A.3 Soil moisture (VWC [A] and matric suction [B]) in shallow cover system for 2008 monitoring year.

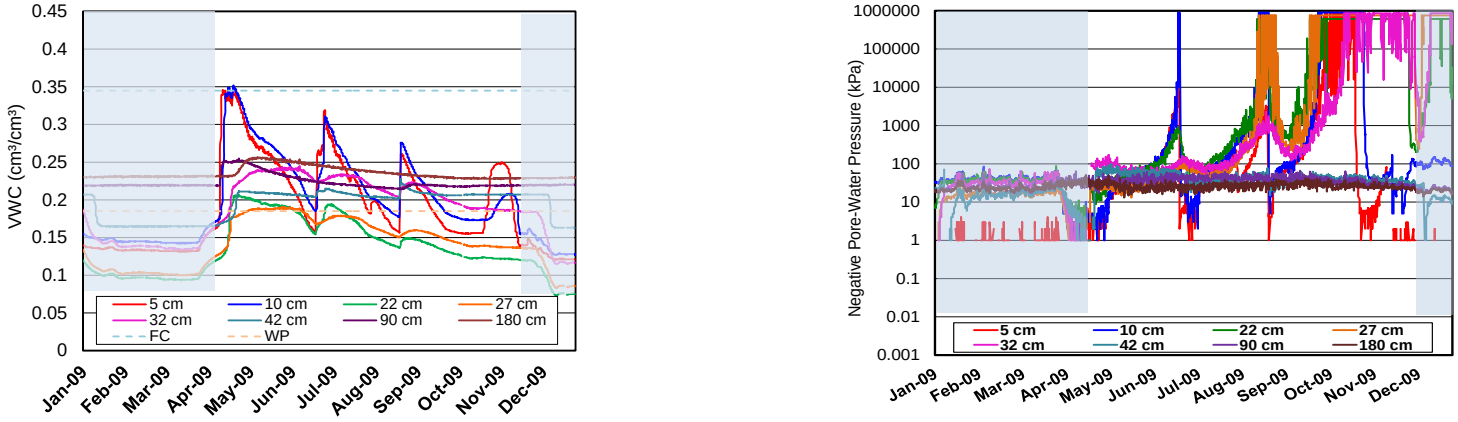

Figure A.4 Soil moisture (VWC [A] and matric suction [B]) in shallow cover system for 2009 monitoring year.

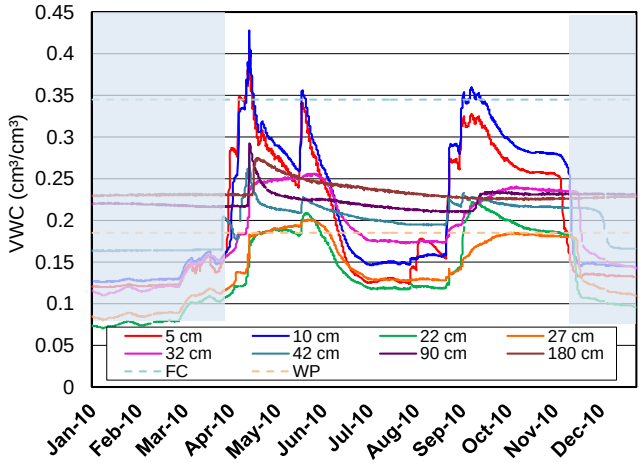

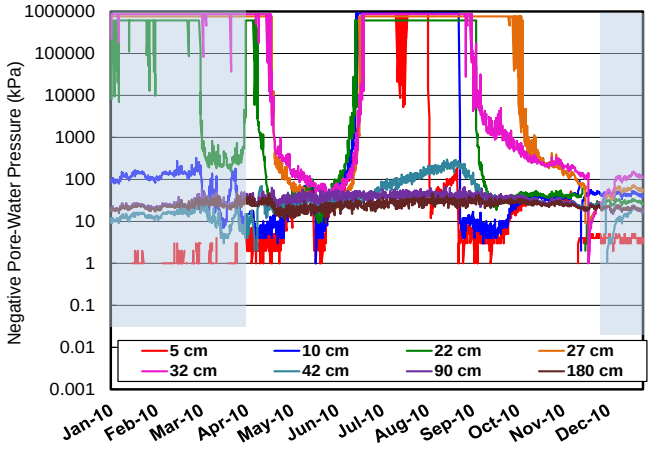

Figure A.5 Soil moisture (VWC [A] and matric suction [B]) in shallow cover system for 2010 monitoring year.

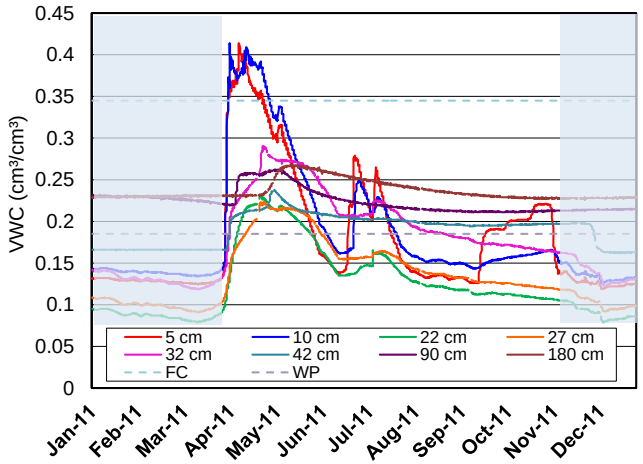

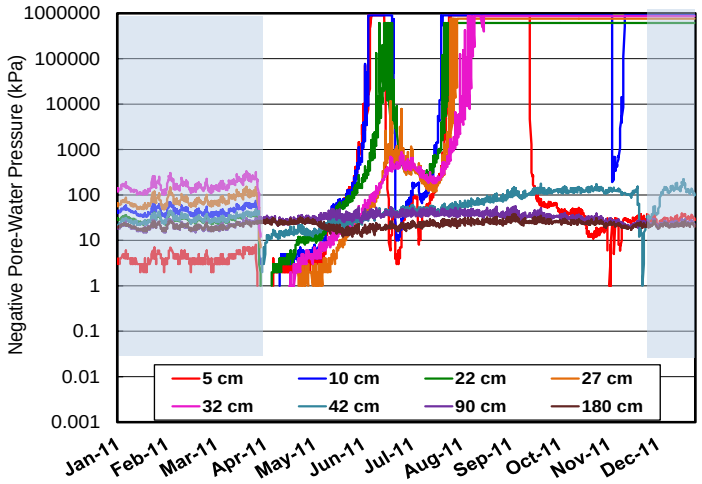

Figure A.6 Soil moisture (VWC [A] and matric suction [B]) in shallow cover system for 2011 monitoring year.

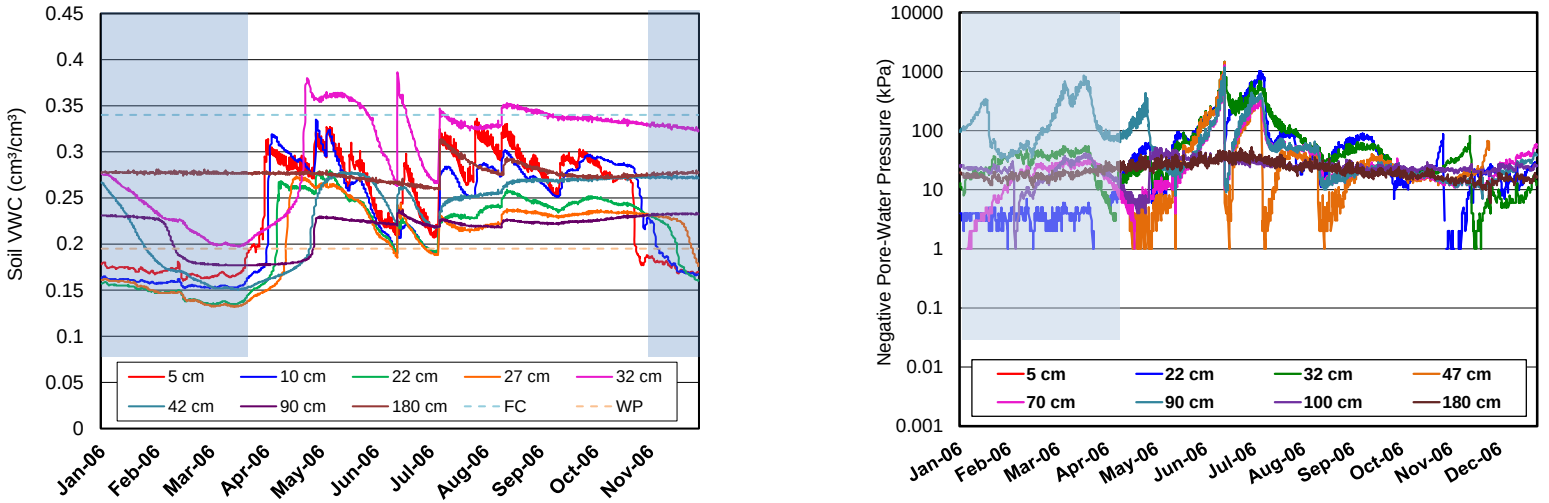

Figure A.7 Soil moisture (VWC [A] and matric suction [B]) in deep cover system for 2006 monitoring year.

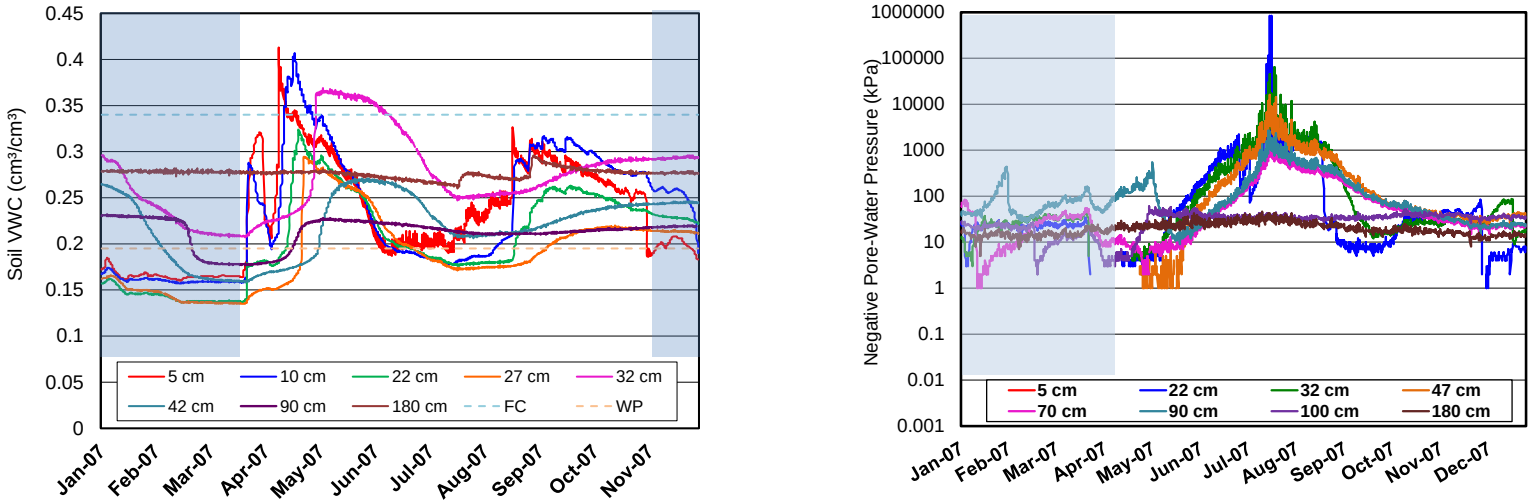

Figure A.8 Soil moisture (VWC [A] and matric suction [B]) in deep cover system for 2007 monitoring year.

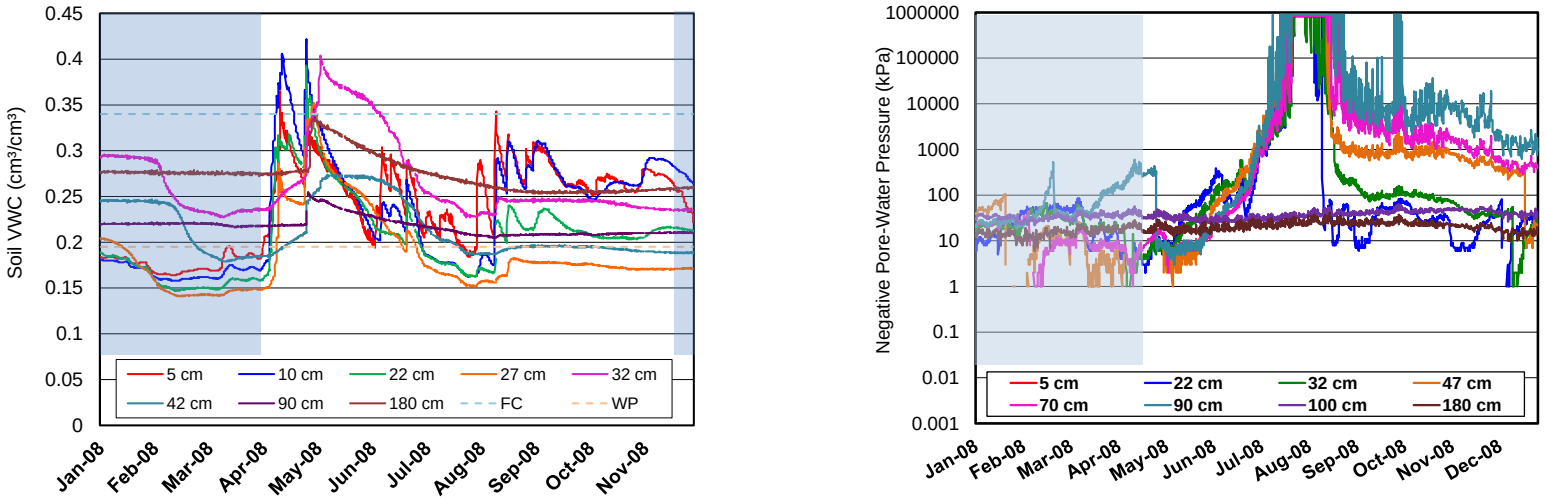

Figure A.9 Soil moisture (VWC [A] and matric suction [B]) in deep cover system for 2008 monitoring year.

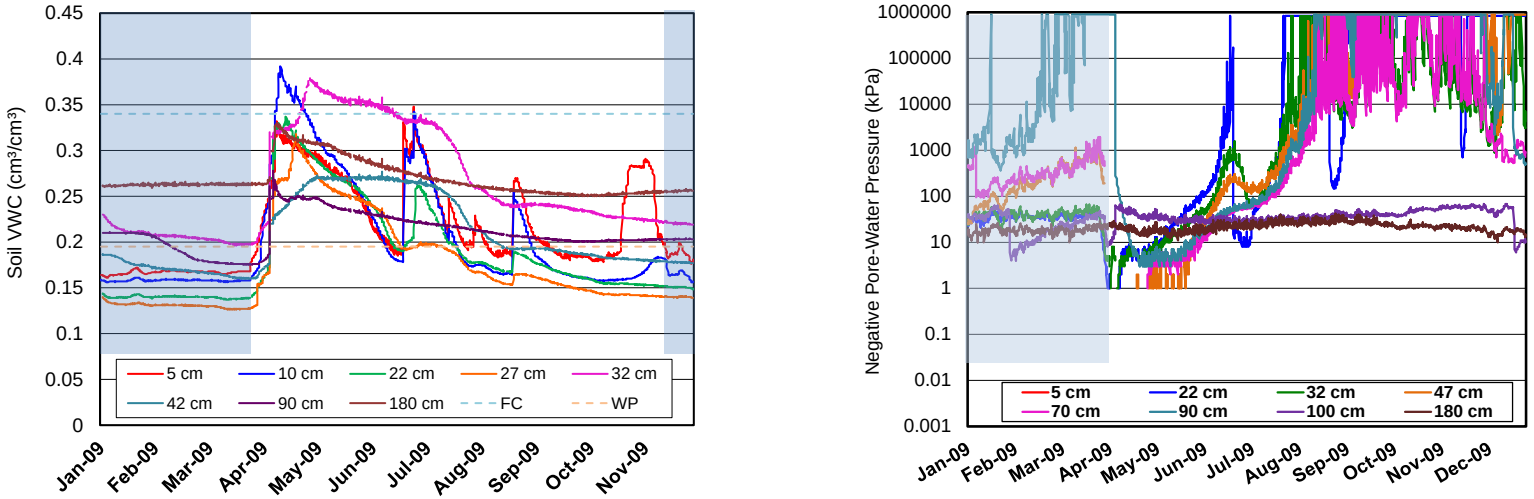

Figure A.10 Soil moisture (VWC [A] and matric suction [B]) in deep cover system for 2009 monitoring year.

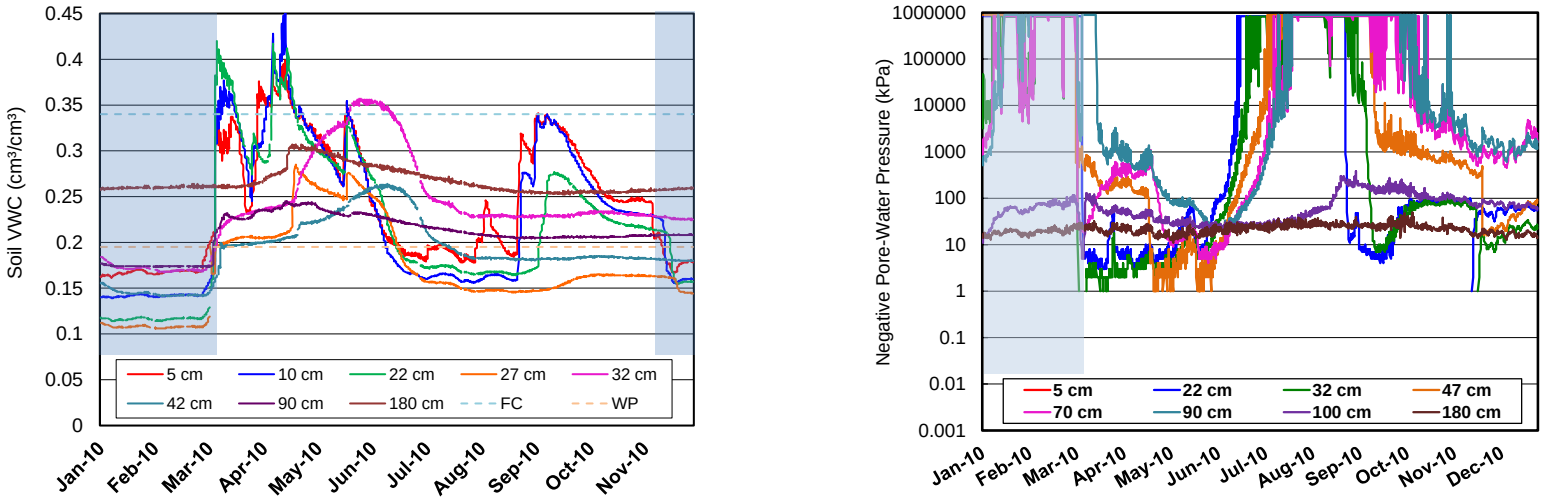

Figure A.11 Soil moisture (VWC [A] and matric suction [B]) in deep cover system for 2010 monitoring year.

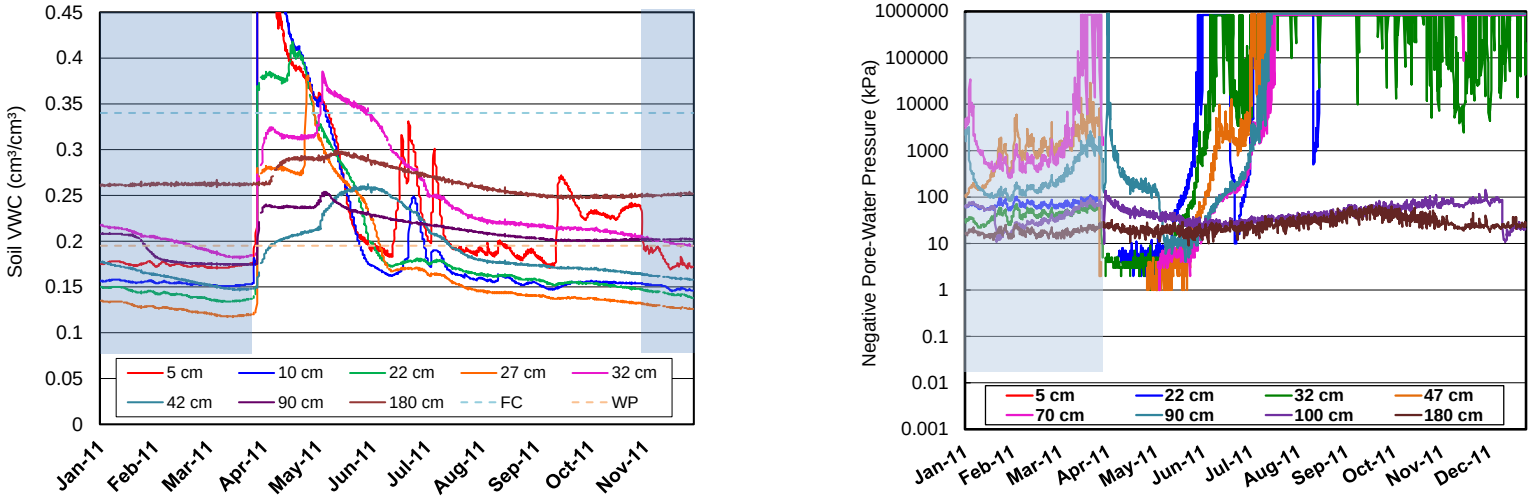

Figure A.12 Soil moisture (VWC [A] and matric suction [B]) in deep cover system for 2011 monitoring year.

Appendix B

Electronic Supplements

Due to the volume of data collected while investigating this research topic, several data sets have been compiled as supplements to this thesis. A complete list of data sets is as follows:

- Ambient Air Temperature 2005-2014
- Ambient PET 2005-2014
- Ambient PPT 2005-2014
- Berm Differential Pressures
- Deep Cover Differential Pressures
- Deep Cover Matric Suction
- Deep Cover Soil Temperatures
- Deep Cover VWC
- Deep Cover Water Balance – 2006
- Deep Cover Water Balance – 2007
- Deep Cover Water Balance – 2008
- Deep Cover Water Balance – 2009
- Deep Cover Water Balance – 2010
- Deep Cover Water Balance – 2011
- Deep Cover Water Balance – 2012
- Deep Cover Water Balance – 2013
- Deep Cover Water Balance – 2014
- Shallow Cover Differential Pressure
- Shallow Cover Matric Suction
- Shallow Cover Soil Temperature
- Shallow Cover VWC

- Shallow Cover Water Balance - 200
- Shallow Cover Water Balance – 2007
- Shallow Cover Water Balance – 2008
- Shallow Cover Water Balance – 2009
- Shallow Cover Water Balance – 2010
- Shallow Cover Water Balance – 2011
- Shallow Cover Water Balance – 2012
- Shallow Cover Water Balance – 2013
- Shallow Cover Water Balance - 2014